Feary, D.A., Hine, A.C., Malone, M.J., et al., 2000
*Proceedings of the Ocean Drilling Program, Initial Reports* Volume 182

# 10. Site 1132[1]

Shipboard Scientific Party[2]

## BACKGROUND AND OBJECTIVES

Site 1132 is located on the Great Australian Bight upper slope in 218.3 m of water (Fig. F1). The primary objective at Site 1132 was to obtain a detailed record of Neogene shelf edge and upper slope cool-water carbonate deposition and, in particular, to intersect the thin proximal portion (to contrast with the distal section at Site 1130) of an inferred Paleocene–middle Eocene progradational siliciclastic wedge (Fig. F2) identified and mapped as seismic Sequence 7 (Feary and James, 1998, reprinted as Chap. 2). This east-west–oriented, elongate sediment body increases in thickness seaward to 230 m and then abruptly downlaps onto the underlying Cenomanian/lower Cenozoic unconformity. Sequence 7 extends at least 300 km along the Eucla Basin, seaward of a prominent basement high (see "Seismic Stratigraphy," p. 31).

Site 1132 was projected to intersect seismic Sequences 2, 3, 4, 6A, 6B, and 7 to recover a record of Neogene cool-water carbonate deposition punctuated by hiatuses representing both sequence boundaries and intrasequence disconformities. The Sequence 2 interval at Site 1132 offered the opportunity to examine along-slope variations in sedimentation rates and depositional facies by comparison of this site with the much thicker Sequence 2 succession intersected at Sites 1127, 1129, and 1131 to the east. Similarly, comparison with the Sequence 2 interval intersected at Site 1130 on the uppermost slope provided an opportunity to describe downslope facies variability. Site 1132 was expected to intersect the most complete section through Sequence 3 of any of the Leg 182 drill sites to characterize the facies deposited in the interpreted aggradational shelf succession (Feary and James, 1998, reprinted as Chap. 2). Seismic data (Fig. F2) show that a thin unit containing mounds immediately overlies the Sequence 7 progradational wedge at Site 1132. This interval was mapped as the distal edge of Sequence 6B, interpreted as an Eocene–middle Miocene interval predominantly de-

F1. Map showing Site 1132 in relation to other Leg 182 sites and the AGSO169 seismic lines, p. 36.

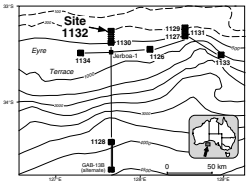


F2. Portion of seismic Line AGSO169/13a showing seismic stratigraphic sequences at Site 1132, p. 37.

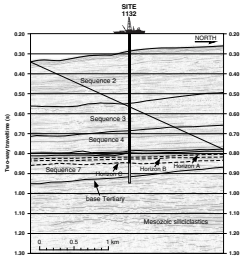


[1] Examples of how to reference the whole or part of this volume.
[2] Shipboard Scientific Party addresses.

Ms 182IR-110

posited on the shelf, but with a thinning wedge containing mounds extending into deeper water (Feary and James, 1998, reprinted as Chap. 2). Site 1132 was located to intersect one of these small Sequence 6B mounds.

The scientific objectives for Site 1132 were to

1. Recover a detailed record of shelf edge siliciclastic deposition at a proximal site, evaluate the sedimentary response to Paleogene sea-level fluctuations, and evaluate the complex interaction between sea-level variation, accommodation space, and subsidence;
2. Determine the characteristics of cool-water carbonate facies within the Neogene/Quaternary succession;
3. Determine paleoceanographic parameters within a shelf edge setting in Sequences 2 to 4 to complement other components of the shelf-to-basin transect;
4. Evaluate sea-level control on Neogene facies within an upper slope/shelf edge setting; and
5. Evaluate the diagenetic history and processes within Neogene facies in an upper slope/shelf edge setting.

# OPERATIONS

## Transit to Site 1132

The 44-nmi sea voyage to Site 1132 required 4.25 hr at 10.4 kt. A beacon was deployed at 2221 hr on 20 November, initiating Site 1132.

## Hole 1132A

The ship was stabilized on position, and Hole 1132A was spudded at 0100 hr on 21 November. The bit was positioned at 229.5 meters below rig floor (mbrf), and Core 1H recovered 9.22 m (Table T1). However, the excessive recovery was not appropriate for the establishment of a good mudline, and the hole was terminated.

T1. Site 1132 coring summary, p. 70.

## Hole 1132B

The ship was not moved, and the bit was positioned at 227.5 mbrf. Hole 1132B was spudded at 0130 hr on 21 November. Core 1H recovered 6.78 m, indicating a water depth of 218.5 meters below sea level (mbsl), which suggests the previous assessment of an inappropriate mudline in Hole 1132A was correct. Advanced hydraulic piston (APC) coring advanced to 168.3 meters below seafloor (mbsf), ceasing after four of the five last APC cores were recovered with split liners. Cores 3H–18H were oriented and Adara temperature tool heat-flow measurements were taken on Cores 4H, 8H, and 12H. The nonmagnetic shoe and flapper valve with a steel 10-finger core catcher were run on Cores 3H, 5H, 7H, 9H, 11H, and 13H. A Davis-Villinger temperature probe (DVTP) was deployed after Core 18H at 168.3 mbsf. Extended core barrel (XCB) cores deepened the hole from 168.3 to 284.6 mbsf. Drilling times increased after Core 24X (219.5 mbsf) and recovery was poor below Core 28X (257 mbsf; Table T1); thus, Hole 1132B was terminated four cores later. The fishing vessel *Bolzano* was hired to deliver to the *Resolution* six self-contained underwater breathing apparatus, two air-

tank filler fittings, and 10 air-filling station filters. The *Bolzano* arrived at Site 1132 at 0200 hr on 21 November, discharged its cargo in four crane lifts, and departed at 0315 hr. The hole was plugged with mud, and the drill string was pulled to the rig floor at 0425 hr on 22 November, ending Hole 1132B.

### Hole 1132C

The ship was moved 20 m northwest, and the standard rotary core barrel (RCB)/bottom-hole assembly (BHA) was run to the seafloor, spudding Hole 1132C at 0735 hr on 22 November. The hole was drilled to 161.6 mbsf with a center bit in 3.5 hr. The center bit was retrieved, and RCB Cores 1R and 2R were cut from 161.6 to 180.4 mbsf in a successful effort to sample a low-recovery interval from Hole 1132B. The hole was then drilled from 180.4 to 255.8 mbsf in 3.25 hr. Coring resumed with the RCB from 255.8 to 603.2 mbsf with low recovery in interbedded cherts and packstones (Table **T1**). With no recovery in the last four cores and vigorous backflow occurring on pipe connections, a precautionary wiper trip was made to verify hole conditions. The pipe was pulled up to 535 mbsf with heavy backflow. The bit deplugger was dropped in case the annulus was plugged with debris, causing the backflow. The bottom was tagged at 574 mbsf, indicating 29 m of fill in the bottom of the hole. We cleaned the hole to continue coring, ultimately clearing out 9 m of the fill. However, the pipe became stuck with 40 kilopounds (kips) overpull, stalling the rotary. The pipe was worked free, and another mud sweep was circulated. A full wiper trip was made to 105 mbsf with heavy backflow and fill was tagged at 560 mbsf (43 m off the bottom). With these unstable conditions, it appeared unlikely that the hole could be safely deepened at these shallow-water depths. Thus, coring was terminated, another mud sweep was circulated, the bit was dropped with the mechanical bit release, and the sleeve was closed. The hole was loaded with 150 bbl of mud in an effort to stabilize the hole.

The end of pipe was pulled to 105 mbsf for logging. The triple combination logging tool (triple combo) log was run from 470 to 397 mbsf and rerun from 560 mbsf to the mudline. The Formation MicroScanner (FMS)/sonic tool could not be worked past 163 mbsf, so it was run from 163 to 80 mbsf. The open-ended pipe was advanced from 105 to 189 mbsf to guide the logging tool through a presumed ledge; however, the FMS/sonic tool could not pass 203 mbsf. The pipe was advanced again to push past any obstructions and reached 242 mbsf where it stopped with 25 kips weight on the pipe. The drill string started hydraulically lifting when an attempt was made to circulate, which suggested that it was buried in fill. The end of pipe was pulled up to 105 mbsf and the FMS/sonic tool was rerun in attempt to log the upper portion of the hole. However, the tool could not pass 180 mbsf, and the log was run from that depth. The hole was plugged with mud, the drill string was retrieved, and both beacons were recovered. The rig was secured for transit, and the vessel was under way at 1815 hr on 24 November.

## LITHOSTRATIGRAPHY

### Introduction

Site 1132 is located at a water depth of 218.3 m immediately seaward of the shelf-slope break of the eastern Eyre Terrace in the western Great

Australian Bight. A Quaternary–Eocene succession of carbonate sediments, 603.2 m thick, was penetrated. It records the temporal evolution from shallow neritic Eocene, through bathyal early Oligocene and middle Miocene, to outer neritic–upper bathyal late Pleistocene and Holocene deposition. The lower Oligocene and middle Miocene intervals are thickly developed, the lower Miocene is represented by a major hiatus, the upper Miocene–lower Pliocene is condensed, and the Pleistocene interval is relatively thick (see "Biostratigraphy," p. 13). The succession shows a wide variety of lithologies, and a total of six litho-stratigraphic units are recognized (Fig. F3). Core recovery is good for the upper 250 mbsf, and lithostratigraphic boundaries are well defined. Recovery is poor below this level, and the positions of boundaries are accordingly more tentative. The most remarkable lithology encountered at the site is a thickly developed bryozoan floatstone-dominated package characterizing the upper 100 mbsf. Seismic evidence shows that deposition of this interval took place in a complex of overlapping and laterally migrating low biogenic mounds (see "Seismic Stratigraphy," p. 31).

F3. Site 1132 summary of litho-stratigraphy, p. 38.

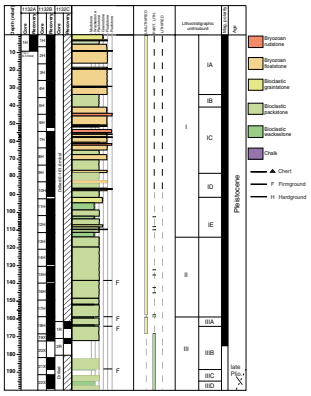


## Lithostratigraphic Units

### Unit I

Interval: Core 182-1132B-1H through Section 13H-2, 75 cm
Depth: 0–113.55 mbsf
Age: Pleistocene

Unit I consists of bryozoan floatstone and rudstone alternating with bryozoan packstone; the lower part also includes bioclastic wackestone with bryozoans. The sediment is predominantly unlithified, although thin, widely spaced, partially lithified beds are present below ~100 mbsf. The abundant bryozoan fauna is highly diverse and includes a variety of growth forms (e.g., Bone and James, 1993). A unique benthic foraminifer assemblage was found in association with the bryozoan mounds of Subunits IA and IB (see "Benthic Foraminifers," p. 18). The sediments are unlithified and burrow mottled, and the color is dominantly light gray with pale olive and white intervals. The unit represents a major bryozoan mound complex composed of well-defined lithostratigraphic packages that form the basis for division into five subunits. The boundaries between subunits are defined at sharp textural and compositional changes between lithologic types.

#### *Subunit IA*

Interval: Core 182-1132B-1H through Section 4H-6, 61 cm
Depth: 0–33.90 mbsf
Age: late Pleistocene

Subunit IA consists of unlithified, thick-bedded bryozoan floatstone, together with a few beds of bryozoan rudstone and packstone, mainly <0.5 m thick. The color is light gray, light olive gray, and pale yellow. The floatstone contains granule- to cobble-sized flat robust branching, encrusting, and delicate branching bryozoan growth forms floating in a matrix consisting of fine sand-sized bioclasts, debris of delicate branching and articulated zooidal bryozoans, and soft fecal pellets. Serpulids are common in the lower part, together with coralline algal rods. In addition, the matrix fine fraction contains coccoliths, bioclasts, benthic

and planktonic foraminifers, echinoid spines, ostracodes, and sponge and tunicate spicules (see "Site 1132 Smear Slides," p. 63). The rudstone and packstone beds contain the same components, but the packstone is dominated at some levels by bryozoan debris and other bioclasts. The sediment is strongly bioturbated, and distinct burrows can be recognized at some levels.

### *Subunit IB*

Interval: Sections 182-1132B-4H-6, 61 cm, through 5H-4
Depth: 33.90–41.30 mbsf
Age: late Pleistocene

Subunit IB consists of packstone with less than 15% "floating" granule-sized bryozoan fragments. The upper boundary is placed where the packstone is overlain by the thick bryozoan floatstone-dominated Subunit IA. The color is light gray, light olive gray, and pale olive. The most common larger bryozoan growth forms are delicate branching and flat robust branching. Serpulids occur scattered throughout. The matrix contains articulated zooidal bryozoans, bioclasts, benthic foraminifers, sponge spicules, planktonic foraminifers, echinoid spines, gastropods, and blackened grains. The sediment is strongly bioturbated, although well-defined burrows are rare to absent.

### *Subunit IC*

Interval: Sections 182-1132B-5H-5 through 9H-3, 131 cm
Depth: 41.30–77.60 mbsf
Age: late Pleistocene

Subunit IC consists mainly of bryozoan floatstone, with intercalated bryozoan rudstone and packstone beds in the upper part, mainly <1 m thick, and with thicker bryozoan packstone beds in the lower part. A 35-cm-thick wackestone occurs between 51 and 52 mbsf. The upper boundary of Subunit IC is placed where a thick floatstone is overlain by the uniform packstone of Subunit IB. The color is light gray and light olive gray, and white intervals occur in the lower part. The floatstone contains granule- to pebble-sized nodular, arborescent, delicate branching, and flat robust branching bryozoan growth forms, and serpulids are common at certain levels. The matrix between the large bryozoans consists of fine to medium sand-sized bioclastic packstone that contains dominant bioclasts and abundant benthic foraminifers and bryozoans. Bivalves, sponge spicules, ostracodes, and planktonic foraminifers are also present. The rudstone, packstone, and floatstone are of similar composition, but the packstone also contains numerous (<25%) blackened grains.

### *Subunit ID*

Interval: Section 182-1132B-9H-3, 131 cm, through Core 10H
Depth: 77.60–91.70 mbsf
Age: late Pleistocene

Subunit ID is dominated by bioclastic packstone packages, ~2.5–5 m thick, intercalated with two floatstone-rudstone packages, 0.8–1.5 m thick. The upper boundary is placed where the upper packstone is abruptly overlain by the bryozoan floatstone of Subunit IC. The color is light gray, pale yellow, and white. The bioclastic packstone is poorly sorted very fine to fine sand, and the content of dark grains increases up-

ward within each package. The lower packstone contains scattered flat robust branching, fenestrate, and nodular bryozoans. The sand fraction of the packstone contains dominant bioclasts, present benthic and planktonic foraminifers, and traces of echinoid spines. The fine fraction includes abundant bioclasts and coccoliths, common tunicate spicules, present sponge spicules, rare dolomite rhombs, and traces of benthic foraminifers and pyrite (see **"Site 1132 Smear Slides,"** p. 63). The sediment is strongly bioturbated throughout, as reflected by muddy and grainy patches with diffuse outlines.

### *Subunit IE*

Interval: Core 182-1132B-11H through Section 13H-2, 75 cm
Depth: 91.70–113.55 mbsf
Age: Pleistocene

Subunit IE consists of alternating packages of bioclastic grainstone, packstone, and wackestone, together with two beds of bryozoan floatstone, 10 and 40 cm thick, at ~109 mbsf. The upper boundary is placed at the contact where the bryozoan-rich Subunit ID overlies lithologies with few or no bryozoans. Packstone is the dominant lithology of Subunit IE, and the scarcity or near absence of bryozoans, except for the thin floatstone beds, is a characteristic feature. The color is gray, light gray, light greenish gray, and white. The grainstone and packstone sand fraction consists of dominant bioclasts, common benthic foraminifers, present to rare planktonic foraminifers, echinoid spines, sponge spicules, tunicate spicules, quartz grains, and traces of bryozoans and glauconite. Blackened grains are common at many levels. The two floatstone beds contain medium sand to granule fragments of bryozoans, dominated by flat robust branching, delicate branching, articulated zooidal, and encrusting growth forms. The fine fraction includes abundant bioclasts and benthic foraminifers, rare sponge spicules, and traces of planktonic foraminifers. The wackestone contains bioclasts, minor benthic and planktonic foraminifers, and tunicate spicules. The subunit is intensely bioturbated, and some burrow fills are grainy and slightly carbonate cemented.

## Unit II

Interval: Sections 182-1132B-13H-2, 75 cm, through 17H-7, 68 cm
Depth: 113.50–158.48 mbsf
Age: Pleistocene

Unit II consists of bioclastic packstone with bryozoans. The sediments are mainly unlithified, but thin partially lithified horizons are present below 130 mbsf. The color is dominantly light gray, with light olive gray, olive, and white intervals. The lithology alternates between packstone with well-sorted bioclastic debris and packstone with a diverse fauna of centimeter-sized bryozoans floating in the matrix. The sand-sized matrix includes articulated zooidal and other bryozoan fragments, benthic and planktonic foraminifers, sponge spicules, small spines of infaunal echinoids, glauconite, and blackened grains. The larger grains comprise a diverse, well-preserved fauna of bryozoans, including delicate branching, flat robust branching, nodular, and arborescent forms that commonly float in the matrix with apparently random orientations. Serpulids constitute a significant faunal component, and partially lithified gray intraclasts are present at some levels. The sediment is com-

pletely bioturbated and scattered discrete burrows are recognized, mostly at minor lithologic changes.

## Unit III

Intervals: Section 182-1132B-17H-7, 68 cm, through Core 28X; Cores 182-1132C-1R through 2R
Depth: 158.48–257.20 mbsf (Hole 1132B); 161.60–180.40 mbsf (Hole 1132C)
Age: late Miocene–Pleistocene

Unit III consists of unlithified bioclastic packstone and minor wackestone and grainstone, with a thin package of foraminiferal ooze and chalk at the base. The upper boundary is placed at a prominent firmground where the light olive gray, partially lithified packstone with bryozoans of Unit II overlies gray unlithified packstone. The color is dominantly light olive gray with thinner olive, pale olive, and white intervals. The sediments are strongly burrowed. Unit III is dominantly unlithified; however, there are a few thin partially lithified intervals down to 168 mbsf, and the unit is partially lithified below that level. The presence of several prominent firmgrounds associated with minor but distinct lithologic and textural changes allows division into five subunits. Core recovery is good in the upper part but decreases below ~240 mbsf.

### *Subunit IIIA*

Interval: Sections 182-1132B-17H-7, 68 cm, through 18H-4, 11 cm
Depth: 158.30–163.41 mbsf
Age: Pleistocene

Subunit IIIA consists of unlithified bioclastic packstone. The color is gray, light gray, and light olive gray. The upper boundary of the subunit coincides with the top of Unit III, and the base is placed at a prominent firmground where unlithified bioclastic packstone overlies the burrowed bioclastic wackestone of Subunit IIIB. The sand fraction is well sorted, very fine to fine grained, and contains dominant bioclasts, common benthic and planktonic foraminifers, and present articulated zooidal bryozoans and echinoid spines. The sediment is strongly bioturbated, and abundant *Chondrites* occur below the top firmground.

### *Subunit IIIB*

Interval: Sections 182-1132B-18H-4, 11 cm, through 21X-5, 29 cm
Depth: 163.41–188.09 mbsf
Age: Pleistocene

Subunit IIIB consists of bioclastic packstone. The color is light olive gray, pale olive, and white. The sediment is unlithified in the upper 4 m and partially lithified below that level. The lower subunit boundary is placed at a distinct firmground where a partially lithified, light gray bioclastic packstone overlies a light olive gray bioclastic wackestone (Fig. F4). The sand fraction is well-sorted very fine and fine sand and contains dominant bioclasts and present benthic and planktonic foraminifers, echinoid spines, articulated zooidal bryozoans, and glauconite. The sediment is strongly bioturbated and distinct burrows occur, most commonly in the lower part.

F4. Firmground that marks the boundary between Subunits IIIB and IIIC, p. 41.

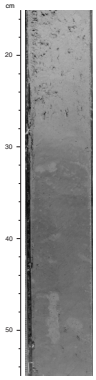

### *Subunit IIIC*

Interval: Sections 182-1132B-21X-5, 29 cm, through 22X-3, 50 cm

Depth: 188.09–194.80 mbsf
Age: late? Pliocene–Pleistocene

Subunit IIIC consists of bioclastic wackestone in the top 50 cm, overlying bioclastic packstone. The color is light gray and light olive gray, and the sediment is partially lithified. The sand fraction is poorly sorted fine sand and contains dominant bioclasts; common to present benthic foraminifers, tunicate spicules, and quartz; and rare planktonic foraminifers and sponge spicules. The sediment is strongly burrowed.

### *Subunit IIID*

Interval: Section 182-1132B-22X-3, 50 cm, through Core 27X
Depth: 194.80–247.90 mbsf
Age: late Miocene–late? Pliocene/Pleistocene

Subunit IIID consists of bioclastic packstone and two minor intervals of bioclastic wackestone, one forming the top 2.5 m, and the other at 207.2–208.2 mbsf. The color is light gray, light olive gray, pale olive, olive, and pale yellow, and the sediment is partially lithified. The lower boundary is placed where light olive gray bioclastic packstone of Subunit IIID overlies white foraminiferal ooze of Subunit IIIE. Although the boundary occurs within an uncored interval between Cores 182-1132B-27X and 28X, the lithologic contrast is marked. The sand fraction is poorly sorted fine sand and contains dominant bioclasts, common sponge spicules, common to present benthic foraminifers, and present to rare bryozoans, serpulids, ostracodes, and glauconite. The grains are commonly partially covered by small carbonate crystals. The basal 50 cm of the subunit contains granule-sized intraclasts and macrofossils, including bryozoans and serpulids. The sediment is strongly bioturbated, with common subhorizontal burrows including *Planolites* with a coarse, commonly greenish fill.

### *Subunit IIIE*

Interval: Core 182-1132B-28X
Depth: 247.90–257.20 mbsf
Age: late Miocene

Subunit IIIE consists of foraminiferal ooze and foraminiferal chalk, together with two thin beds of partially lithified bioclastic packstone. The color is white, light gray, and gray. Core recovery is poor above and below the subunit, and, as a result, the upper boundary cannot be precisely placed. The dominant ooze and chalk lithologies are, however, markedly different from both the packstone lithology of Subunit IIID and the chert-bearing grainstone and packstone lithologies of the underlying Unit IV. The chalk and the packstone are partially lithified, and it is possible that the unconsolidated nature of the ooze is due to drilling disturbance. The sand fraction of the ooze and chalk includes dominant planktonic foraminifers, common benthic foraminifers and bioclasts, present glauconite, rare ostracodes, and traces of echinoid spines and bryozoans. The fine fraction includes dominant nannofossils, common benthic foraminifers, and present planktonic foraminifers. The packstone sand fraction contains dominant bioclasts, common planktonic foraminifers, common to present glauconite, rare benthic foraminifers, and traces of echinoid spines.

## Unit IV

Intervals: Cores 182-1132B-29X through 32X; Cores 182-1132C-3R through 22R
Depth: 257.20 mbsf to bottom of hole (Hole 1132B); 255.80–441.50 mbsf (Hole 1132C); the top is defined in Hole 1132C
Age: middle Miocene

The interval containing Unit IV is characterized by very poor core recovery. Recognition of a distinct lithostratigraphic unit that differs markedly from the overlying and underlying deposits is, however, possible. Unit IV consists of partially lithified grainstone with light gray, dark gray, and almost black chert. It is significant that the chert is restricted to this single unit and has not been observed in overlying or underlying units. The chert is thus considered an important primary constituent of Unit IV, and it cannot have been emplaced in the cores by drilling contamination. The upper boundary is placed at the first downhole occurrence of chert; the lower boundary, by the last occurrence (LO) of chert. The first appearance is at roughly the same depths in Holes 1132B and 1132C. The color of the grainstone is light gray, olive gray, and white in one case, and the sediments are partially to strongly lithified. The sand fraction contains abundant bioclasts and planktonic foraminifers; common benthic foraminifers; and present to rare echinoid spines, sponge spicules, quartz, and glauconite. A thin section (Sample 182-1132C-13R-CC, 10–12 cm) shows a gray, very fine grained, partially dolomitized microbioclastic packstone with ostracode and zooidal? bryozoan fragments and planktonic foraminifers. The matrix consists of silt-sized microbioclasts. Silt- and sand-sized dolomite rhombs are common.

The chert is light gray or, more commonly, dark gray to almost black. Recovered fragments have mostly been crushed or brecciated by drilling, although centimeter-sized nodules with their original shapes preserved are common. The nodules have a white rim, 1–2 mm thick, consisting of poorly silicified carbonate. Abundant ghosts after small, partially silicified calcareous fossils occur within the nodules. Porous, partly silicified, white to light gray carbonate infills of commonly cylindrical burrows penetrate many nodules. The chert nodules were formed by partial to complete silicification of grainstone, by replacement of carbonate.

## Unit V

Interval: Core 182-1132C-23R through Section 31R-1, 100 cm
Depth: 441.50–517.70 mbsf
Age: early Oligocene–early Miocene

The interval containing Unit V is characterized by very poor core recovery. The available material shows, however, that it is lithologically distinct from overlying and underlying units. The unit consists of bioclastic and foraminiferal packstone and grainstone, without chert. The upper boundary is placed at the top of bioclastic grainstone lacking significant amounts of chert, and the lower boundary is placed at a prominent mineralized and bored hardground where white bioclastic grainstone overlies pale yellow echinoid wackestone (Fig. F5). The color of the subunit is pale yellow, very pale brown, and pale brown, and the sediment is strongly lithified. The sand fraction is very fine to fine sand and

F5. Bioclastic grainstone from the basal part of Unit V, p. 42.

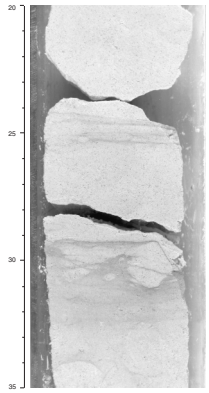

contains bioclasts, benthic and planktonic foraminifers, and glauconite. The lowest grainstone (516.8–517.7 mbsf) contains delicate branching bryozoans and serpulids. Dolomite and abundant glauconite are present at 507.1–507.3 mbsf. A thin section of Sample 182-1132C-26R-CC, 7–9 cm (468.7 mbsf), consists of gray, very fine to fine-grained foraminiferal packstone to local wackestone. Planktonic and benthic foraminifers dominate, and brachiopod, echinoid, ostracode, and bryozoan fragments are common. The matrix is a microsparite. The echinoderm grains are dolomitized and overgrown with dolomite rhombs. A thin section of Sample 182-1132C-31R-1, 56–59 cm (517.3 mbsf), from the base of Unit V, consists of white to gray, very fine to fine-grained, partially dolomitized planktonic foraminiferal wackestone to local packstone (see **"Site 1132 Thin Sections,"** p. 64). Particles are dominated by planktonic and benthic foraminifers, ostracodes, and echinoid fragments; clear, sand-sized dolomite rhombs are common.

## Unit VI

Interval: Section 182-1132C-31R-1, 100 cm, through Core 35R
Depth: 517.70–555.95 mbsf
Age: middle–late Eocene

Unit VI is complex and may well represent several discrete packages that could have been defined as subunits, if recovery had been better. The unit is represented by five cores containing lithologies that are different from core to core and with recovery gaps of 5–9 m between cores. The individual packages are described in turn from top to bottom to allow a possible future assignment to separate lithostratigraphic subunits or even units. Thin sections yield important information on the rather fragmentary succession and are, therefore, also described (see **"Site 1132 Thin Sections,"** p. 64).

The top interval of Unit VI, between 517.7–520.6 mbsf (Section 31R-1, 100 cm, through 31R-4), contains several firmgrounds and hardgrounds (Figs. **F6, F7, F8**). The upper boundary of the unit is a mineralized hardground showing brecciation, borings, and possible neptunian dikes (Fig. **F6**). It forms the top surface of a lithified, pale yellow echinoid wackestone, 55 cm thick, that contains brachiopods and bryozoans—in addition to echinoid fragments in the very coarse sand fraction—and a dolomite content of ~20%. A thin section of Sample 182-1132C-31R-2, 55–58 cm (518.8 mbsf), consists of gray to white, fine to medium sand-sized, partially dolomitized planktonic foraminiferal wackestone to packstone. The sediment is dominated by planktonic foraminifers with common bryozoan fragments (mostly delicate branching forms), glauconite grains, clear dolomite rhombs, and medium to coarse sand-sized echinoid and brachiopod fragments.

The echinoid wackestone overlies a pale yellow lithified bioclastic packstone that is rich in glauconite and contains bryozoans, solitary corals, echinoid fragments, and gastropods. The sediments are strongly bioturbated and include *Thalassinoides* burrows. A thin section of Sample 182-1132C-31R-3, 36–38 cm (520.1 mbsf), consists of white to gray, fine-grained, glauconitic, partially dolomitized chalk with a bioclastic wackestone to local packstone texture. The dominant particles are planktonic foraminifers, common benthic foraminifers, glauconite, and fine sand-sized dolomite rhombs. Echinoid and bryozoan particles are also present.

F6. Hardground marking the top of Unit VI, **p. 43.**

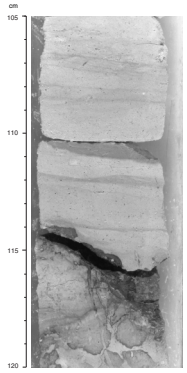


F7. Unit VI burrowed firmground to hardground, **p. 44.**

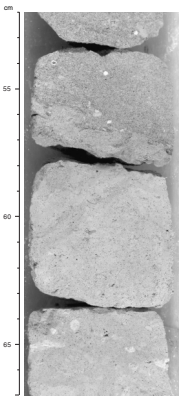


F8. Unit VI complex mineralized hardground in bioclastic packstone, **p. 45.**

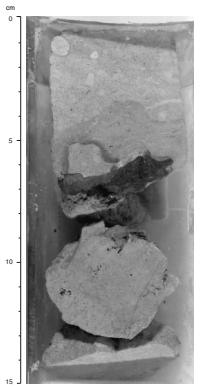

The packstone rests on a burrowed firmground at 520.3 mbsf (Section 31R-3) that forms the top surface of a bioclastic wackestone with floating bryozoans, at least 15 cm thick, which in turn overlies a mineralized hardground at 545.5 mbsf (Section 31R-CC) with sponge borings and debris of bryozoans, serpulids, echinoids, and bivalves (Figs. F7, F8).

The interval from 526.3 to 529.7 mbsf (Core 32R) consists of lithified bioclastic packstone with abundant, green, very fine grained material that is possibly a precursor clay to glauconite. The packstone is light gray to pale yellow, and the green material occurs in densely spaced, gently curved, wispy solution seams, which give the sediment package a characteristic finely striped appearance. Scattered centimeter-sized mollusk and bryozoan fragments are common, and the sediment is strongly bioturbated. A thin section of Sample 182-1132C-32R-1, 40–42 cm (526.7 mbsf), consists of gray to white, fine to coarse sand-sized bryozoan wackestone to local packstone. Bryozoan particles dominate and represent a diverse fauna with many different growth forms. Planktonic foraminifers and echinoid particles with replacing limonite, glauconite, and angular quartz silt are also present. A thin section of Sample 182-1132C-32R-2, 124–126 cm (528.9 mbsf), consists of gray to white, fine-grained, partially dolomitized planktonic foraminifer wackestone. Planktonic foraminifers dominate, and bryozoan, echinoid and ostracode fragments, benthic foraminifers, quartz silt, and clear dolomite rhombs are common.

A package at 535.9–536.4 mbsf (Core 33R) consists of lithified yellow to reddish yellow bioclastic grainstone. The grains are medium sand-sized in the upper part and fine to medium sand-sized in the lower part. Bryozoan fragments are common. The sediment is strongly bioturbated. Burrows filled with reddish, fine sand-sized bioclastic packstone are common in the lower part.

The interval from 545.5 to 547.5 mbsf (Core 34R) consists of yellow to red bioclastic grainstone and packstone. The grainstone contains granule-sized bryozoan fragments and whitish burrow fills. The grains are mainly medium to coarse sand sized. The packstone is composed of fine to medium sand-sized bioclasts; scattered granule-sized bryozoan fragments are also present.

The lowest cored material at 555.1–555.9 mbsf (Core 35R) consists of pale to dark red bioclastic grainstone and packstone. The grains are fine to medium sand sized, and scattered granule-sized bryozoan and shell fragments are present. Two pebbles of coarse sand- to granule-sized calcareous sandstone are composed of subrounded to subangular quartz grains, green lithic fragments, and sedimentary rock fragments. A thin section of Sample 182-1132C-35R-1, 45–47 cm (551.6 mbsf), consists of orange, medium to coarse sand-sized bryozoan wackestone and packstone. Most grains are somewhat rounded and abraded, with conspicuous microborings filled by limonite. The dominant grains are bryozoans, with mostly flat robust branching, articulated branching, and nodular growth forms. Benthic and planktonic foraminifers are common, and dolomite rhombs are rare. Presence of the planktonic foraminifer *Acarinina collactea* gives a middle–late Eocene age for the deepest cored part of the succession (see **"Biostratigraphy,"** p. 13).

## Discussion

The succession encountered in Holes 1132B and 1132C is 556 m thick and spans the Eocene–Pleistocene time interval. It shows an over-

all punctuated deepening to shallowing trend, from an Eocene shallow-marine shelf, to mid-Oligocene and middle Miocene deep-slope conditions, and then back to upper bathyal to outer neritic water depths in the late Pliocene–Holocene.

The oldest cored sediments, Unit VI of middle–late Eocene age, were deposited in a high-energy shallow-marine environment as reflected by the body and trace fossil fauna and rapidly varying lithology. Succeeding deposition took place in progressively deeper water, probably in an upper slope environment with relative sea-level falls reflected by repeated occurrences of firmgrounds and mature, mineralized hardgrounds with sponge borings. There is no direct evidence for latest Eocene–earliest Oligocene deposition, and the Eocene Unit VI is apparently overlain by mid-Oligocene chert-free slope carbonates of Unit V. The early Oligocene hiatus and the marked landward facies shift probably reflect sea-level rise, backstepping, and marked condensation in the middle and lower slope regions. A second major hiatus appears to coincide with the boundary between the chert-free mid-Oligocene Unit V and chert-bearing middle Miocene slope carbonates of Unit IV. The cause of the hiatus is unclear, but a direct sea-level control seems unlikely because the carbonate facies of the two units appear similar. The hiatus is more likely to reflect scouring, winnowing, or nondeposition related to a change in deeper water-current regimes, which may have some combination of climatic, plate tectonic-paleogeographic, or sea-level causes. However, the poor core recovery prevents firm conclusions on this aspect at present. Late Miocene–early Pleistocene deposition of Unit III reflects gradual shallowing, represented by stacking of probably middle to upper slope carbonate packages topped by firmgrounds. Upper slope depths were reached at the Pliocene–Pleistocene transition, recorded by the incoming of delicate bryozoans floating in the fine-grained carbonates of Unit II. This can be considered the first phase of widespread bryozoan colonization of the seafloor, which eventually led to establishment in the Pleistocene of the bryozoan mound complex of Unit I. This type of ecological facies succession is well known from the upper Maastrichtian–lower Danian carbonates of Denmark (Surlyk, 1997). The mound complex shows a cyclic internal upbuilding characterized by packages, which coarsen upward from packstone and grainstone to floatstone and rudstone with rich and diverse bryozoan faunas. Several orders of cycles are recognized, corresponding to Subunits IA to IE. The larger cycles illustrate the establishment, aggradation, and lateral migration of major mound systems. The smaller cycles may reflect possible Milankovitch-driven rhythmicity in either productivity or current velocity. The main subunit boundaries within the bryozoan mound complex appear to correlate well to seismic reflectors seen in dip sections across the shelf-slope break (Feary and James, 1998, reprinted as **Chap. 2**). Combined analysis of facies successions and trends in the mound complex and seismic reflection patterns will yield important information on the dynamic architecture and temporal evolution of the impressive >100-m-thick bryozoan mound complex. There are no signs of deposition within the photic zone. During the Holocene, the long-term slope progradation recorded at Holes 1132B and 1132C reached water depths corresponding to the present-day position of the site, immediately beyond the shelf-slope break in slightly more than 200 m of water.

# BIOSTRATIGRAPHY

## Introduction

Calcareous nannofossils and planktonic foraminifers indicate that drilling at Site 1132 recovered a thick Pleistocene–middle Eocene sequence (~550 m thick) overlying a relatively thin barren section (~45 m) (Fig. F9). Calcareous nannofossils from the basal Pleistocene section registered a nannofossil event, the "*Braarudosphaera* Event," which previously was recorded at Sites 1127, 1130, and 1131, representing a brief and dramatic change in surface-water conditions over a large area. A thin interval (~20 m) with poor core recovery separates a thick Pleistocene–upper Pliocene? section (~230 m) with nannofossil combined Zones NN21–NN20 and Zone NN19 from an equally thick middle–lower Miocene section (~200 m) with nannofossil Zone NN6 and combined Zones NN5–NN4. Hiatuses are likely within this thin interval, as the contained nannofossils and planktonic foraminifers are suggestive of late Miocene age. Another similarly thin interval (~20 m) with poor core recovery, also likely to contain hiatuses, underlies the middle–lower Miocene section. Immediately below this thin interval is an ~45-m section with lower–middle Oligocene nannofossil and planktonic assemblages. The Eocene age indicated for the section below 517 mbsf was determined from foraminifers in thin section from two depths, ~530 and ~547 mbsf. In our shipboard examination, no calcareous nannofossils were found in this Eocene section.

Five main benthic foraminiferal assemblages are identified. These indicate upper to middle bathyal paleodepth for the Pleistocene–Oligocene section. A striking, well-preserved Pleistocene assemblage, characterized by many large (>1 mm) agglutinated forms, is found in bryozoan-rich accumulations. This assemblage probably reflects diverse, highly dynamic ecosystems that became established at the seafloor at various times during the Pleistocene, coincident with bryozoan mound development. Changes in the composition of this assemblage may relate to sea-level and/or circulation changes during the growth of bryozoan buildups.

F9. Calcareous nannofossil and planktonic foraminifer zones, with benthic foraminiferal assemblages, p. 46.

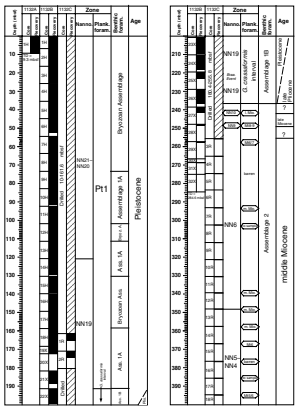

## Calcareous Nannofossils

A Pleistocene–lower Oligocene succession of calcareous nannofossil assemblages is recorded from Site 1132. Core recovery deteriorated rapidly below the Pleistocene section. Frequent chert layers in the Miocene and Oligocene sections hampered both core recovery and biostratigraphic refinement (see "Operations," p. 2). No calcareous nannofossils were found below the Oligocene section in our shipboard analysis.

The succession at Site 1132 is differentiated into three main biostratigraphic packages: Pleistocene (~230 m thick), middle–lower Miocene (~200 m thick), and lower–middle Oligocene (~45 m thick). These packages are separated by two thin intervals (each ~20 m thick) representing condensed sections that probably include one or more hiatuses. The younger interval contains assemblages of late Miocene age, separating the Pleistocene and middle–lower Miocene successions. The older interval contains an assemblage of earliest Miocene age, between the middle Miocene and the lower–middle Oligocene. Calcareous nannofossils from the basal Pleistocene section registered a brief crisis event in the surface-water ecosystem, the "*Braarudosphaera* Event," as previously recorded at Sites 1127, 1130, and 1131.

## Pleistocene

Assemblages indicative of the combined Zones NN21–NN20 are recorded down to Sample 182-1132B-12H-CC (111.10 mbsf). Species present throughout this interval include *Calcidiscus leptoporus, Gephyrocapsa caribbeanica,* small *Gephyrocapsa* spp. (including *Gephyrocapsa aperta*), *Helicosphaera carteri,* and *Syracosphaera* spp. The LO of *Pseudoemiliania lacunosa* is in Sample 182-1132B-13H-CC (121.05 mbsf), indicating Zone NN19. In this sample, *Gephyrocapsa* spp. (small) registered their highest abundance acme.

Zone NN19 assemblages are recorded down to Sample 182-1132B-26X-CC (236.55 mbsf). Preservation is mostly moderate in the upper part of the zone, but deteriorates rapidly in its lower part. The moderately preserved assemblages from the upper part of Zone NN19, at 121.05–139.17 mbsf, contain *Calcidiscus*? *macintyrei, Dictyococcites productus, G. caribbeanica, Helicosphaera carteri, Helicosphaera*? *sellii, Rhabdosphaera clavigera,* and *Reticulofenestra minuta,* in addition to abundant small *Gephyrocapsa* spp., and few *P. lacunosa*. Preservation of the few specimens of *Helicosphaera sellii* and *Calcidiscus macintyrei* observed in these assemblages is particularly poor, suggesting that they may be reworked. The highest occurrences of these two species could not be confidently located in our shipboard study.

An abundance peak of *Braarudosphaera bigelowii* is recorded at the base of Zone NN19 in Sample 182-1132B-25X-CC (222.91 mbsf). A similar acme of this species from a similar stratigraphic level has also been recorded at other Leg 182 shallow-water sites in both the eastern and western transects (see **"Biostratigraphy,"** p. 9, in the "Site 1127" chapter, **"Biostratigraphy,"** p. 10, in the "Site 1130" chapter, and **"Biostratigraphy,"** p. 9, in the "Site 1131" chapter). This indicates that a brief dramatic change in surface-water conditions occurred over a large area of the Great Australian Bight during the early Pleistocene.

## Miocene

Poorly to moderately preserved assemblages indicating a late Miocene age are recorded from Samples 182-1132B-27X-CC and 28X-CC; both sections contain chert nodules. The rare discoasters found in these assemblages are heavily calcified, making species identification uncertain. Only tentative zonal assignment can be made, as zonal assignment in much of the upper Miocene relies on species of *Discoaster.* The younger assemblage from Sample 182-1132B-27X-CC (241.60 mbsf) is assigned to Zone NN10, on the basis of the tentative identification of *Discoaster bellus, Discoaster calcaris,* and *Discoaster variabilis;* the key species for Zones NN9 and NN11. *Discoaster hamatus, Discoaster berggrenii,* and *Discoaster quinqueramus* were not found. Other species present include *Dictyococcites antarcticus, Calcidiscus macintyrei, C. oamaruensis, Helicosphaera carteri, Helicosphaera rhomba, Reticulofenestra gelida, Reticulofenestra haqii, Reticulofenestra minutula, R. pseudoumbilicus, Sphenolithus abies, Sphenolithus neoabies, Syracosphaera* spp., and *T. rugosus*. Reworking from Paleogene sediments is indicated by the presence of *Calcidiscus oamaruensis*. The assemblage from Sample 182-1132B-28X-CC (250.73 mbsf) probably belongs to Zone NN9, on the basis of tentative identification of *D. hamatus*. In addition to the taxa, other than the species of *Discoaster,* listed above for Zone NN10, the Zone NN9 assemblage contains *B. bigelowii, Pontosphaera multipora,* and *Coccolithus pelagicus,* as well as reworked Paleogene taxa (e.g., *Dictyococcites bisectus*).

The assemblages from Samples 182-1132B-29X-CC (257.43 mbsf) and 182-1132C-3R-CC (255.87 mbsf) to 13R-CC (348.10 mbsf) are readily assignable to the middle Miocene Zone NN6. Key elements of these assemblages include *Dictyococcites antarcticus, Calcidiscus leptoporus, Calcidiscus macintyrei, Calcidiscus premacintyrei, Coccolithus miopelagicus, Helicosphaera carteri, Reticulofenestra pseudoumbilicus,* and *Triquetrorhabdulus rugosus*. The index species for the combined Zones NN5–NN4, *Sphenolithus heteromorphus,* occurs in Samples 182-1132C-14R-CC (357.60 mbsf) to 22R-CC (432.3 mbsf). *Calcidiscus premacintyrei* ranges down into combined Zones NN5–NN4, together with *Dictycoccites antarcticus, Calcidiscus leptoporus, Cyclicargolithus abisectus, Cyclicargolithus floridanus,* and *R. pseudoumbilicus*.

Sample 182-1132C-23R-CC (441.68 mbsf) contains the association of *B. bigelowii, C. abisectus, C. floridanus, Helicosphaera euphratis, Sphenolithus dissimilis,* and *Sphenolithus moriformis,* which places it in Zone NN1, of early Miocene age.

Zones NN3–NN2 are missing or condensed in the interval between Samples 182-1132B-22X-CC and 23R-CC. The underlying Sample 182-1132B-24X-CC contains an assemblage assignable to Zone NP23, of early–middle Oligocene age, indicating that Zones NP25 and NP24 are either missing or condensed in the interval between Samples 182-1132B-23X-CC and 24R-CC. Thus, the ~20-m interval (between 432.30 and 450.94 mbsf) containing the lower Miocene Zone NN1 represents a highly condensed section with possible multiple hiatuses (see Fig. **F10**).

F10. Sedimentation rate curve from datum levels for Site 1132, **p. 48.**

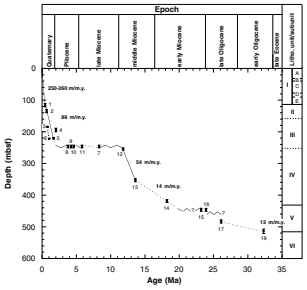


## Oligocene

Zone NP23 is based on the assemblages recorded from Samples 182-1132C-24R-CC (450.94 mbsf) to 30R-CC (507.27 mbsf). These assemblages contain *B. bigelowii, Clausicoccus fenestratus, Chiasmolithus altus, C. abisectus, C. floridanus, D. bisectus, Helicosphaera obliqua, S. moriformis,* and *Zygrhablithus bijugatus*. The key taxa for Zones NP25, NP24, and the upper part of Zone NP23, *Sphenolithus distentus* and *Sphenolithus ciperoensis,* are not present. Although this indicates that the assemblages are assignable to Zone NP23, it does not exclude the possibility of the assemblages being younger than Zone NP23. At Site 1130, *S. ciperoensis* was recorded within a short interval (see **"Biostratigraphy,"** p. 10, in the "Site 1130" chapter). The stratigraphic ranges of *S. ciperoensis* and *S. distentus* in southern Australia are unlikely to correspond to those in the tropics. Shafik (1990) concluded that the incursions of *S. distentus* and *S. ciperoensis* in southern Australia occurred as responses to brief episodes of warm-water influence, brought about by an intermittent proto-Leeuwin Current. A detailed postcruise study will be necessary to determine whether these species occur at Site 1132.

The key species for Zone NP22, *Reticulofenestra umbilicus,* is recorded from the lowest core-catcher sample obtained from Hole 1132C that contains calcareous nannofossils. The Zone NP22 assemblage in Sample 182-1132C-31R-CC (520.60 mbsf) is similar to those from Zone NP23 above, although without *H. obliqua*. It contains, in addition, *Chiasmolithus oamaruensis, Dictyococcites scrippsae,* and *Micrantholithus entaster.*

# Planktonic Foraminifers

Planktonic foraminifers indicate that sediments recovered at Site 1132 are of Pleistocene, late Pliocene, middle Miocene, Oligocene, and Eocene age. Except in the upper part of the section (<100 mbsf), plank-

tonic foraminifers are generally poorly preserved because of cementation and recrystallization. Preliminary results indicate that the Pleistocene section extends down to at least 190 mbsf and overlies a succession of probable late Pliocene age (190–240 mbsf). A condensed upper Miocene unit lies unconformably between the Pliocene–Pleistocene section and the underlying middle Miocene sediments. The condensed unit and hiatus represent >6.5 m.y. Mainly middle Miocene assemblages were recorded from the Miocene sediments between 240 and 450 mbsf, suggesting that large parts of the lower and upper Miocene are either highly condensed or missing. Further downhole, an Oligocene succession (~440–515 mbsf) overlies disconformably a limestone of middle to late Eocene age, indicating a hiatus of ~1.5 m.y. at the Oligocene/Eocene boundary (Fig. F9).

## Pleistocene

Planktonic foraminifers are relatively rare from Cores 182-1132B-1H through 7H in sediments dominated by bryozoan debris. Their abundance increases slightly downhole, to ~10% of the >63 µm residue, although preservation deteriorates. Common species include *Globorotalia truncatulinoides, Globorotalia inflata, Globigerinoides ruber, Zeaglobigerina rubescens, Globigerina bulloides, Globigerina falconensis, Globigerina quinqueloba, Neogloboquadrina pachyderma,* and *Orbulina universa*. This assemblage occurs down to ~190 mbsf (Core 182-1132B-21X), indicating the Pleistocene Zone Pt1 of Berggren et al. (1995) and SN14 of Jenkins (1993) (Fig. F5, p. 47, in the "Explanatory Notes" chapter). *Globorotalia tosaensis* is the species used by Berggren et al. (1995) to subdivide the zone, although its single occurrence in Sample 182-1132B-15H-CC, 14–17 cm (139.2 mbsf), cannot be applied here for a similar purpose. The exceedingly poor preservation makes reliable recognition of the taxon very difficult, and we suspect that we have not found its true last appearance in this section.

The *G. truncatulinoides* assemblage has been widely documented in Quaternary sediments around the Great Australian Bight as representative of the southern temperate planktonic foraminifer fauna (Almond et al., 1993; Li et al., 1996a, 1996b, in press; Wells and Okada, 1996). Rare specimens of such warm-water taxa as *G. trilobus, Globigerinoides quadrilobatus,* and *Globorotalia menardii* were found in Cores 182-1132B-8H, 9H, 14H, and 21X, although not all of them occurred together in a single sample. Their periodic appearances probably reflect warmer climatic conditions and/or stronger flows of the Leeuwin Current (McGowran et al., 1997a).

The Pleistocene/Pliocene boundary in the region has been placed at the first occurrence of *G. truncatulinoides* (Jenkins, 1993; McGowran et al., 1997b). At Site 1132, this datum level was recorded at 188.6 mbsf (Sample 182-1132B-21X-CC, 28–31 cm). However, whether the sediments across this level are conformable cannot be determined in this shipboard study.

## Upper? Pliocene

As found previously at Sites 1127, 1130, and 1131, the Pleistocene *G. truncatulinoides* assemblage was succeeded downhole by an assemblage mainly composed of *Globorotalia crassaformis, Globorotalia puncticulata,* and *Globorotalia crassula*. The "*G. crassaformis* interval" occurred at Site 1132 between 190 and 240 mbsf, in Cores 182-1132B-

22X through 26X (Fig. F9). Also present are *Globorotalia inflata, Globigerina bulloides,* and *G. ruber.* The assemblage is similar in composition to the upper Pliocene fauna of New Zealand (Hornibrook et al., 1989). Accordingly, we tentatively place this interval in the upper Pliocene.

## Miocene

Poorly preserved planktonic foraminifers indicating a Miocene age were recorded in the interval between 241 and 442 mbsf (Cores 182-1132B-27X through 29X, and 182-1132C-3R through 23R). Except for the lowermost and uppermost samples, this interval is characterized by middle Miocene planktonic foraminiferal assemblages. Sample 182-1132B-27X-CC, 34–37 cm (241.8 mbsf), contains *Zeaglobigerina woodi, Jenkinsiana mayeri,* and typical specimens of the *Globoconella miozea–Globoconella conoidea* bioseries, as well as other lower–upper Miocene species. Their association with *Globorotalia plesiotumida* and *Globoconella conomiozea* suggests the late Miocene rather than middle Miocene because these two taxa did not appear until the middle part of the late Miocene (see Table T4, p. 64, in the "Explanatory Notes" chapter). The middle Miocene from ~260 to 425 mbsf is indicated by the consistent occurrence of *Fohsella peripheroronda, Z. woodi, Globigerinoides trilobus,* and *Globoquadrina dehiscens*. On the basis of the successive occurrences of *Zeaglobigerina nepenthes, Zeaglobigerina druryi, Orbulina suturalis, Praeorbulina glomerosa,* and *Globigerinoides sicanus,* Sample 182-1132B-28X-CC, 32–35 cm, was assigned to Zone Mt8; Samples 182-1132B-29X-CC, 23–26 cm, and 182-1132C-3R-CC, 7–8 cm, to Zone Mt7; Sample 182-1132C-15R-CC, 0–2 cm, to Zone Mt6; Sample 182-1132C-20R-CC, 22–25 cm, to Subzone Mt5b; and Samples 182-1132C-21R-CC, 23–26 cm, and 22R-CC, 10–13 cm, to Subzone Mt5a (Fig. F9). A more detailed biostratigraphy for this interval was not possible because of poor recovery (see "Operations," p. 2). Further downhole, Sample 182-1132C-23R-CC, 18–21 cm (441.7 mbsf), contains few planktonic foraminifers, although the sparse assemblage does include *G. dehiscens,* a species first appearing in the early Miocene.

The Miocene planktonic foraminifer biofacies was succeeded at 450.9 mbsf (Sample 182-1132C-24R-CC, 14–17 cm) by assemblages of probable early Oligocene age. This indicates that much of the early Miocene and late Oligocene are either missing or highly condensed.

## Oligocene

Unlike those found in the Neogene, the Oligocene assemblages from Cores 182-1132C-24R through 29R are characterized by poorly preserved, small specimens. They mainly include *Globorotaloides suteri, Globorotaloides testarugosa, Tenuitella munda, Tenuitella clemenciae, Tenuitellinata juvenilis, Globigerina praebulloides, Globigerina officinalis,* and *Paragloborotalia opima nana*. Their co-occurrence with *Globigerina euapertura* (in Cores 182-1132C-24R through 27R) and *Zeaglobigerina* cf. *labiacrassata* (in Sample 182-1132C-25R-CC, 17–20 cm) suggests a middle Oligocene age (Li et al., 1992). *Subbotina angiporoides* is common in the interval from 487.9 to 497.6 mbsf (Samples 182-1132C-28R-CC, 20–21 cm, and 29R-CC, 24–26 cm). Berggren (1992) dated the LO of *S. angiporoides* at ~30 Ma, in the early Oligocene. Its presence indicates an association equivalent to the early Oligocene Zone SP13 of Jenkins (1993) or older. An early Oligocene age, however, appears to be contradicted by the absence of *Chiloguembelina cubensis,* the most conspicuous Eocene–

lower Oligocene species. *Chiloguembelina cubensis* has been widely recorded in southern middle to high latitudes, including southern Australia (Berggren, 1992; McGowran et al., 1992). It is also common in the lower Oligocene assemblage from Site 1126 (see "Biostratigraphy," p. 12, in the "Site 1126" chapter). This suggests that a more accurate dating of the Oligocene section at Site 1132 is not possible without detailed postcruise studies.

### Eocene

Sediments of lithostratigraphic Unit VI from 517 to 555.95 mbsf at Site 1132 are assigned to the Eocene (see "Lithostratigraphy," p. 3). No planktonic foraminifers were found in the washed core-catcher samples. However, several thin-section samples prepared for lithologic analysis contain middle–upper Eocene assemblages. Although extremely rare, specimens of *S. angiporoides–Subbotina linaperta* complex were detected in Sample 182-1132C-32R-1, 40–42 cm. In Sample 182-1132C-35R-CC, 45–47 cm, *A. collactea, Globigerinatheka*? *index,* and *S. linaperta,* together indicating a later middle Eocene age, occur in a matrix with numerous benthic foraminifers. This species association has been documented in Eocene sediments from Jerboa-1 in the operational area of Leg 182 (McGowran, 1991) and from the St. Vincent Basin, South Australia (McGowran, 1989, 1990; McGowran et al., 1992).

## Benthic Foraminifers

Benthic foraminifers were studied in all core-catcher samples from Holes 1132B and 1132C. However, poor core recovery below Core 27X in Hole 1132B and throughout Hole 1132C led to an extremely discontinuous faunal record in older sediments. Benthic foraminifers are relatively abundant and well preserved down to Core 182-1132B-21X, although abundance decreases significantly and preservation deteriorates markedly below Core 182-1132B-21X. Between 100 and 300 benthic foraminifers were picked from the >63-µm fraction, except in samples in which abundance was low. The benthic foraminiferal assemblages at Site 1132 include a high proportion of cosmopolitan taxa; however, they probably also contain species with a more geographically restricted distribution. Postcruise studies are needed to fully document benthic foraminiferal distribution at Site 1132 during the Pleistocene and to investigate how faunal changes relate to climate, sea-level, and/or circulation fluctuations within a sequence stratigraphic framework. The following benthic foraminiferal assemblages are recognized in the Cenozoic succession of Site 1132.

### Bryozoan Assemblage (Pleistocene)

#### *Cores 182-1132B-1H through 8H, 12H, and 15H through 17H*

This is a diversified, extremely well-preserved assemblage found in samples containing abundant and well-preserved bryozoan fragments. The assemblage includes unusually large specimens (>1 mm) of *Bigenerina nodosaria, Hoeglundina elegans, Textularia* spp., *Cibicidoides* spp., and miliolids. Also present are *Sphaeroidina bulloides, Sigmoilina obesa, Cancris auriculus, Martinottiella communis, Uvigerina hispidocostata, Bulimina marginata, Loxostomum* spp., *Loxostomoides* spp., *Sigmoilina* spp., *Tritaxia* spp., and *Anomalinoides* spp. The presence of *S. bulloides, H. elegans, B. nodosaria,* and *B. marginata* indicates upper bathyal paleodepths. Similar

benthic foraminifer assemblages were found in comparable bryozoan buildups at Sites 1129 and 1131. The assemblages probably represent a diverse, highly dynamic ecosystem that became established at the seafloor at various times during the Pleistocene, coincident with bryozoan buildup development. Changes in the composition of this assemblage may relate to different stages during growth of bryozoan buildups. Further work on the benthic and planktonic foraminiferal assemblages is likely to provide a record of sea-level, circulation, and surface productivity changes during the growth of these Pleistocene bryozoan buildups.

## Assemblage 1A (Pleistocene)

### *Cores 182-1132B-9H through 21X, except Cores 12H and 15H through 17H*

This assemblage is characterized by fluctuating abundances of *U. hispidocostata, Loxostomum* spp., *Loxostomoides* spp., *Tritaxia* spp., *Triloculina* spp., *Quinqueloculina* spp., *Spiroloculina* spp., *Elphidium* spp., and *Rosalina* spp. Also present as rare to few constituents of the assemblage are *H. elegans, S. bulloides, Cibicides refulgens, Planulina wuellerstorfi, Spiroloculina* spp., *Patellina corrugata, Spirillina* spp., *Cibicidoides* spp., *Anomalinoides* spp., *Siphonina* spp., and various nodosariids. Upper bathyal paleodepths are suggested by the presence of the depth-indicative species *H. elegans, S. bulloides,* and *U. hispidocostata.* Small, sorted specimens (63–150 µm) of *Triloculina* spp., *Spiroloculina* spp., *Elphidium* spp., *Quinqueloculina* spp., and *Patellina* spp., typical of inner to middle neritic environments, are also present in variable abundance, indicating that downslope transport periodically varied in intensity during the Pleistocene. The scale and the nature of this cyclicity remains to be determined by high-resolution postcruise studies. Remarkably high numbers of *U. hispidocostata, Tritaxia* spp., and *Loxostomum* spp. are found in the lowermost sample (Sample 182-1132B-21X-CC), above an interval in which benthic foraminiferal diversity and abundance are extremely low (Cores 182-1132B-22X through 26X). Their unusual abundance in Sample 182-1132B-21X-CC indicates an enhanced carbon flux to the seafloor after a major oceanographic change. Similar high-productivity assemblages were documented from Holocene sediments off northwest Africa (Lutze and Coulbourne, 1984) and from Cretaceous organic-rich sediments along the West African margin (Holbourn et al., 1999).

## Assemblage 1B (Late Pliocene)

### *Cores 182-1132B-22X through 26X*

This impoverished assemblage is characterized by *P. wuellerstorfi, U. hispidocostata, Bolivina* spp., *Loxostomum* spp., and *Cibicidoides* spp. Calcareous nannofossil assemblages from this interval are dominated by *B. bigelowii* (see **"Calcareous Nannofossils,"** p. 13), suggesting that a major ecological crisis affected the planktonic ecosystem during the late Pliocene. The acme of *B. bigelowii* occurs in Sample 182-1132B-25X-CC, which is virtually barren of benthic foraminifers. This suggests that the ecological crisis may have affected organisms throughout the water column.

### Assemblage 2 (Late Miocene–Middle Miocene)

*Cores 182-1132B-27X through 29X and Cores 182-1132C-3R through 22R*

This assemblage is characterized by *Cibicidoides mundulus, S. bulloides, Rectuvigerina striata, Heterolepa dutemplei, Hanzawaia ammophila, Laticarinina pauperata, Siphonina tenuicarinata, P. corrugata, Dorothia* sp., *Elphidium* spp., *Tritaxia* spp., and *Rosalina* spp. Abundance is generally low and preservation poor in the lower Miocene cores, which recovered mainly hard chert fragments. Higher abundance and improved preservation are recorded in Sample 182-1132B-27X-CC of late Miocene age, which occurs in an interval of bioclastic packstone (see **"Lithostratigraphy,"** p. 3). Upper to middle bathyal paleodepths are indicated by the presence of *S. bulloides, R. striata, L. pauperata,* and *S. tenuicarinata*. However, this interpretation is tentative as few bathymetric indicators are present in this sparse assemblage.

### Assemblage 3 (Oligocene)

*Cores 182-1132C-23R through 29R*

This assemblage is characterized by numerous, small *Trifarina* spp. and *Bolivina* spp. Also present are *P. corrugata, H. ammophila, Globocassidulina subglobosa,* and *S. tenuicarinata*. Assemblage 3 is found in a discrete lithostratigraphic unit consisting of bioclastic packstone and grainstone, lacking chert, but with abundant glauconite (see **"Lithostratigraphy,"** p. 3). Upper bathyal paleodepths are suggested by the presence of the depth-indicative species *H. ammophila, G. subglobosa,* and *S. tenuicarinata,* and by the absence of deeper water indicators.

### Assemblage 4 (Eocene)

*Cores 182-1132C-30R through 35R*

A marked lithologic change from bioclastic packstone and wackestone to lithified bioclastic packstone and wackestone with prominent firmgrounds, hardgrounds, and solution seams occurs below Core 182-1132C-30R (see **"Lithostratigraphy,"** p. 3). Disaggregated samples from this lithostratigraphic unit were barren of benthic foraminifers, except for Sample 182-1132C-31R-CC, which contained a single miliolid test. However, study of thin sections revealed the frequent occurrence of *Stilostomella* spp., *Cibicidoides* spp., *Bolivina* spp., and miliolids in the calcareous cement of the sandy limestone.

## Sedimentation Rates

Sediment accumulation rates, shown in Fig. **F10,** were calculated from preliminary biostratigraphic and paleomagnetic results for Site 1132. The biostratigraphic datum levels and relevant paleomagnetic data used to calculate sedimentation rates are listed in Table **T2.** The placement of the onset of the Brunhes Chron is made with confidence, whereas the placement of the termination of the Jaramillo is tentative (see **"Paleomagnetism,"** p. 21).

A very high sedimentation rate, between 250 and 260 m/m.y., was determined for the upper part of the Pleistocene section, and a significantly lower rate of 85–95 m/m.y. for the remainder of the Pleistocene and upper Pliocene?. Paleomagnetic data support the lower accumulation rate for the lower Pleistocene section, between 180 and 220 mbsf.

T2. Datum levels used in the graph of sedimentation rate, **p. 72.**

A condensed upper Miocene unit lies between the Pliocene–Pleistocene and middle Miocene sections. A hiatus of 4 m.y. (~1.7–5.8 Ma) is inferred above the condensed unit and a hiatus of 3.5 m.y. (8.3–11.8 Ma) is inferred beneath it. Poor core recovery, however, makes the interpretation uncertain. The middle and lower Miocene sections recorded an average sedimentation rate of 21 m/m.y. A condensed unit of lowest Miocene occurs at 440 m in a condensed unit with hiatuses inferred above and below. Poor core recovery combined with few datum levels obscures the details. Based on the absence of zones, it appears the upper hiatus lasts 5 m.y. from 18.3 to 23.2 Ma, and the lower hiatus may last 4.5 m.y. from 23.9 to 28.5? Ma, spanning the Paleogene/Miocene boundary.

# PALEOMAGNETISM

All cores from Holes 1132B and 1132C with sufficient recovery to make long-core measurements feasible were measured as half cores using the 2-G 760-R magnetometer. Measurements were made of natural remanent magnetization (NRM) and after 20-mT demagnetization. Four sections of whole cores were measured to compare with the standard archive half-core measurement. The experimental nonmagnetic shoe was used for odd-numbered cores from Hole 1132B from Cores 182-1132B-3H to 13H. The nonmagnetic shoe again had a significant effect on the coring contamination (see **"Appendix: Magnetics Experiment"**). Discrete samples were taken from both soft sediments cored using APC and from biscuits in the XCB and RCB cores for NRM and rock magnetic analysis. However, the magnetization of these samples was so weak that their NRM could not be measured; thus, their analysis must await shore-based studies.

## Long-Core Measurements

Long-core measurements revealed an extensive section of normally magnetized sediments, continuing through all of the APC cores and most of the XCB cores. In the XCB cores, the signal was weak, and measurement was confounded by the presence of mud, which had become remobilized and remagnetized in the coring process. We therefore measured large discrete biscuits from cores to improve the signal-to-noise ratio. The first indication of reversed rocks came in Core 182-1132B-21X. Subsequent analysis of large biscuits in Core 182-1132B-22X confirmed that there was indeed a change of polarity between Cores 182-1132B-20X and 22X. However, Core 182-1132B-21X was badly disturbed by coring, and only small biscuits remained. It is possible that the few reversed readings at the bottom of Core 182-1132B-21X mark the end of the normal sequence at 190 mbsf. Certainly in Section 182-1132B-22X-2 at 194 mbsf, the results are reversed (Fig. **F11**). A substantial sequence of predominantly reversed rocks occurred below the reversal, until a return to normal polarity at 230 mbsf. This polarity was maintained for the remainder of the available record from Hole 1132B.

After removal of readings from the beginning and end of cores and sections, the intensity of magnetization showed some fluctuations with a wavelength of ~15 m (Fig. **F11**). These are comparable with those seen in the cores from other sites with high sedimentation rates (e.g., at Site 1127). The intensity fluctuations at Site 1132 were obscured by noise,

F11. Magnetic intensity in Hole 1132B from 0 to 250 mbsf, **p. 49.**

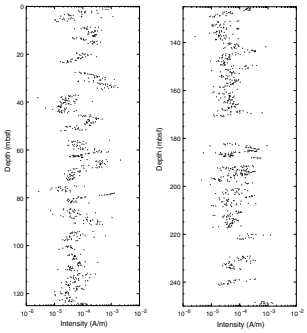

although there is a possibility of high-resolution correlation between sites with high sedimentation rates.

In Hole 1132C, poor recovery precluded long-core measurements, with the exception of Cores 182-1132C-31R to 35R. These cores included a hardground with a mineralized crust. The intensity of magnetization was anomalously high in the region of strong mineralization and remained high in red skeletal limestones below. A polarity change, associated with the hardground, extended to a depth of ~10 cm below the mineralized crust.

The comparison between whole core and archive core was performed in conjunction with the coring tests using the nonmagnetic cutting shoe and APC assembly and will be discussed in more detail in the **"Appendix: Magnetics Experiment."** However, it is noteworthy that the comparison between archive-half and whole-core measurements showed no significant difference in the core taken using the nonmagnetic shoe, whereas significant differences were observed in the core taken using the standard core-barrel assembly.

### Susceptibility

Magnetic susceptibility measured using the multisensor track (MST) yielded negative diamagnetic values near the noise level of the instrument. From ~159 to 250 mbsf, the magnetic susceptibility (MS) approaches zero, suggesting an increase in ferrimagnetic susceptibility (Fig. **F12**). At the mineralized hardground, the susceptibility is strongly positive and continues at high levels in the underlying red skeletal limestone below.

F12. Magnetic susceptibility and intensity of magnetization in Hole 1132B from 0 to 250 mbsf, **p. 50.**

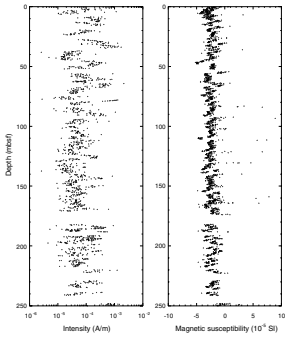


### Magnetostratigraphy

The Brunhes/Matuyama boundary is placed in Core 182-1132B-21X because of individual XCB biscuits, which recorded normal polarity in Core 182-1132B-20X and reversed polarity in Core 182-1132B-22X (Fig. **F13**). The occurrence of the Brunhes/Matuyama boundary at ~180 m gives a sedimentation rate of ~230 m/m.y. for the Brunhes. The return to normal polarity at 230 mbsf is possibly the Jaramillo termination. If the sedimentation rate calculated from the Brunhes/Matuyama boundary extends below the boundary, the 200,000 yr of the Matuyama above the Jaramillo should be represented by between 40 and 50 m of section. The observed section depth is ~40 m; thus, we interpret the polarity change as the top of the Jaramillo and suggest that the sedimentation rate of ~230 m/m.y. does indeed continue to the Jaramillo (Fig. **F13**). A second possibility, which is more consistent with biostratigraphic data (see **"Biostratigraphy,"** p. 13), places the Jaramillo between 186 and 193 mbsf and the termination of the Olduvai between 222 and 229 mbsf.

F13. Magnetic inclination and magnetostratigraphy, **p. 51.**

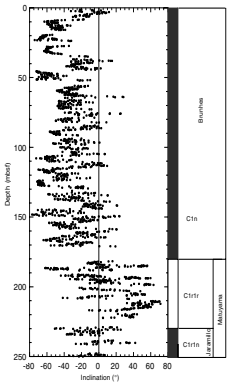


## ORGANIC GEOCHEMISTRY

At Site 1132, in addition to routine monitoring of hydrocarbon gases for safety, analyses were conducted for inorganic carbon, total carbon, nitrogen, and sulfur. The analytical procedures are described in **"Organic Geochemistry,"** p. 16, in the "Explanatory Notes" chapter.

### Volatile Hydrocarbons and Hydrogen Sulfide

At Site 1132, concentrations of volatile hydrocarbons and hydrogen sulfide ($H_2S$) were routinely determined in samples from Holes 1132B and 1132C using the standard Ocean Drilling Program headspace sampling procedure. As at Sites 1126, 1128, and 1130, only low concentrations of methane ($C_1$) are present at Site 1132 (Table T3). Of the four sites, Site 1132 has the highest $C_1$ content, with a maximum value of 54 ppm. Ethane ($C_2$), at concentrations <5 ppm, was present between 53.8 and 249.4 mbsf. No heavier hydrocarbon gases ($C_{3+}$) were detected. Unlike the other low-$C_1$ sites, $H_2S$, at low concentrations, was present at Site 1132 from 68.3 to 125.3 mbsf.

### Inorganic and Organic Carbon, Sulfur, and Nitrogen

Calcium carbonate ranges from 85 to 95 wt% in Hole 1132B. Values are at the high end of the range near the sediment surface and decline gradually toward the lower end of the range with increasing depth (Table T4; Fig. F14A).

Organic carbon ($C_{org}$) ranges primarily from 0.2 to 0.6 wt% in Hole 1132B, with a few samples having higher or lower values (Table T4; Fig. F14). Values of $C_{org}$ are scattered within this concentration range throughout Hole 1132B samples and exhibit no trend with depth (Fig. F14B).

Nitrogen concentrations are all <0.1 wt%. Sulfur is present in only eight samples, all from the upper 90 mbsf, at low concentrations (Table T4).

## INORGANIC GEOCHEMISTRY

### Interstitial Waters

Interstitial water samples from Hole 1132B were taken at a rate of one per core for the first 15 cores and one every other core thereafter, recovery permitting. As a result of poor recovery, only three samples were taken from Hole 1132C (Cores 182-1132C-14R, 15R, and 31R). No samples were taken from Hole 1132A. Samples were analyzed according to the procedures outlined in "Inorganic Geochemistry," p. 18, in the "Explanatory Notes" chapter. The data are presented in Table T5 and in Figures F15, F16, F17, F18, and F19.

#### Salinity and Chlorinity

Salinity values increase below the fourth core (30.3 mbsf), reaching 71 in Core 182-1132B-23X (205.1 mbsf) and slowly increasing to a maximum of 80 at 518.1 mbsf (Fig. F15). Chlorinity mirrors this pattern and increases from values near normal seawater to 1275 mM in Core 182-1132C-34R (Fig. F15). The increase in $Cl^-$ and salinity suggests the presence of a high-salinity fluid within and below the cored interval.

#### Calcium, Magnesium, Potassium, Lithium, Silica, Strontium, and Iron

The concentration of $Ca^{2+}$ decreases from 11.9 to 8.0 mM at 68.2 mbsf (see Fig. F15), followed by a rapid increase to 39.6 mM at 239.9

T3. Headspace gas compositions, Holes 1132B and 1132C, p. 73.

T4. $CaCO_3$, $C_{org}$, N, and S data, Hole 1132B, p. 74.

F14. $CaCO_3$ and $C_{org}$ contents in samples from Hole 1132B, p. 52.

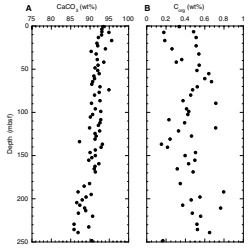

T5. Interstitial water geochemistry, p. 76.

F15. Concentration depth profiles, p. 53.

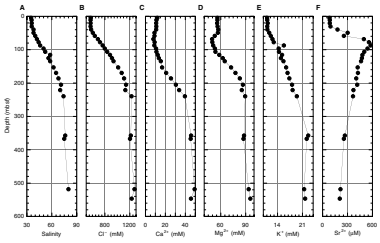

F16. Concentration depth profiles, p. 54.

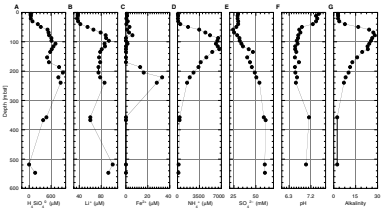

F17. Concentration depth profiles, p. 55.

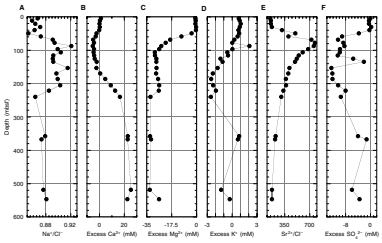

mbsf. We infer that the decrease is caused by precipitation, and the increase by dissolution of carbonate minerals. The $Mg^{2+}$ concentration remains almost constant at values near that of normal seawater for the upper 49.2 mbsf. Below 49.2 mbsf, the $Mg^{2+}$ concentration decreases from 52.8 to 49.8 mM at 77.7 mbsf, probably as a result of the precipitation of dolomite (Figs. F15, F17). As is the case with $Mg^{2+}$, the concentration of $K^+$ remains almost constant at values near that of normal seawater for the upper 49.2 mbsf. Below 49.2 mbsf, the $K^+$ concentration increases to 357.6 mbsf, where it reaches a maximum value of 22.6 mM. The excess $K^+$ concentration shows that ~2.5 mM of $K^+$ is lost from the pore waters (Fig. F17), probably caused by ion-exchange reactions with clay minerals. The $Sr^{2+}$ concentration increases slightly from 83 µM in the upper four cores to 95 µM at 30.3 mbsf. Thereafter, it increases sharply to a maximum concentration of 578 µM at 87.2 mbsf, indicating the onset of carbonate recrystallization (Fig. F15). Note, however, that the high sulfate concentration results in saturation of the pore waters with respect to celestite, thus limiting the maximum $Sr^{2+}$ concentration to values similar to those observed at Site 1130. The concentration of $Li^+$ remains almost constant at ~37 µM in the upper 30 mbsf. Below this depth are two maxima, 94 µM (106.2 mbsf) and 86 µM (239.9 mbsf), separated by a zone of slightly lower $Li^+$ concentrations (76 mM; Fig. F16). This complex pattern reflects (1) the $Li^+$ supply from the brine and (2) the release of $Li^+$ from clay minerals by ion-exchange reactions in the presence of $NH_4^+$ (Shipboard Scientific Party, 1996). The concentration of $H_2SiO_4^0$ remains constant at 48 µM during the first three cores and increases rapidly to 712 µM at 106.2 mbsf. This first maximum is followed by a decrease to 493 µM (153.2 mbsf) and a second maximum of 926 µM at 205.1 mbsf. Below that depth, concentrations of $H_2SiO_4^0$ decline to 166 µM at 546.9 mbsf (Fig. F16). As a result of the dependence of $H_2SiO_4^0$ availability on soluble phases like opal-A, we assume that this pattern reflects the opal-A content of the sediment. In the upper part of Hole 1132B, $Fe^{2+}$ concentrations are very low and generally remain below the detection limit. Below 169.7 mbsf, $Fe^{2+}$ concentration increases sharply to values as high as 32.1 µM (220.9 mbsf), falling again to levels below the detection limit by 357.6 mbsf (Fig. F16).

## Sulfate, Alkalinity, Ammonium, and pH

The concentration of $SO_4^{2-}$ remains near that of normal seawater for the upper 40 mbsf, declining to 24.0 mM at 58.8 mbsf, indicating the onset of sulfate reduction. Below 58.7 mbsf, the concentration of $SO_4^{2-}$ increases slowly to 54.2 mM at 239.9 mbsf. However, calculation of the excess $SO_4^{2-}$ shows that the zone of depleted $SO_4^{2-}$ concentration extends to 357.6 mbsf. Below that depth, $SO_4^{2-}$ concentration attains a stable plateau of 60 mM (±1 mM) until the base of the cored interval (Fig. F16). With increasing sulfate reduction, alkalinity rises to a maximum of 28.01 mM at 77.7 mbsf and subsequently decreases to 2.37 at 516.7 mbsf (Fig. F16). Ammonium, as a by-product of organic matter decomposition in the sulfate reduction zone, approximately follows the alkalinity distribution, although the maximum concentration is shifted downhole (6654 µM at 125.2 mbsf; Fig. F16). The pH declines slowly from 7.52 at 4.5 mbsf to 7.28 at 39.8 mbsf, and then decreases more rapidly to 6.83 at 49.2 mbsf. Below that depth, pH attains values as low

as 6.54 at 186.2 mbsf, increasing thereafter to 7.12 at 357.6 mbsf (Fig. F16).

## Discussion

Although the increase in alkalinity and reduction of $SO_4^{2-}$ are lower compared to Site 1130, the depletion of $Mg^{2+}$ is greater at Site 1132. The greater depletion in $Mg^{2+}$ may be a result of increased amounts of dolomite formation at Site 1132 compared to Site 1130, although it would intuitively seem that higher amounts of carbonate recrystallization should occur at Site 1130 because of the higher alkalinity values.

Unlike Site 1130, Site 1132 shows no exceptionally high salinity/depth gradient. A possible explanation for this is evident if salinity is related to absolute depth with respect to the sea surface (Fig. F18). The salinity values of Sites 1130 and 1132 reach a stable plateau of 82 and 80, respectively, at the same depth below the sea surface, which suggests that a brine with similar salinity is located ~520 m below the sea surface at both sites. Therefore, the difference in the salinity depth/gradient between the two sites can be explained simply by the different distances between the seafloor and brine surface (Fig. F18).

A striking feature of Site 1132 is the absence of vertical gradients in the concentrations of both conservative and nonconservative constituents in the upper 30.3 mbsf. A similar phenomenon was noted during Leg 166 on the western margin of Great Bahama Bank and was attributed to the active flushing of seawater. Possible causes for this phenomenon include thermally induced seawater intake (Eberli, Swart, Malone et al., 1997) or rapid sedimentation.

## X-Ray Mineralogy

As is the case with Site 1130, the mineralogy of Site 1132 is characterized by high-frequency alternations between low-Mg calcite (LMC) and high-Mg calcite (HMC). In contrast to Site 1130, Site 1132 shows a higher degree of variability of the minor constituents aragonite and dolomite. Because of the accelerated recrystallization rates (compared to Site 1130; see "Discussion," immediately above), the complete replacement of HMC with LMC and/or dolomite occurs at a much shallower depth than at Site 1130 (Table T6, also in ASCII format). However, isolated peaks of as much as 60 wt% HMC can be observed down to a depth of 155.4 mbsf (Fig. F19). Although the amount of aragonite decreases with depth, concentrations never decrease to zero, as was the case for Site 1130.

# PHYSICAL PROPERTIES

## Introduction

Measurements of physical properties at Site 1132 followed the procedures outlined in "Physical Properties," p. 19, in the "Explanatory Notes" chapter. These included nondestructive measurements of *P*-wave velocity (every 4 cm; Table T7, also in ASCII format), gamma-ray attenuation (GRA) bulk density (every 4 cm; Table T8, also in ASCII format), MS (every 8 cm; Table T9, also in ASCII format), and natural gamma radiation (NGR) (every 16 cm; Table T10, also in ASCII format) using the MST. The *P*-wave logger (PWL) was activated only on APC

F18. Salinity vs. absolute depth, p. 56.

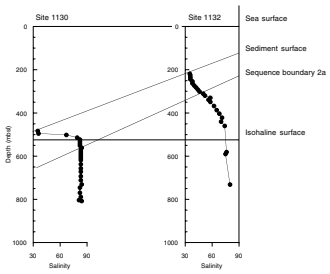


T6. Mineralogical composition data, p. 77.

F19. Variations in mineral concentrations, p. 57.

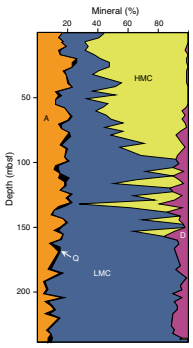


T7. Discrete *P*-wave velocity measurements, p. 78.

T8. GRA-densiometry measurements, p. 79.

T9. Magnetic susceptibility measurements, p. 80.

T10. Natural gamma-ray measurements, p. 81.

cores. Thermal conductivity was measured in unconsolidated sediment at a frequency of one determination per core (Table T11, also in ASCII format), with two additional samples analyzed after deployments of the DVTP and Adara temperature tools. Four in situ measurements of formation temperature were made (Table T12, also in ASCII format). A minimum of two discrete *P*-wave velocity measurements per section were made on the working half of split cores (Table T7), and measurement frequency was increased to five per section after the PWL was turned off. Standard index properties (Table T13, also in ASCII format) and undrained shear strength (only in unconsolidated sediments) (Table T14, also in ASCII format) were measured at a frequency of one per section. Magnetic susceptibility data are discussed in "Paleomagnetism," p. 21.

The following sections describe the quality of the data obtained, downhole variations in sediment physical properties, and their relationships to lithology and downhole logging data (see "Lithostratigraphy," p. 3, and "Downhole Measurements," p. 29).

T11. Thermal conductivity measurements, p. 82.

T12. In situ temperature measurements, p. 83.

T13. Index properties measurements, p. 84.

T14. Undrained shear strength measurements, p. 85.

## Data Quality

Multisensor track data also include measurements of coarse-grained sediment that cascaded into the hole between coring and was generally present in the first section of Cores 182-1132B-1H to 15H at depths shallower than 139 mbsf. For some cores, this sediment fill occupied more than the first section. Affected data were omitted from figures in this report but are included in the data tables (Tables T8, T9, T10, T15, also in ASCII format). High-quality NGR and GRA bulk density data were obtained using the MST, although problems occurred with *P*-wave velocity and MS measurements (see "Paleomagnetism," p. 21). The former was affected by voids between core and liner as a result of the presence of $H_2S$ in the sediments. Difficulties also occurred with the pycnometer used for determination of dry volume for index properties measurements (see "Index Properties," p. 21, in the "Explanatory Notes" chapter).

T15. *P*-wave velocity measurements from the MST, p. 86.

## Index Properties, *P*-wave Velocity, Natural Gamma Radiation, and GRA Densiometry

A close correlation was seen between downhole logging data (see "Downhole Measurements," p. 29) and sediment physical properties measurements. Gamma-ray attenuation bulk densities have similar values to the downhole logging data in the interval 100 to 150 mbsf and exhibit similar patterns. For instance, cyclicity in bulk density in the interval 140–150 mbsf is also seen in both records (Fig. F20) (see "Downhole Measurements," p. 29).

Physical properties data can be separated into five units on the basis of trends in the measured parameters. Physical properties Unit (PP Unit) 1 (0–5 mbsf) is characterized by a high bulk density near the sediment/water interface (>2.0 g/cm³), which decreases rapidly with depth (Fig. F20). Natural gamma radiation increases from 3 to 10 cps. *P*-wave velocity remains unchanged and porosity increases (41%–58%) within this unit (Fig. F20). Physical properties Unit 1 corresponds to a thin package of grainstones that caps lithostratigraphic Unit I (see "Lithostratigraphy," p. 3).

F20. *P*-wave velocity, bulk density, porosity, NGR, and magnetic susceptibility for Site 1132, p. 58.

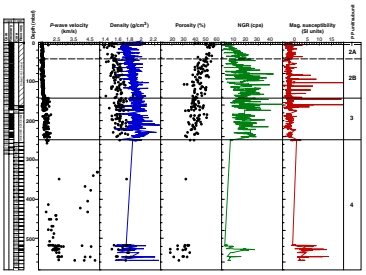

Physical properties Unit 2 (5–142 mbsf) exhibits an overall increase in bulk density with depth (1.7–1.95 g/cm$^3$), with a corresponding but more gradual increase in *P*-wave velocity (~1.6–1.7 km/s) and a decrease in porosity (~58%–41%) (Fig. F20), although there is considerable variation in porosity associated with differences in lithology. Average NGR values generally increase within this unit from ~5 to ~20 cps, with high-frequency cycles superimposed on this trend. PP Unit 2 may be divided into two subunits separated by an apparent firmground at 42 mbsf (Fig. F20).

Physical properties Subunit 2A (5–42 mbsf) exhibits increasing NGR (5–22 cps) and GRA bulk density (1.75–1.8 g/cm$^3$) with depth. A decrease in NGR at 33 mbsf corresponds to a packstone at the boundary between lithostratigraphic Subunits IA and IB (see "Lithostratigraphy," p. 3). *P*-wave velocity and porosity remain nearly constant within PP Subunit 2A (Fig. F20). The base of PP Subunit 2A is marked by an abrupt decrease in NGR (20–10 cps) and an increase in *P*-wave velocity (1.6–1.7 km/s; Fig. F20).

Physical properties Subunit 2B (42–142 mbsf) is characterized by cyclic and generally increasing NGR, bulk density (1.8–1.95 g/cm$^3$), and *P*-wave velocity (1.6–1.7 km/s), and decreasing porosity (50%–38%; Fig. F20). The amplitude of the high-frequency NGR cyclicity is greater in this unit relative to PP Subunit 2A. A low in NGR values within Subunit 2B corresponds to the disappearance of HMC from the sediments (see "Inorganic Geochemistry," p. 23).

Physical properties Unit 3 (142–248 mbsf) is characterized by highly variable *P*-wave velocity and bulk density data superimposed on an increasing trend (Fig. F20). Natural gamma radiation data within PP Unit 3 show a distinct cyclicity on a slightly increasing trend (Fig. F20) that corresponds well to an interval of high NGR variability in the downhole logs (see "Downhole Measurements," p. 29). Porosity decreases throughout PP Unit 3 (43%–38%). Within this unit, peaks in GRA bulk density are generally correlated to more lithified sections recognized in the split-core sections (see "Lithostratigraphy," p. 3). Below 150 mbsf, GRA density is lower than in situ measurements because of incomplete filling of core liners during XCB and RCB coring. The base of PP Unit 3 correlates well to the base of logging Unit 1 (see "Downhole Measurements," p. 29), lithostratigraphic Unit III (see "Lithostratigraphy," p. 3), and the upper/middle Miocene boundary (see "Biostratigraphy," p. 13).

Core recovery within PP Unit 4 (248–603 mbsf) was poor because of numerous chert layers in the sedimentary section alternating with softer carbonate sediment (Fig. F20; see "Lithostratigraphy," p. 3). Recovered cherts had high *P*-wave velocities alternating with lower velocities characteristic of the less indurated sediments. All measured parameters show high variability near the base of PP Unit 4 (Fig. F20).

## Shear Strength

Shear strength at Site 1132 was measured from 1 to 168 mbsf, and values ranged between 2 and 48 kPa (Fig. F21). Although shear strength exhibits an increasing trend with greater depth, the data are highly variable because of differences in lithification and grain size within the upper portion of the recovered sedimentary section (see "Lithostratigraphy," p. 3). However, in some intervals, variability may result from drilling disturbance and cracking of the sediment before failure, resulting in lower values for peak strength. Peaks in shear strength near the

F21. Shear strength data, p. 59.

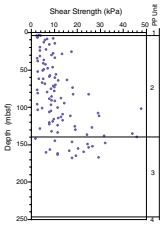

base of PP Unit 2 (Fig. F21) correlate to partially lithified intervals within lithostratigraphic Unit 2 (see "Lithostratigraphy," p. 3).

## Thermal Conductivity

At Site 1132, thermal conductivity was measured between 10 and 250 mbsf (Fig. F22). Values increase from 0.82 W/(m·K) near the top of the hole to 1.24 W/(m·K) within PP Unit 3 (195 mbsf). Below 195 mbsf, thermal conductivity values are highly variable, corresponding to an interval of increasing sediment lithification (see "Lithostratigraphy," p. 3); thus, some values may be invalid as a result of poor contact between sediments and the measurement probe. Overall, thermal conductivity data are significantly controlled by sediment bulk density as demonstrated by the close relationship between the two data sets (Fig. F22).

F22. Thermal conductivity and bulk density data, p. 60.

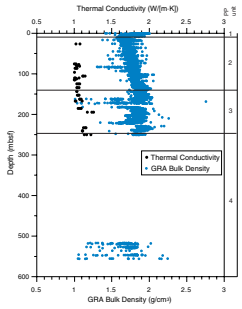


## In Situ Temperature Measurements

Four in situ temperature measurements were made at Site 1132, three using the Adara tool and one using the DVTP. There was some variation in estimates of mudline temperature from 14.5°C to 15.4°C. An additional estimate of seafloor temperature (12.6°C) was obtained using an expendable bathythermograph (XBT). This value was lower than those obtained from the in situ temperature tools, possibly because of calibration differences. None of the in situ temperature measurements was affected by postemplacement movement of the probe, and differences between lower and upper data fits to the decay curve yielded only minor differences in temperature (Table T12).

The three deepest in situ temperature measurements define a linear relationship with depth ($r^2 = 0.99$; $N = 4$) that passes close to the average of all mudline values (14.9°C ± 0.4°C; Fig. F23) but not to the XBT-derived seafloor temperature. If the XBT seafloor temperature is used, it is difficult to explain the magnitude of the geothermal gradient nonlinearity, given the very small change of thermal conductivity with depth at Site 1132. Thus, the XBT temperature was not used (Fig. F23).

F23. Variation of formation temperature with depth below seafloor, p. 61.

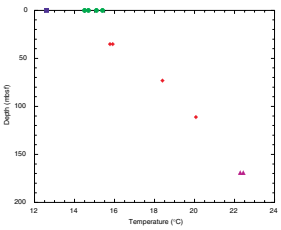


The geothermal gradient derived using Adara mudline temperatures is 41.6°C/km. The defined linear trend does not pass through the first Adara measurement at 35.5 mbsf, where the formation is similar in temperature to the highest estimates of seafloor temperature. This pattern strongly suggests that there is some circulation of seawater within the relatively coarse facies occurring in this interval. This conclusion is consistent with the presence of pore fluids of near-seawater salinity from 0 to 35 mbsf (see "Inorganic Geochemistry," p. 23). The geometric mean of thermal conductivity between 0 and 169 mbsf was used to determine heat flow at the site (0.99–0.074 W/[m·K]). Using this value and the geothermal gradient determined above, heat flow at the site is estimated to be 42–44.7 mW/m². This value is identical to that determined at Site 1131, which has similar low thermal-conductivity sediments and is in a similar position, although somewhat deeper on the shelf margin.

# DOWNHOLE MEASUREMENTS

## Logging Operations

Hole 1132C was prepared for logging after drilling was halted as a result of deteriorating hole conditions (see "Operations," p. 2). The lower limit of the BHA was placed at 105 mbsf for both logging runs (Fig. F24). Two logging tool strings were run in the following order: (1) triple combo and (2) FMS/sonic (see "Downhole Measurements," p. 25, in the "Explanatory Notes" chapter). The triple combo run touched bottom at 561 mbsf. Extensive hole deterioration between triple combo and FMS/sonic runs resulted in only 70 m (140–176 mbsf) of the FMS/sonic tool string being logged after three attempts (Fig. F24). The well seismic tool (WST) and the geologic high-resolution magnetic tool were not run.

F24. Logging runs at Hole 1132C, p. 62.

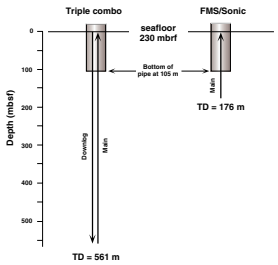


## Data Quality

While we pulled pipe in preparation for logging, weighted mud was added to the borehole to reduce backflow of fluids out of the hole. Barite contained in this mud adversely affected the photoelectric effect values and, as a result, they were unusable. The borehole diameter was generally smooth during the triple combo run except for enlargements (as much as 38 cm) between 145 and 240 mbsf and between 440 and 510 mbsf (Figs. F25, F26). Despite the larger borehole, the diameter is below the saturation limits of the caliper (42 cm) for the entire interval logged. Of the 36 m of FMS collected, the lower 16 m (160–176 mbsf) was of little use because of the severely rugose and sometimes undergauge hole. The remainder of the record was of good quality.

F25. Geophysical logs from the triple combo, plotted vs. depth in the open-hole logged interval, p. 63.

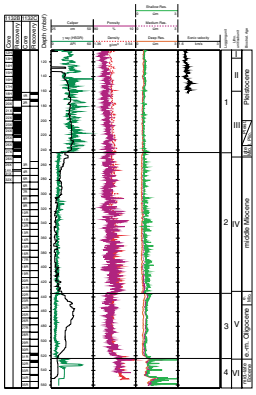

## Preliminary Observations

Downhole logs at Site 1132 were well correlated to lithologic variations observed in the upper 245 mbsf of the section. Below this depth, where recovery was low (~6%), logs will enable the characterization of sedimentary sequences and assist in intersite correlation to provide a detailed record of Eocene to Holocene shelf edge temperate-water carbonate deposition.

The compatibility of wireline log data with physical properties measurements from both whole-core and discrete samples attests to the integrity of the logging data sets (see "Physical Properties," p. 25). Overall, downhole measurement trends show the effects of compaction overprinted by the influence of diagenesis and changes in sediment composition. Compaction causes a gradual increase in sonic velocity and bulk density, and a decrease in porosity with depth (Figs. F25, F26). Downhole variations, resulting from changes in lithology and diagenetic alteration, enable logging data from Site 1132 to be divided into four units (Figs. F25, F26, F27).

Logging Unit 1 (0–242 mbsf) is characterized by high and variable gamma-ray values, mainly resulting from increased uranium concentrations (Fig. F26). Within the interval logged in pipe (0–104 mbsf; Fig. F27), gamma-ray values show distinct variability and are moderately correlated to NGR values from the MST (see "Physical Properties," p. 25). A prominent gamma-ray peak in the downhole logs is seen between 88 and 92 mbsf (Fig. F27). This peak is likely to be spurious, as the gamma-ray values are greater than expected for these high-carbon-

F26. Spectral gamma-ray logs, plotted vs. depth for the open-hole logged interval, p. 64.

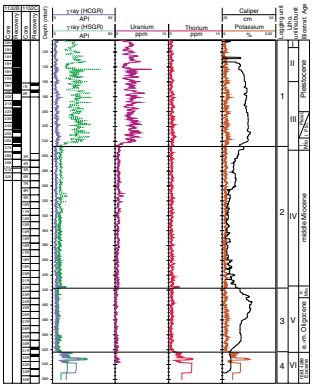

ate sediments when logged through pipe. In addition, no equivalent peak is seen in the NGR data. High and variable uranium values continue for the remainder of the unit, until an abrupt decrease at the boundary with logging Unit 2 (242 mbsf). This decrease in gamma ray may result from diagenesis, as it corresponds to the depth at which HMC becomes a minor component of the sediments (see **"Inorganic Geochemistry,"** p. 23). In the open-hole logged interval of Unit 1, separation of the porosity and density curves indicate a slightly greater density than expected for a clean limestone.

This is likely to result from higher magnesium concentrations occurring within the carbonates of this unit. Downhole resistivity within Unit 1 is nearly constant with a slight separation of shallow and deep values indicating some fluid invasion in the unit (Fig. **F25**). The base of logging Unit 1 correlates well to the base of the upper Miocene (see **"Biostratigraphy,"** p. 13) and the base of lithostratigraphic Subunit III (see **"Lithostratigraphy,"** p. 3), which marks the lower limit of a lithologically variable sediment sequence.

Logging Unit 2 (242–437 mbsf) is characterized by low gamma-ray values (Fig. **F26**). Both density and porosity exhibit greater variability than in Unit 1 and an overall downhole increasing trend that steepens near 402 mbsf to a maximum at 432 mbsf, after which values decrease to the base of the unit (Fig. **F25**). The increased variability in porosity and density correlates well to a sedimentary interval characterized by alternations of chert and bioclastic grainstone (see **"Lithostratigraphy,"** p. 3). Resistivity logs from Unit 2 indicate that significant borehole fluid invasion is occurring within this interval, as shown by the separation of shallow- and deep-resistivity traces (Fig. **F25**). This invasion is likely to be occurring along discrete, relatively thin beds, giving rise to the short wavelength (<1 m) fluctuations in the shallow-resistivity data (Fig. **F25**). The base of logging Unit 2 correlates well to the base of lithostratigraphic Unit IV, which marks the downhole disappearance of chert in the sedimentary section (see **"Lithostratigraphy,"** p. 3). This boundary is characterized by increases in resistivity and decreases in gamma radiation, porosity, and density (Figs. **F25, F26**).

Logging Unit 3 (437–524 mbsf) is characterized by nearly constant values in all data sets except porosity. The sediments within logging Unit 3 correspond to lithostratigraphic Unit V, which is dominated by apparently homogeneous bioclastic grainstones (on the basis of limited recovery; see **"Lithostratigraphy,"** p. 3). The separation of deep- and shallow-resistivity curves indicate that fluid invasion is occurring within Unit 3, although this invasion is more uniform than in the units above and below as expected from the more porous and homogeneous sediments occurring within this unit (Fig. **F25**). The base of logging Unit 3 is marked by an increase in gamma-ray values, density, and resistivity, and a decrease in porosity (Figs. **F25, F26**). This boundary is well correlated to the Oligocene/Eocene boundary (see **"Biostratigraphy,"** p. 13).

Logging Unit 4 (524–537 mbsf) is characterized by increased variability in both gamma-ray and resistivity within the limited section logged (Figs. **F25, F26**). Resistivity measurements indicate deep invasion of borehole fluids along discrete intervals (Fig. **F25**). Increased gamma-ray values in Unit 4 largely result from greater Th and K (Fig. **F27**), indicating the presence of terrigenous minerals within the dominantly carbonate sediments in this unit (~85% $CaCO_3$; see **"Organic Geochemistry,"** p. 22). Density values are high and porosity values are low throughout this unit (Fig. **F25**). Logging Unit 4 correlates well to an interval of

F27. Spectral gamma-ray logs, plotted vs. depth for the interval logged through pipe, **p. 65.**

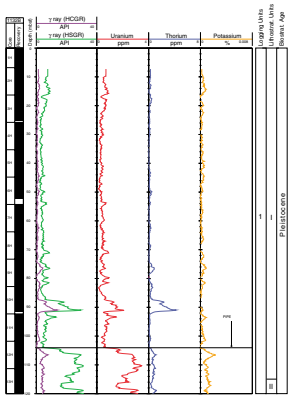

Eocene sediments within lithostratigraphic Unit VI (see "Lithostratigraphy," p. 3).

# SEISMIC STRATIGRAPHY

## Introduction

Site 1132 (Fig. F28) was predicted to intersect Cenozoic seismic Sequences 2, 3, 4, 6A, 6B, and 7 (sequences defined in Feary and James, 1998, reprinted as Chap. 2). However, as was the case with Site 1130, hole instability within Sequence 7 sandstones severely restricted penetration and caused coring to be terminated. The high-resolution site-survey seismic data (Fig. F29), together with the regional seismic database, indicated that significant hiatuses should occur at all sequence boundaries.

## Time–Depth Conversion

A check-shot survey was not planned at this site because there was an expectation that the time–depth conversion parameters derived from Site 1130 (only ~11.5 km to the south and intersecting a broadly similar succession) would be applicable at Site 1132. However, hole restriction or collapse (see "Operations," p. 2) encountered during deployment of the FMS/sonic tool string would have prevented a check-shot survey in any case. Because the FMS/sonic tool string was only run over a short interval, it was not even possible to derive a useful integrated sonic curve as a guide to time–depth conversion. Accordingly, the time–depth relationship for sequence boundaries and horizons located on seismic data was estimated to correspond, as was the case at Site 1130, to a line tracking immediately below the envelope defined by the six stacking velocity curves for the immediate vicinity of Site 1132 (Fig. F30A). On this basis, estimates of depth errors of as great as 15 m between predicted and corrected depths to boundaries can be determined (Table T16), although these values must be viewed as only very approximate estimates.

## Seismic Sequence Characteristics

The data collected at Site 1132, particularly lithostratigraphic and biostratigraphic information, provide an opportunity to interpret the site data within a more regional context and also allow a description of the characteristics of seismic sequences intersected at this site (see "Lithostratigraphy," p. 3, and "Biostratigraphy," p. 13). The final best-fit correlation of lithostratigraphic and biostratigraphic data with seismic stratigraphy (Fig. F31) was based both on the regional moderate-resolution multichannel seismic data collected by the Japan National Oil Corporation (JNOC) in 1990 (Feary and James, 1998, reprinted as Chap. 2) and on the high-resolution site-survey seismic data collected by the Australian Geological Survey Organisation (AGSO) in 1996 (Feary, 1997). This correlation shows that the predicted seismic stratigraphy (Fig. F29) is considerably different from the sequences actually intersected at Site 1132, and at present only some of this variance can be explained. Detailed postcruise work will be necessary to clarify and explain the difference between the sequences encountered at nearby Site 1130 and the stratigraphy at this site.

F28. Seismic site-survey tracks for Site 1132 in relation to other Leg 182 sites and the AGSO169 site-survey seismic lines, p. 66.

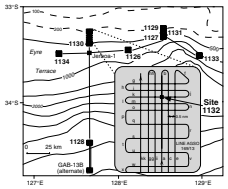


F29. Portion of seismic Line AGSO169/13a showing seismic stratigraphic sequences, p. 67.

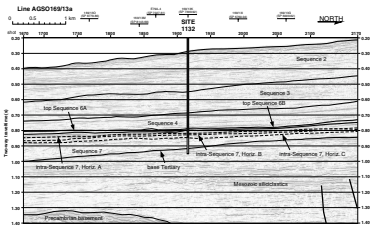


F30. Predicted and corrected depths and interval velocities, p. 68.

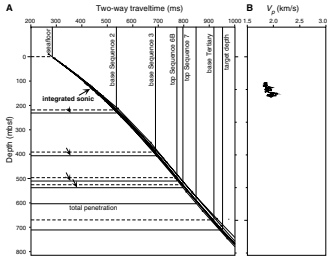


T16. Differences between depths to key horizons and corrected depths, p. 87.

F31. Lithostratigraphic units, seismic sequences, biostratigraphic hiatuses, and ages, p. 69.

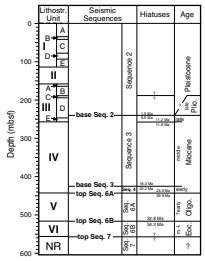

## Sequence 2

Comparison of the high-resolution site-survey seismic data at Site 1132 with regional seismic data indicates that the Sequence 2 interval intersected at Site 1132 should represent a quite different facies succession compared to the adjacent Site 1130. Seismic data shows that the component of Sequence 2 intersected at Site 1132 should contain a hiatus surface toward the base, corresponding to the possible top Pliocene boundary at 188 mbsf. Apart from this surface, Sequence 2 appears essentially complete. The uppermost part of Sequence 2 displays a dramatic mounded appearance, corresponding to the bryozoan mounds of lithostratigraphic Unit I (see **"Lithostratigraphy,"** p. 3). This unit consists of bryozoan floatstone and rudstone alternating with bryozoan packstone and contains an abundant and diverse bryozoan fauna. The portion of Sequence 2 underlying the mounded zone and overlying the hiatus surface contains much more evenly stratified and continuous reflections, corresponding to the bioclastic packstones with variable bryozoan component of lithostratigraphic Unit II and Subunits IIIA and IIIB. Several firmgrounds are present in this interval, and the hiatus surface visible on seismic data correlates to a firmground at the top Subunit IIIC boundary at 188 mbsf. The lowermost component of Sequence 2, beneath the hiatus surface, corresponds to lithostratigraphic Subunit IIIC and most of Subunit IIID. Sediments in this upper? Pliocene or basal? Pleistocene interval (see **"Biostratigraphy,"** p. 13) consist of bioclastic packstone with bioclastic wackestone interbeds. Bryozoan bioclasts are not as abundant within this interval as they are in the overlying part of Sequence 2. The base of Sequence 2 (at 240 mbsf) corresponds to a dramatic decrease in gamma-ray values observed on the downhole logs (see **"Downhole Measurements,"** p. 29). This surface also represents a hiatus of some 6.5 m.y. (Fig. **F31**).

## Sequence 3

Sequence 3 provides the greatest difficulty in correlating between Sites 1132 and 1130. Seismic data from the upper Miocene succession comprising Sequence 3 at Site 1130 appear to correlate to seismic data from the basal part of Sequence 3 at Site 1132. However, biostratigraphic information (see **"Biostratigraphy,"** p. 13) indicates that Sequence 3 is represented at Site 1132 by a thin interval (17 m) of upper Miocene sediment overlying a substantial thickness of middle Miocene sediment (168 m), indicating that a previously unrecognized major disconformity/erosional surface presumably exists between these two sites. Identification of the exact nature and location of this surface will require postcruise work. The thin upper Miocene component of Sequence 3 consists of foraminiferal ooze and chalk, in contrast to the overlying packstone-dominated lithologies of Sequence 2. The thick middle Miocene interval consists of very poorly recovered, variably silicified, and partially dolomitized bioclastic grainstone, with the silicification distinguishing this unit from underlying and overlying units.

## Sequence 4

Poor recovery of both the overlying middle Miocene Sequence 3 interval and the lower Miocene Sequence 4 interval resulted in a lack of lithostratigraphic expression of the ~5-m.y. hiatus at the base of Sequence 3 (indicated by biostratigraphic data). Regional correlation indi-

cates that the thin interval (~16 m) of lower Miocene sediment at Site 1132 should be assigned to seismic Sequence 4. It appears that this occurrence of Sequence 4 may represent the feather edge of a thinning-seaward sequence present beneath the modern outer shelf. Lithostratigraphic data indicate that Sequence 4 consists of bioclastic grainstone and packstone.

### Sequence 6

A combination of regional biostratigraphic and seismic data indicate that the 76-m-thick lower Oligocene interval intersected at Site 1132 (lithostratigraphic Unit V) corresponds to seismic Sequence 6A, and the 38-m-thick upper Eocene interval (lithostratigraphic Unit VI) corresponds to seismic Sequence 6B. These sequences are considerably thicker at Site 1132 than predicted before drilling, and they will necessitate a postcruise reinterpretation of the seismic grid in this vicinity. Sequence 6 sediments were poorly recovered, but sufficient lithostratigraphic information exists to categorize Sequence 6A as partially dolomitized bioclastic and foraminiferal packstone and grainstone overlying a mineralized and bored hardground that marks the top Sequence 6B boundary. Seismic data show that Sequence 6B at Site 1132 corresponds to a distinct mound; however, poor recovery of this interval precludes a detailed analysis of mound composition. Recovered core consists of a diverse range of lithologies, including echinoid wackestone, bioclastic packstone, bioclastic wackestone, and bioclastic grainstone, with bioclasts dominated by bryozoan, brachiopod, echinoid, and bivalve fragments. Abundant firmgrounds and hardgrounds are present throughout lithostratigraphic Unit VI, and it appears likely that this interval represents mound development on a shallow marine shelf (see **"Lithostratigraphy,"** p. 3).

### Sequence 7

The lack of recovery within the ~45-m-thick interval of seismic Sequence 7 intersected at Site 1132 is attributed to the loose, unconsolidated character of the sand inferred to constitute the succession underlying lithostratigraphic Unit VI. The unconsolidated nature of these sediments resulted in collapse around the drill bit, which caused the drill string to jam and required that the hole be abandoned. It is likely that pebbles of coarse sand- to granule-sized calcareous sandstone at the base of lithostratigraphic Unit VI either may have been derived from Sequence 7 or may actually represent the uppermost part of Sequence 7. If the latter is true, then the drilling difficulties encountered deeper in the hole would seem to indicate a variable distribution of calcareous cement surrounding siliciclastic grains within this unit.

## REFERENCES

Almond, D.O., McGowran, B., and Li, Q., 1993. Late Quaternary foraminiferal record from the Great Australian Bight and its environmental significance. *Mem. Assoc. Australas. Palaeontol.,* 15:417–428.

Berggren, W.A., 1992. Paleogene planktonic foraminifer magnetobiostratigraphy of the Southern Kerguelen Plateau (Sites 747–749). *In* Wise, S.W., Jr., Schlich, R., et al., *Proc. ODP, Sci. Results,* 120 (Pt. 2): College Station, TX (Ocean Drilling Program), 551–568.

Berggren, W.A., Kent, D.V., Swisher, C.C., III, and Aubry, M.-P., 1995. A revised Cenozoic geochronology and chronostratigraphy. *In* Berggren, W.A., Kent, D.V., Aubry, M.-P., and Hardenbol, J. (Eds.), *Geochronology, Time Scales and Global Stratigraphic Correlation.* Spec. Publ.—Soc. Econ. Paleontol. Mineral. (Soc. Sediment. Geol.), 54:129–212.

Bone, Y., and James, N.P., 1993. Bryozoans as carbonate sediment producers on the cool-water Lacepede Shelf, Southern Australia. *Sediment. Geol.,* 86:247–271.

Eberli, G.P., Swart, P.K., Malone, M.J., et al., 1997. *Proc. ODP, Init. Repts.,* 166: College Station, TX (Ocean Drilling Program).

Feary, D.A., 1997. ODP pollution prevention and safety panel: Leg 182 safety package—Cenozoic cool-water carbonates of the Great Australian Bight. *Aust. Geol. Surv. Org.,* 28.

Feary, D.A., and James, N.P., 1998. Seismic stratigraphy and geological evolution of the Cenozoic, cool-water, Eucla Platform, Great Australian Bight. *AAPG Bull.,* 82:792–816.

Holbourn, A., Kuhnt, W., El Albani, A., Pletsch, T., Luderer, F., and Wagner, T., 1999. Upper Cretaceous palaeoenvironments and benthonic foraminiferal assemblages of potential source rocks from the western African margin, Central Atlantic. *Geol. Soc. Spec. Publ. London,* 153:195–222.

Hornibrook, N. de B., Brazier, R.C., and Strong, C.P., 1989. Manual of New Zealand Permian to Pleistocene foraminiferal biostratigraphy. *Paleontol. Bull. N.Z. Geol. Surv.,* 56:1–175.

Jenkins, D.G., 1993. Cenozoic Southern mid- and high-latitude biostratigraphy and chronostratigraphy based on planktonic foraminifera. *In* Kennett, J.P., and Warnke, D.A. (Eds.), *The Antarctic Paleoenvironment: A Perspective on Global Change.* Antarct. Res. Ser., 60:125–144.

Li, Q., James, N.P., Bone, Y., and McGowran, B., 1999. Palaeoceanographic significance of Recent foraminiferal biofacies on the southern shelf of Western Australia: a preliminary study. *Palaeogeogr., Palaeoclimatol., Palaeoecol.,* 147:101–120.

Li, Q., McGowran, B., James, N.P., and Bone, Y., 1996a. Foraminiferal biofacies on the mid-latitude Lincoln Shelf, South Australia: oceanographic and sedimentological implications. *Mar. Geol.,* 129:285–312.

Li, Q., McGowran, B., James, N.P., Bone, Y., and Cann, J.H., 1996b. Mixed foraminiferal biofacies on the mesotrophic, mid-latitude Lacepede Shelf, South Australia. *Palaios,* 11:176–191.

Li, Q., Radford, S.S., and Banner, F.T., 1992. Distribution of microperforate tenuitellid planktonic foraminifers in Holes 747A and 749B, Kerguelen Plateau. *In* Wise, S.W., Jr., Schlich, R., et al., *Proc. ODP, Sci. Results,* 120: College Station, TX (Ocean Drilling Program), 569–594.

Lutze, G.F., and Coulbourn, W., 1984. Recent benthic foraminifera from the continental margin of Northwest Africa: community structure and distribution. *Mar. Micropaleontol.,* 8:361–401.

McGowran, B., 1989. The later Eocene transgression in southern Australia. *Alcheringa,* 13:45–68.

————, 1990. Fifty million years ago. *Am. Sci.,* 78:30–39.

————, 1991. Maastrichtian and early Cainozoic, southern Australia: foraminiferal biostratigraphy. *In* Williams, M.A.J., De Deckker, P., and Kershaw, A.P. (Eds.), *The Cainozoic of the Australian Region.* Geol. Soc. Aust. Spec. Publ., 18:79–98.

McGowran, B., Li, Q., Cann, J., Padley, D., McKirdy, D.M., and Shafik, S., 1997a. Biogeographic impact of the Leeuwin Current in southern Australia since the late middle Eocene. *Palaeogeogr., Palaeoclimatol., Palaeoecol.,* 136:19–40.

McGowran, B., Li, Q., and Moss, G., 1997b. The Cenozoic neritic record in southern Australia: the biogeohistorical framework. *In* James, N.P., and Clarke, J., *Cool-Water Carbonates*. Spec. Publ.— Soc. Econ. Petrol. Mineral., 56:185–203.

McGowran, B., Moss, G., and Beecroft, A., 1992. Late Eocene and early Oligocene in southern Australia: local neritic signals of global and oceanic changes. *In* Prothero, D.R., and Berggren, W.A. (Eds.), *Eocene-Oligocene Climatic and Biotic Evolution:* Princeton (Princeton Univ. Press), 178–201.

Shafik, S., 1990. The Maastrichtian and early Tertiary record of the Great Australian Bight Basin and its onshore equivalents on the Australian southern margin: a nannofossil study. *BMR J. Australian Geol. Geophys.,* 11:473–497.

Shipboard Scientific Party, 1996. Site 975. *In* Comas, M.C., Zahn, R., Klaus, A., et al., *Proc. ODP, Init. Repts.,* 161: College Station, TX (Ocean Drilling Program), 113–177.

Surlyk, F., 1997. A cool-water carbonate ramp with bryozoan mounds: late Cretaceous-Danian of the Danish Basin. *In* James, N.P., and Clarke, J D.A. (Eds.), *Cool-water Carbonates*. Spec. Publ.—Soc. Econ. Paleontol. Mineral., 56:293–307.

Wells, P., and Okada, H., 1996. Holocene and Pleistocene glacial palaeoceanography off southeastern Australia, based on foraminifers and nannofossils in Vema cored hole V18-222. *Aust. J. Earth Sci.,* 43:509–523.

**Figure F1.** Map showing the location of Site 1132 on the uppermost continental slope, immediately below the shelf edge, in relation to other Leg 182 sites and the Australian Geological Survey Organisation Survey 169 (AGSO169) seismic lines.

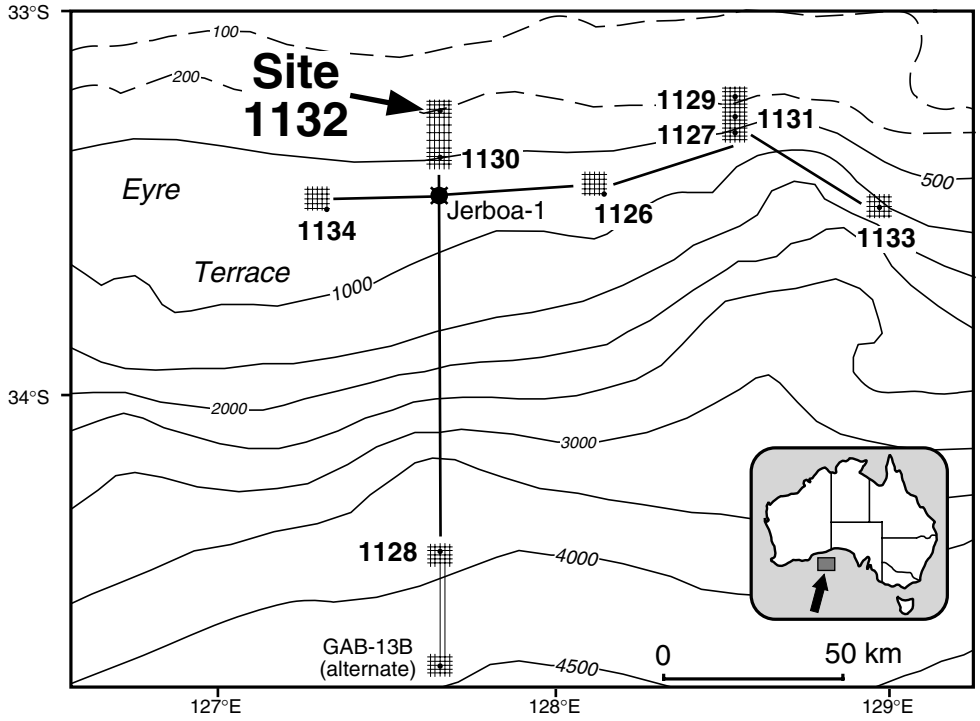

**Figure F2.** Portion of seismic Line AGSO169/13a showing the pre-drill seismic stratigraphic interpretation at Site 1132 and showing sequences planned (shown in white) and actually intersected (shown in black) at this site.

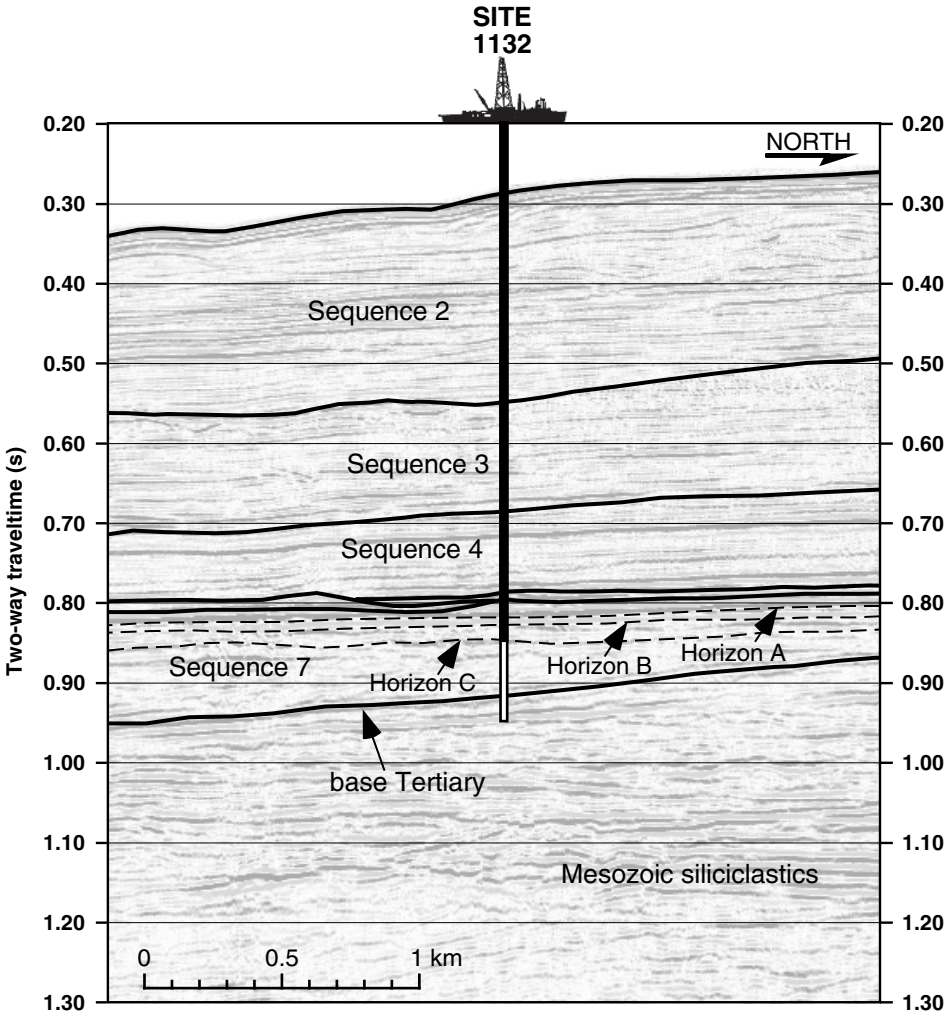

**Figure F3.** Summary of lithostratigraphy, Site 1132. Subdivision of Units IV and V is not possible due to poor core recovery. Ages are from "Biostratigraphy," p. 13. ? = magnetic intensity too low to be measured. (Continued on next two pages.)

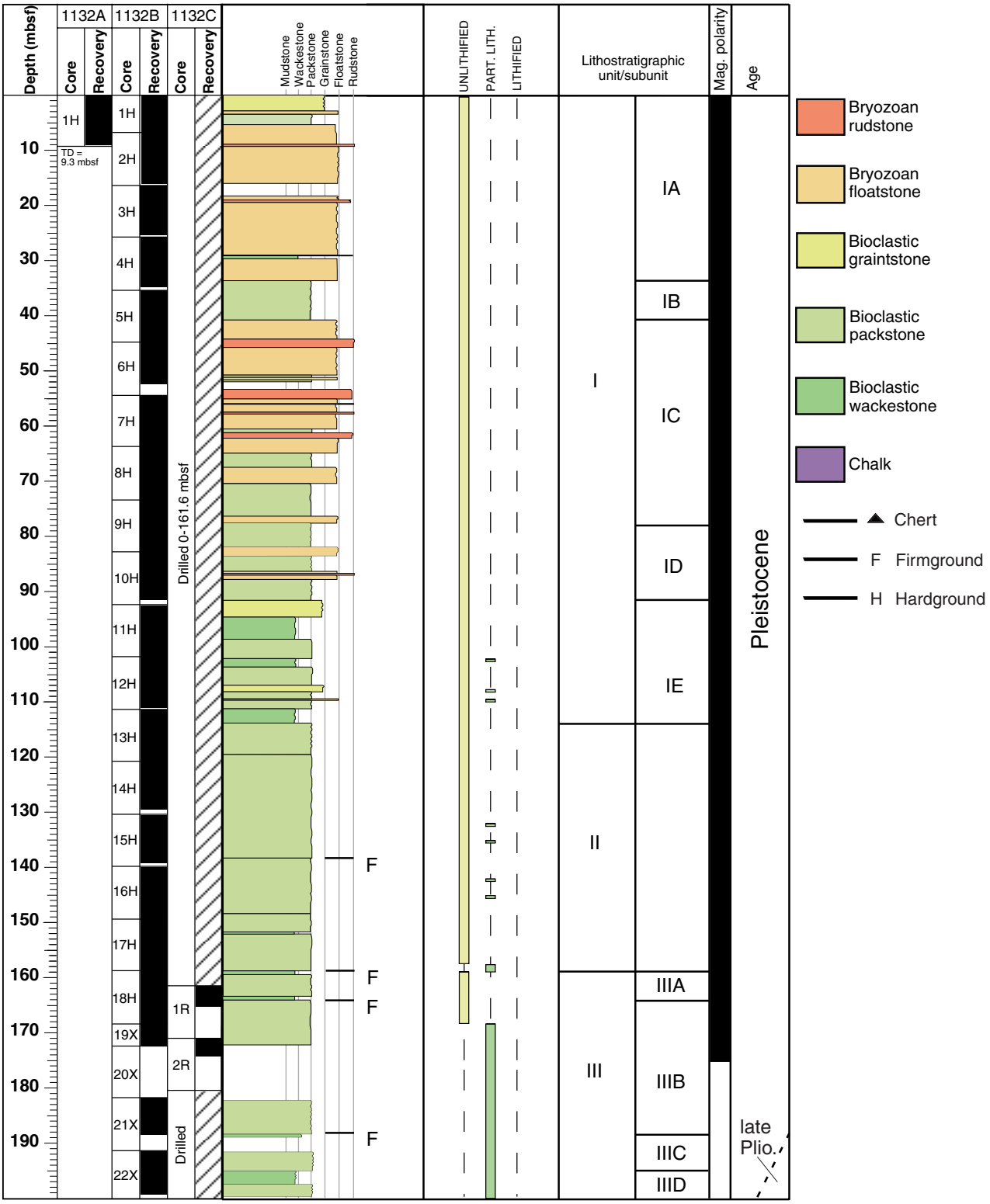

Figure F3 (continued).

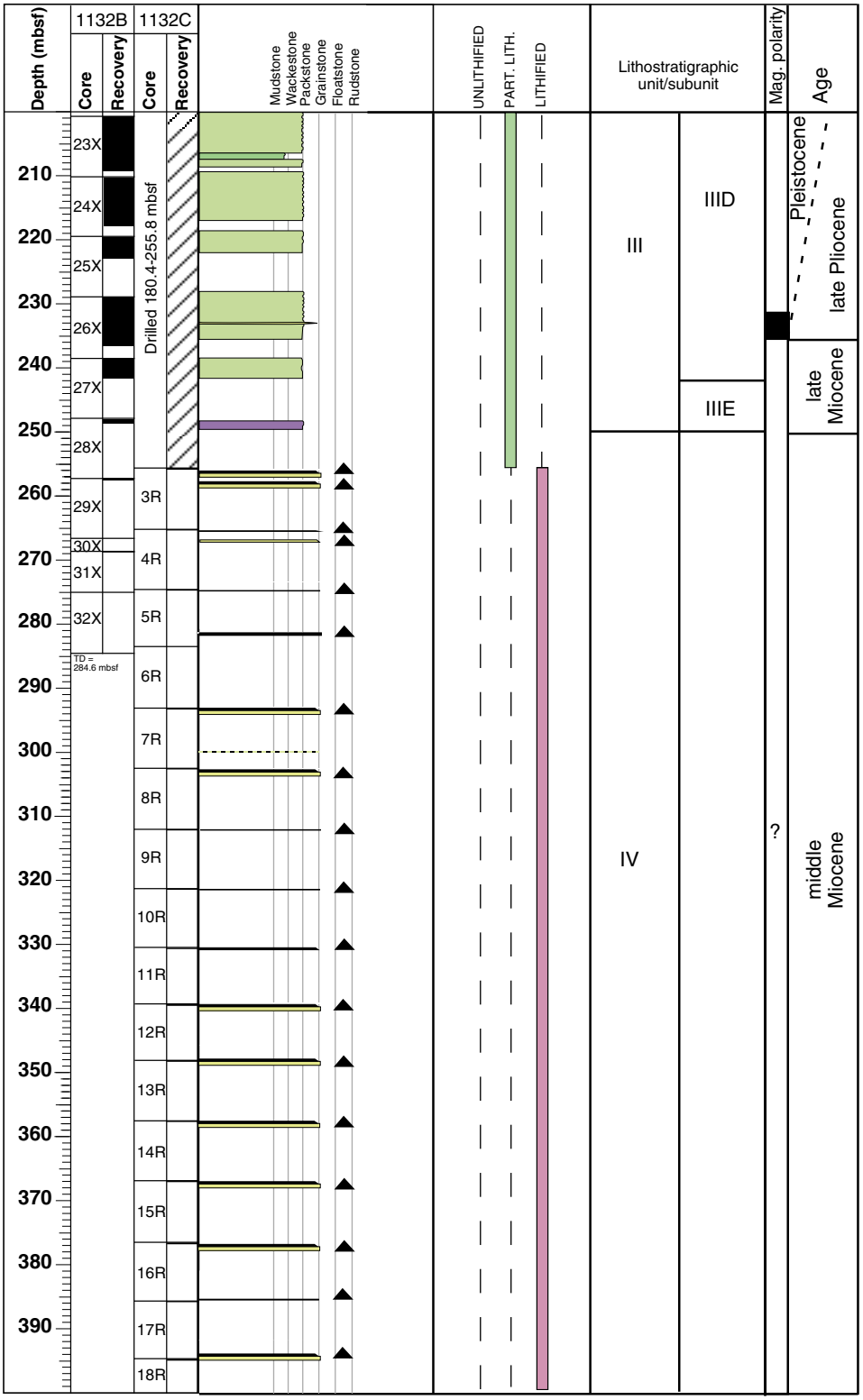

**Figure F3 (continued).**

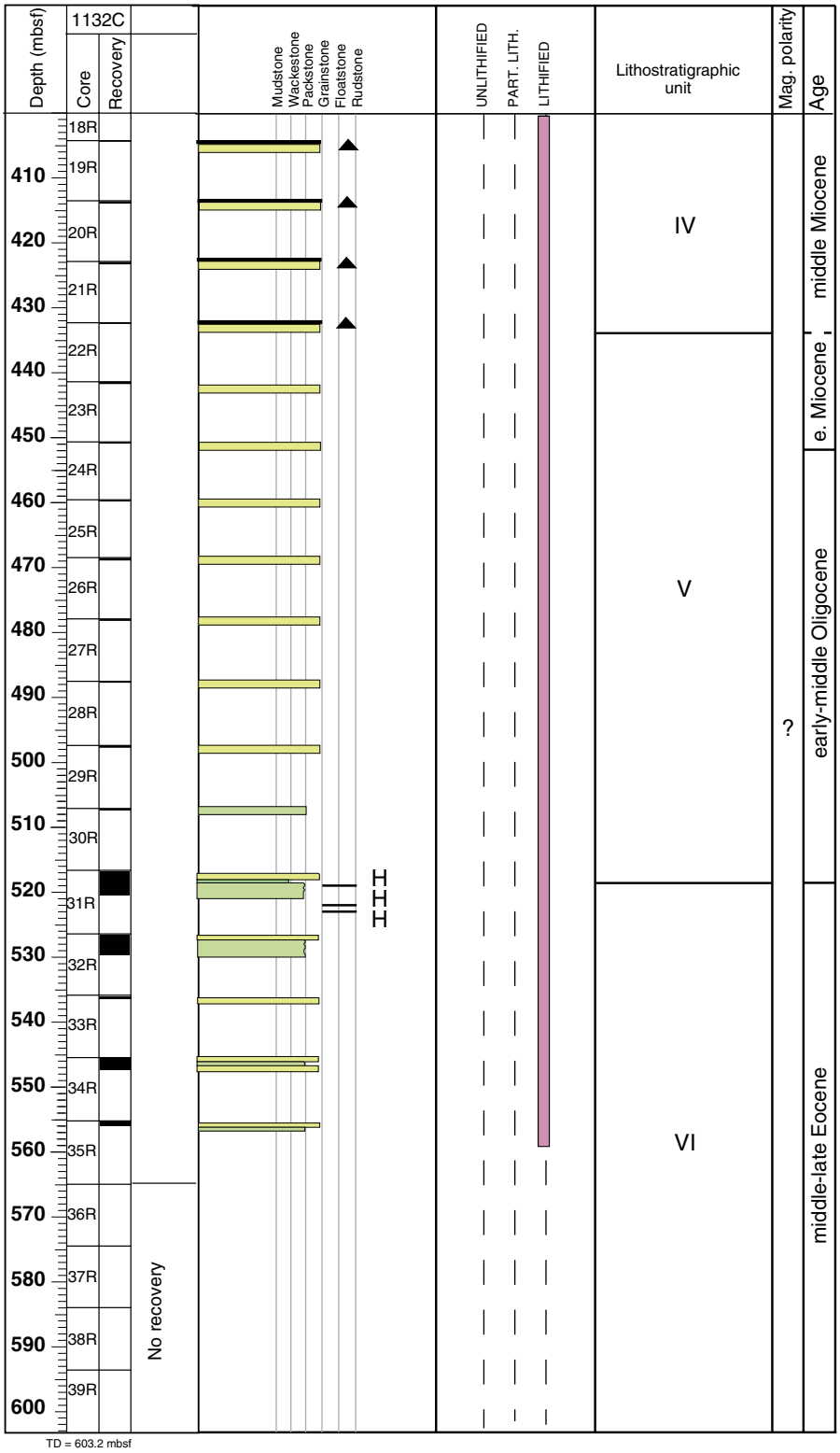

**Figure F4.** Firmground in light olive gray bioclastic wackestone overlain by light gray bioclastic packstone at 29 cm. The top of the firmground marks the boundary between Subunits IIIB and IIIC. The boundary is diffuse due to burrow mottling. Note how the lighter packstone is piped down into the upper 23 cm of the darker wackestone. The vertical 1-cm-wide burrow that extends downward from 46 to 51.5 cm probably belongs to a new ichnogenus (interval 182-1132B-21X-5, 15–55 cm).

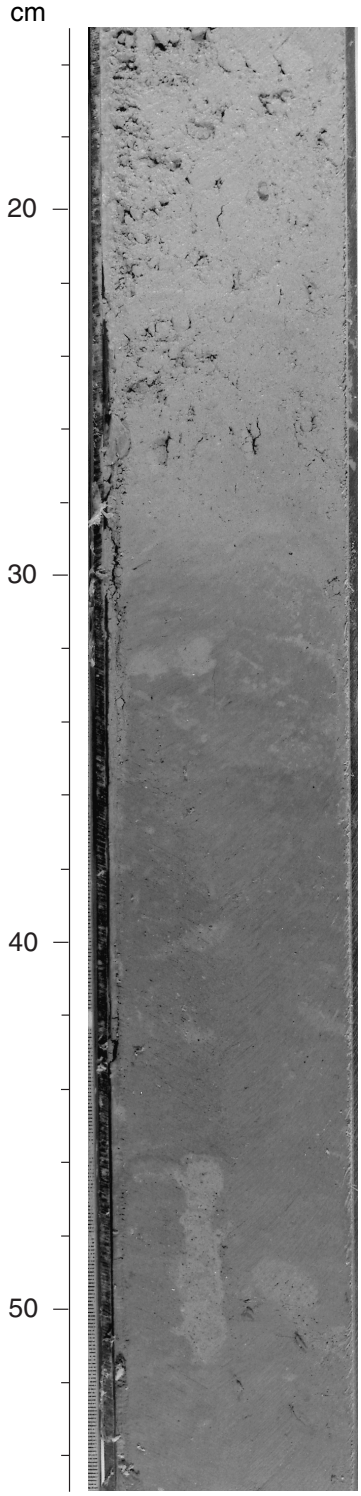

**Figure F5.** Bioclastic grainstone from the basal part of Unit V, showing preferential nodular hardening of *Planolites* (25 cm) and *Thalassinoides*-like burrow fills, enhanced by solution seams (interval 182-1132C-31R-1, 20–35 cm).

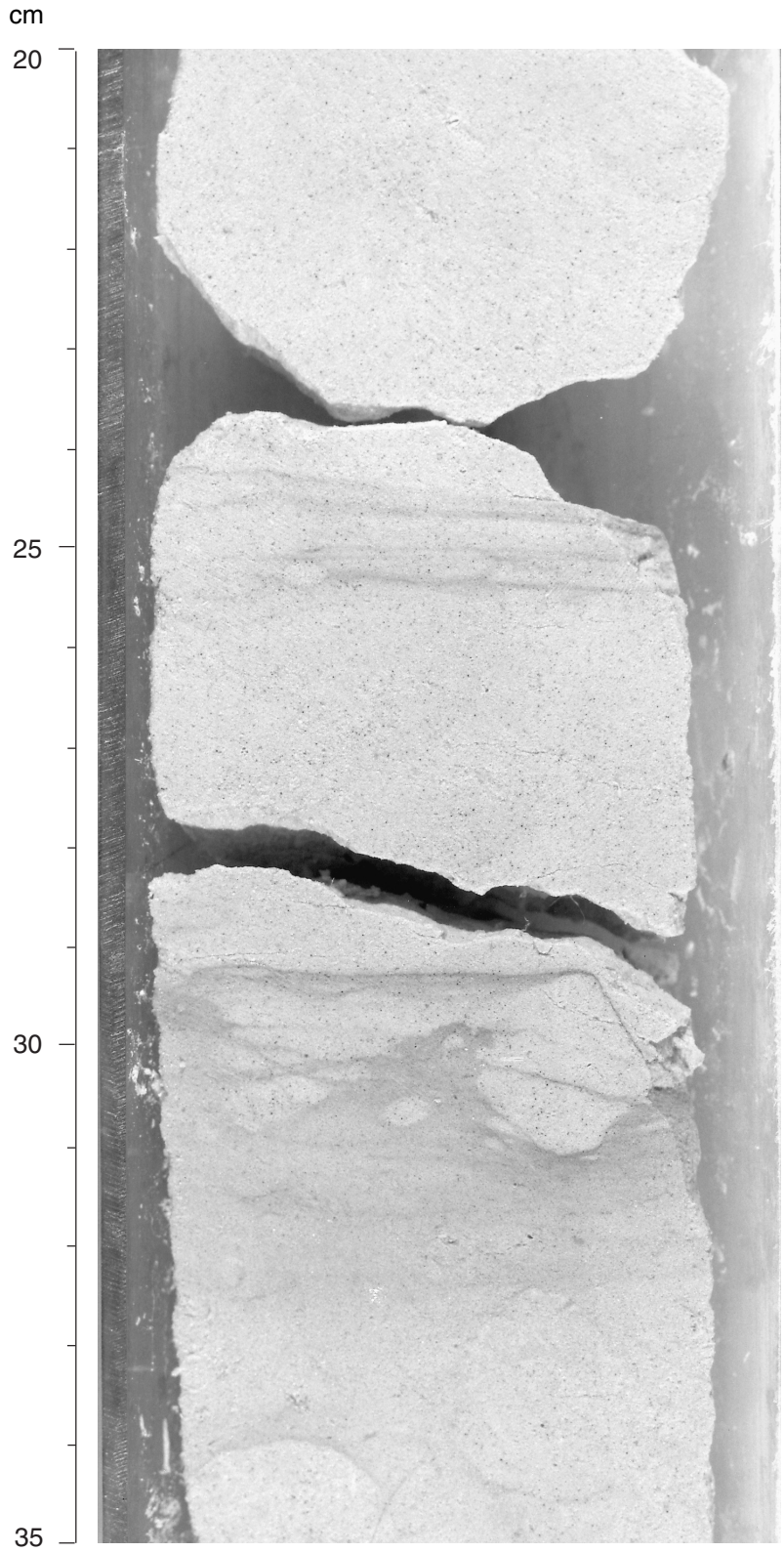

**Figure F6.** Hardground marking the top of Unit VI (114–117.5 cm). The hardground is mineralized, and the burrow gallery at 119–120 cm was empty at the time of hardground formation, as seen by the mineralized and bored underside of the hardened layer at 119 cm. The 2-mm-long boring in the lower right (119.2 cm) is clearly visible due to the white burrow fill. The upper surface of the hardground is also bored, notably to the upper left. A 1- to 2-mm-wide crack, filled with sediment from above, extends obliquely downward from the top of the hardground. It is a Neptunian dike (interval 182-1132C-31R-105-120).

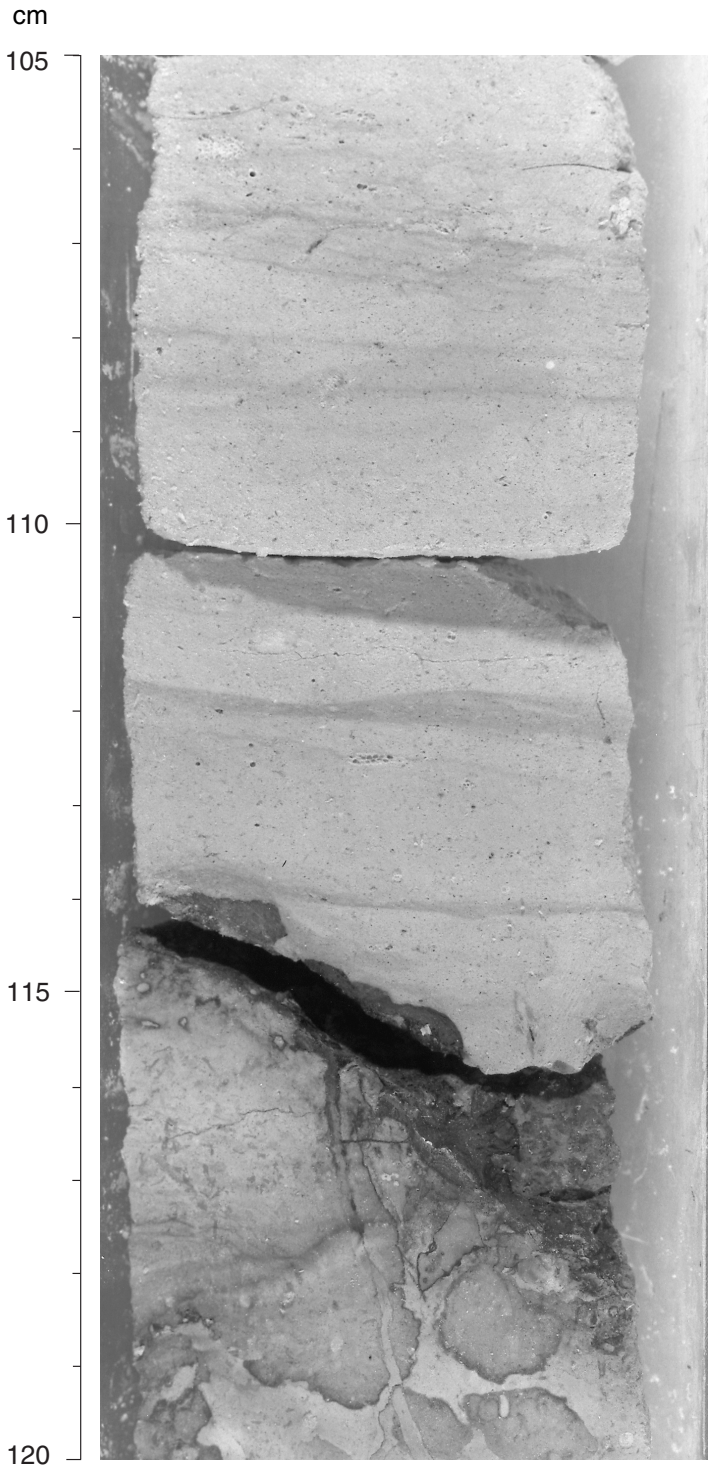

**Figure F7.** Burrowed firmground to hardground at the top of a light gray bioclastic wackestone (55.5–57 cm), overlain by bioclastic packstone. Note the poorly sorted nature of both deposits and the large bioclasts in the packstone (Unit VI; interval 182-1132C-31R-3, 52–67 cm).

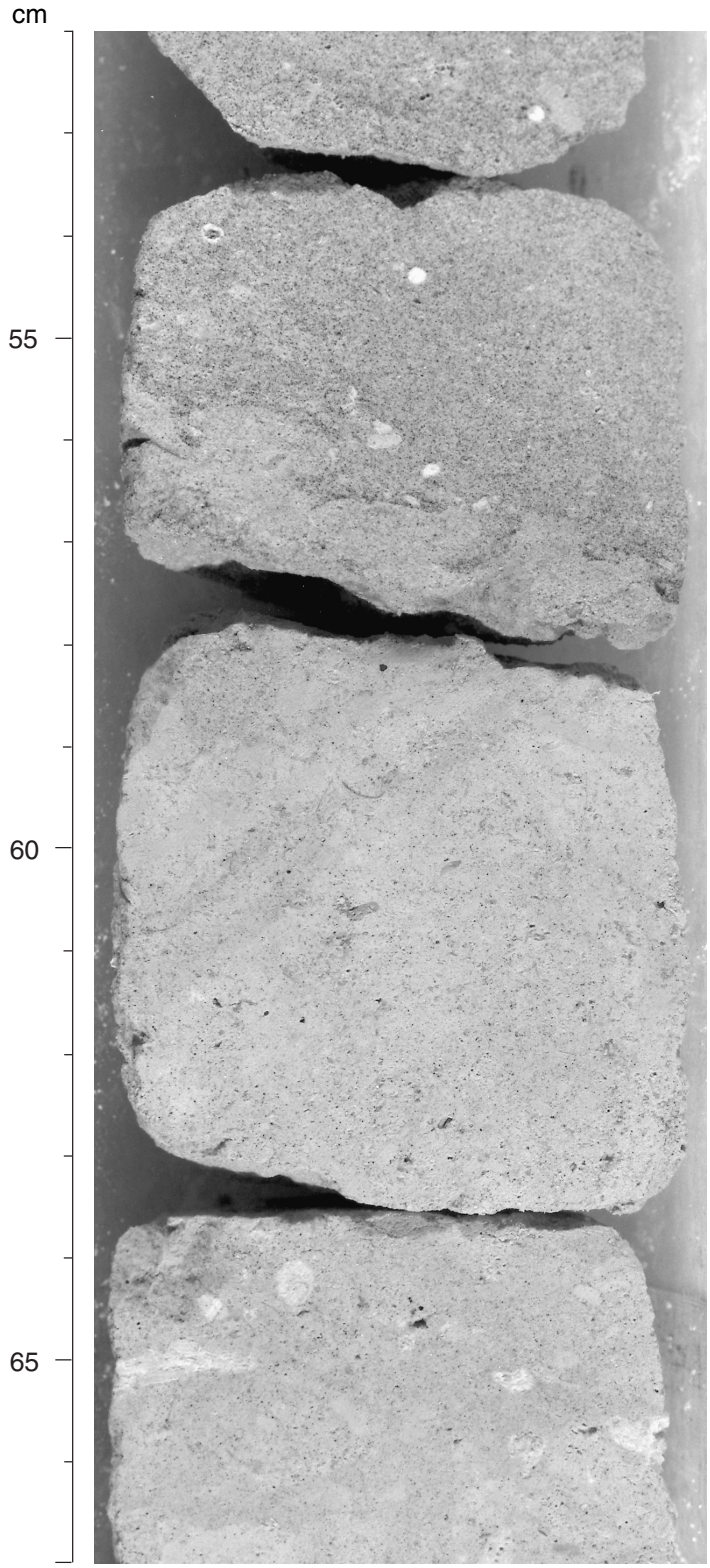

**Figure F8.** Complex mineralized hardground in bioclastic packstone of Unit VI. Note the succession of two densely spaced firmground to hardground surfaces and the high content of large bioclasts, fossils, vugs, and burrows, notably in the upper part. The material infilling the shell to the upper left differs from the surrounding sediment, indicating an earlier fill period, reworking, and embedding during renewed sedimentation (interval 182-1132C-31R-CC, 0–15 cm).

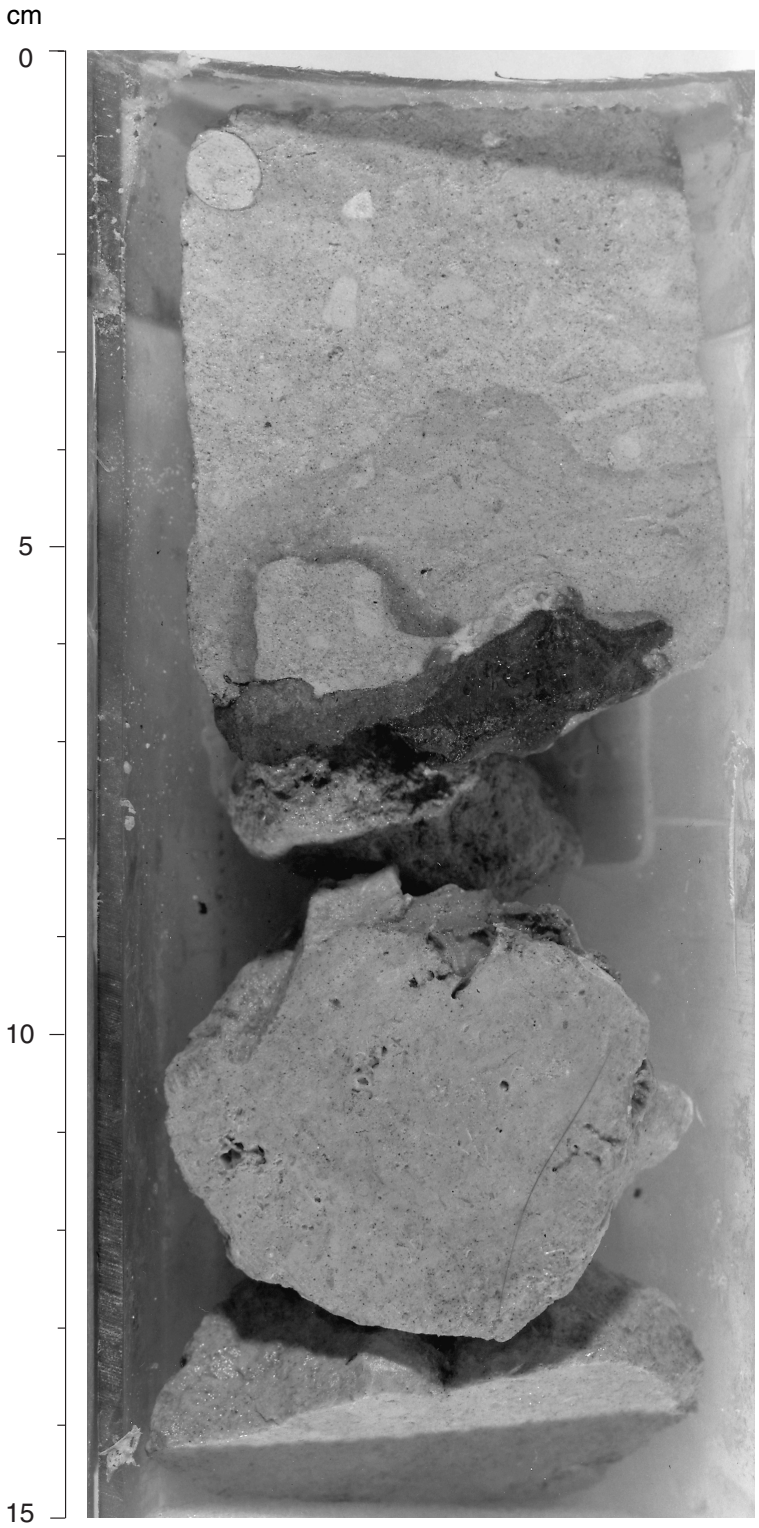

**Figure F9.** Stratigraphic position of calcareous nannofossil and planktonic foraminifer zones, together with benthic foraminiferal assemblages, at Site 1132. Dashed boundaries imply uncertainty. No sample means that the core catcher, if recovered, did not contain enough sediment to prepare for foraminifers. (Continued on next page.)

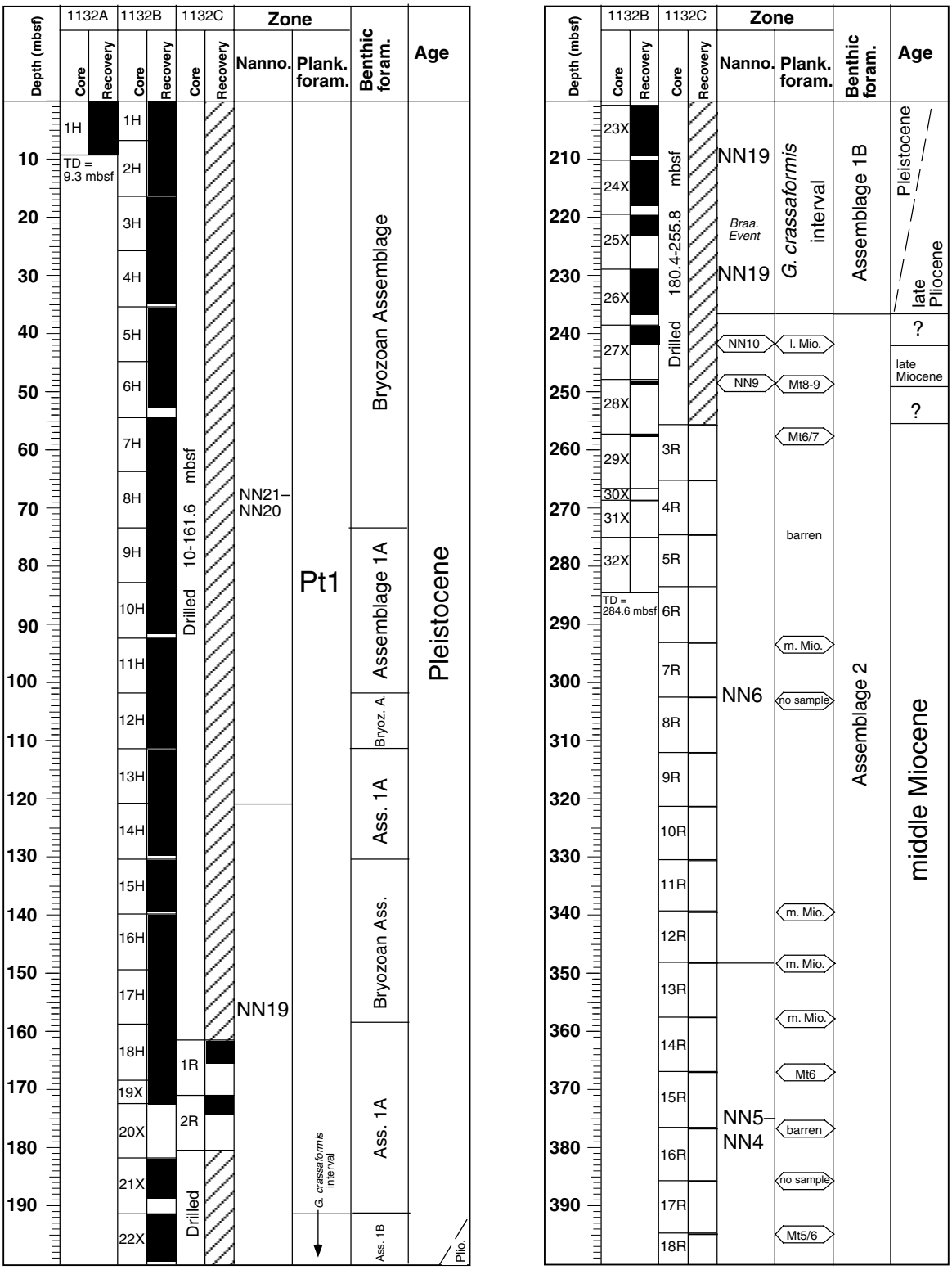

Figure F9 (continued).

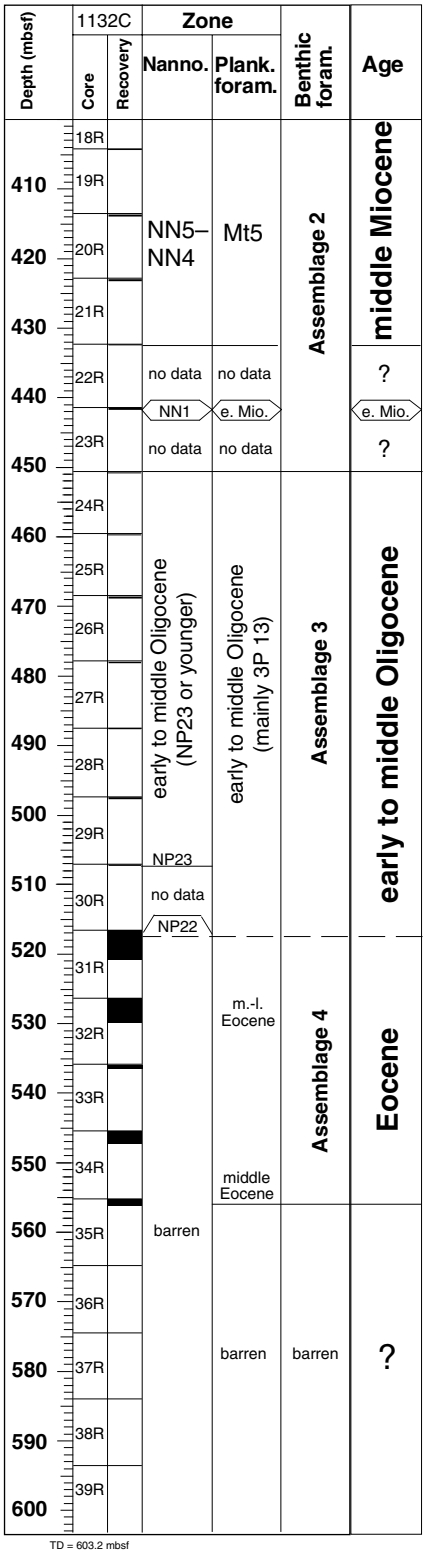

**Figure F10.** Sedimentation rate curve constructed from the datum levels listed in Table T2, p. 72. Stratigraphic error varies between ±0.72 and ±6.67 m, as indicated by the length of error bars.

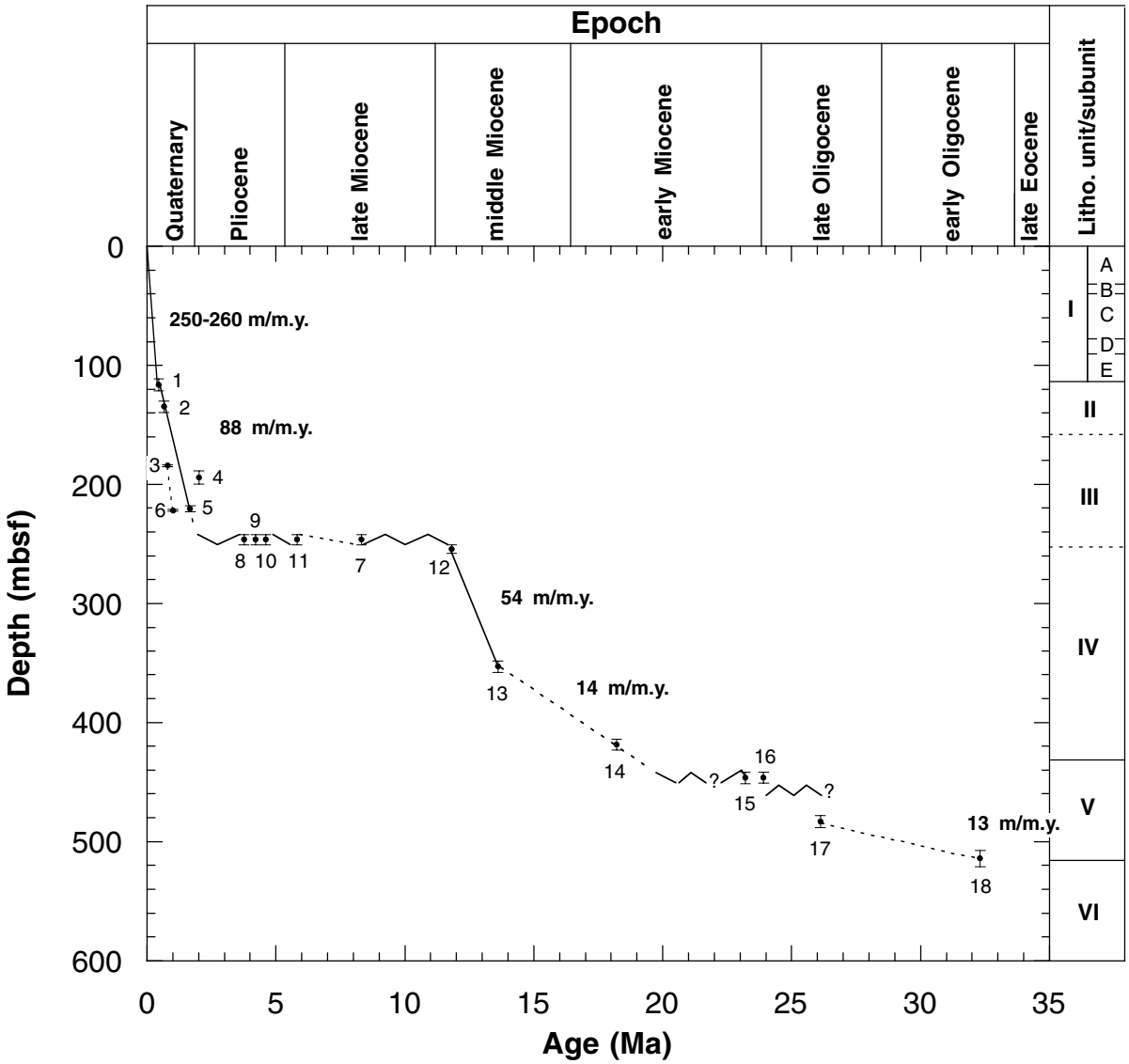

**Figure F11.** Magnetic intensity in Hole 1132B from 0 to 250 mbsf. The record has been cleaned by removing results from the tops and bottoms of cores and sections, which reveals fluctuations in intensity with wavelengths of ~15 m.

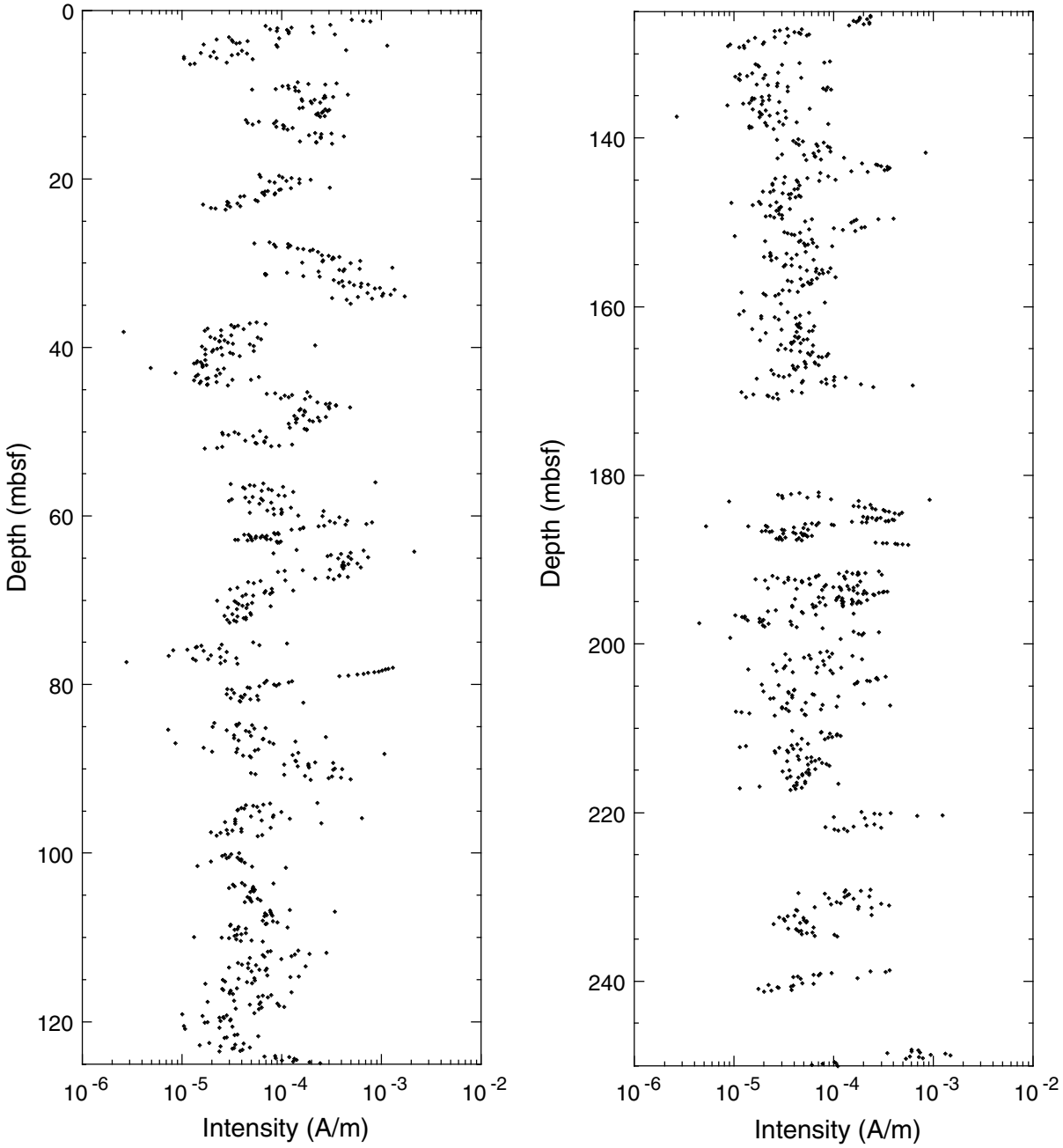

**Figure F12.** Magnetic susceptibility and intensity of magnetization in Hole 1132B from 0 to 250 mbsf. Magnetic susceptibility is diamagnetic throughout and approaches zero between 150 and 250 mbsf. Intensity of magnetization decreases in the top 150 mbsf and stabilizes in the depth range of higher susceptibility.

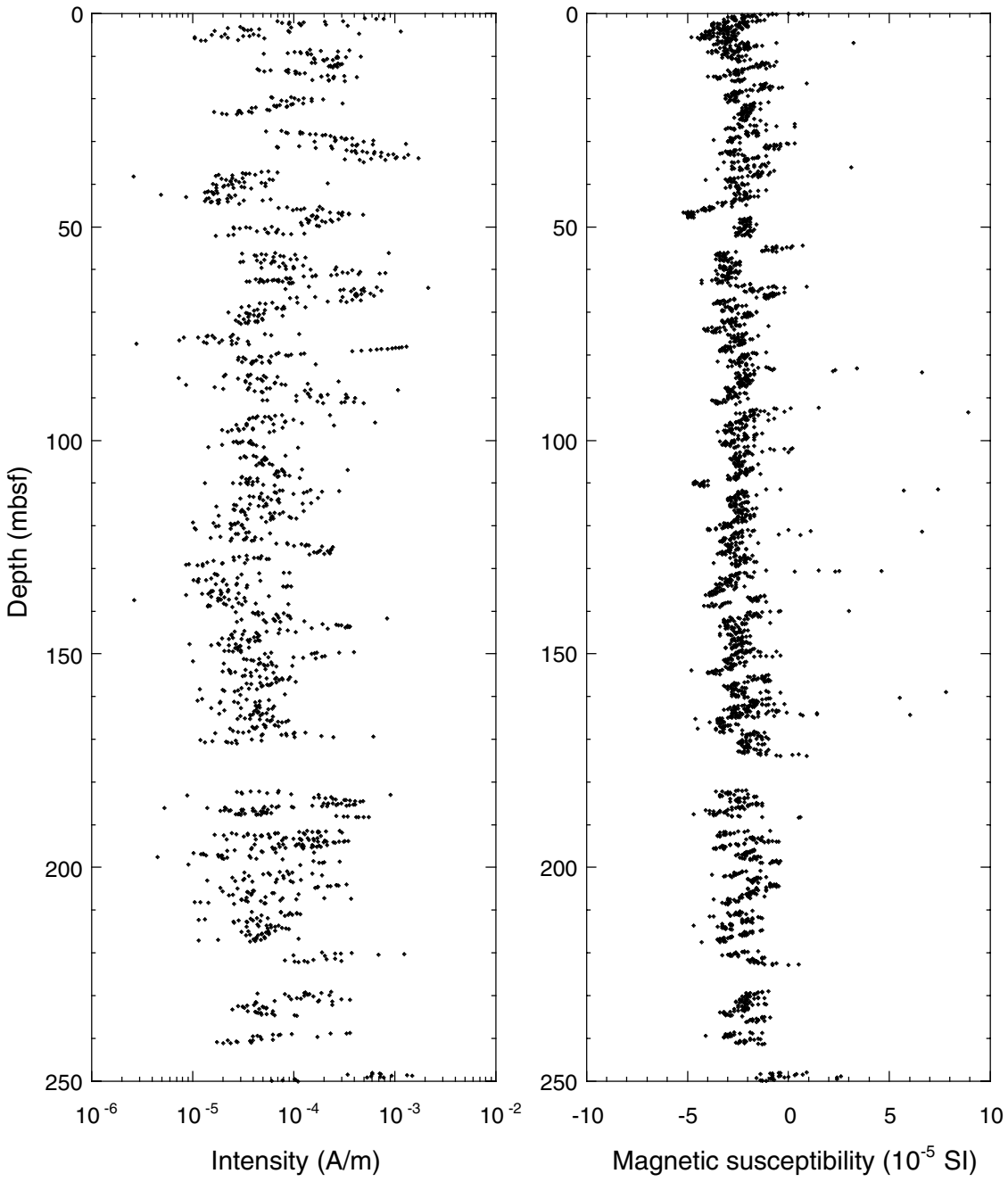

**Figure F13.** Magnetic inclination and magnetostratigraphy of the upper 250 mbsf of Hole 1132B. Magnetic polarity and chron are shown on the right of the figure: the Brunhes/Matuyama boundary (C1n/C1r1r) and the top of the Jaramillo Subchron (C1r1n) are identified.

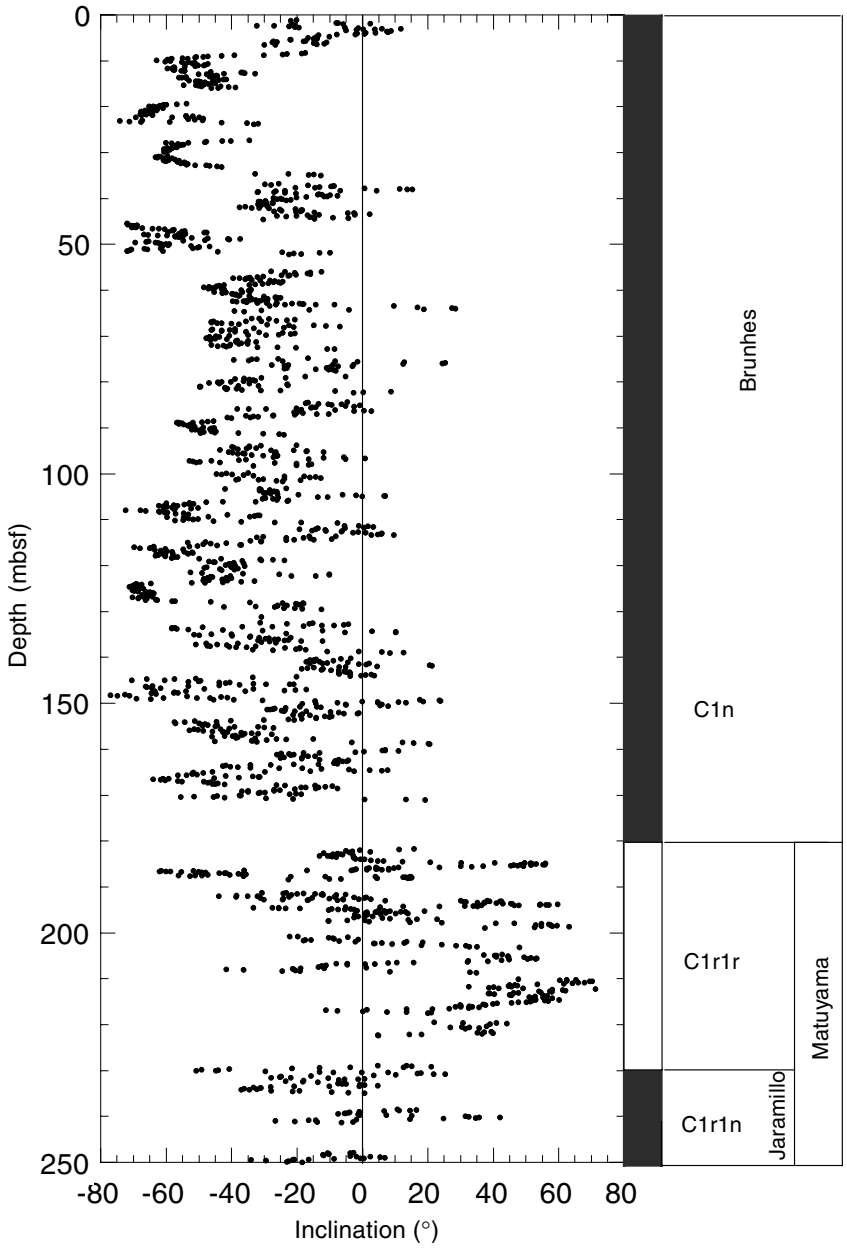

**Figure F14.** **(A)** Calcium carbonate and **(B)** organic carbon contents in samples from Hole 1132B.

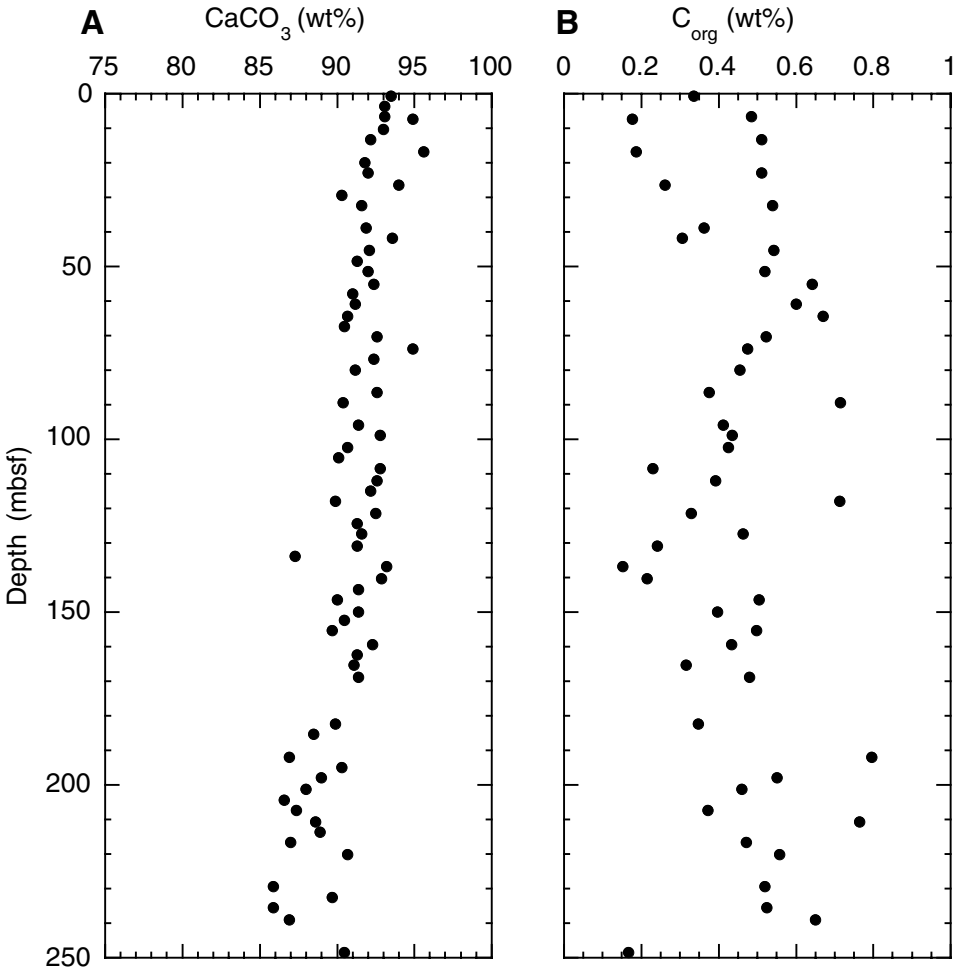

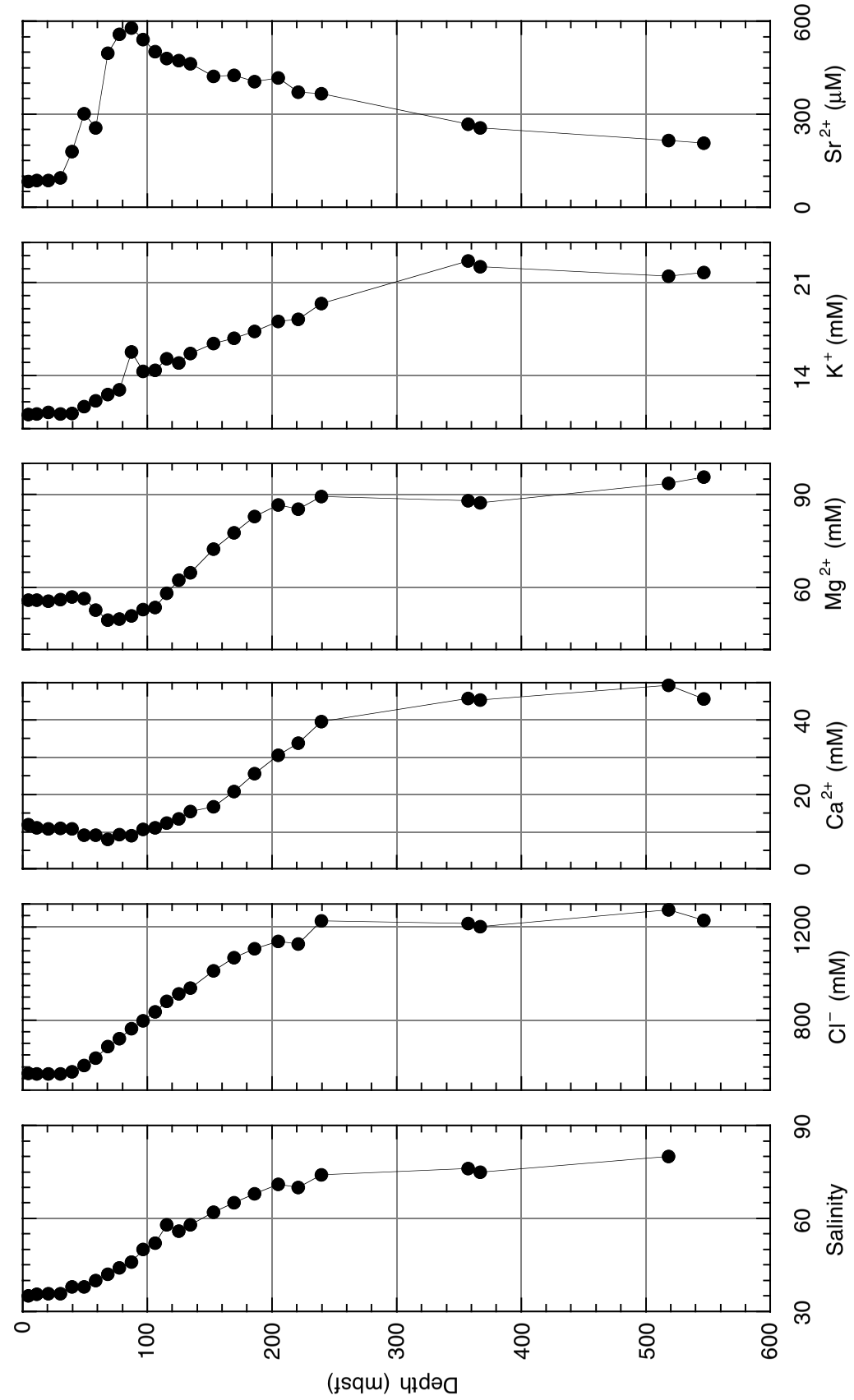


**Figure F15.** Depths vs. concentration profiles for (A) salinity, (B) $Cl^-$, (C) $Ca^{2+}$, (D) $Mg^{2+}$, (E) $K^+$, and (F) $Sr^{2+}$.

**Figure F16.** Depths vs. concentration profiles for (**A**) $H_4SiO_4^0$, (**B**) $Li^+$, (**C**) $Fe^{2+}$, (**D**) $NH_4^+$, (**E**) $SO_4^{2-}$, (**F**) pH, and (**G**) alkalinity.

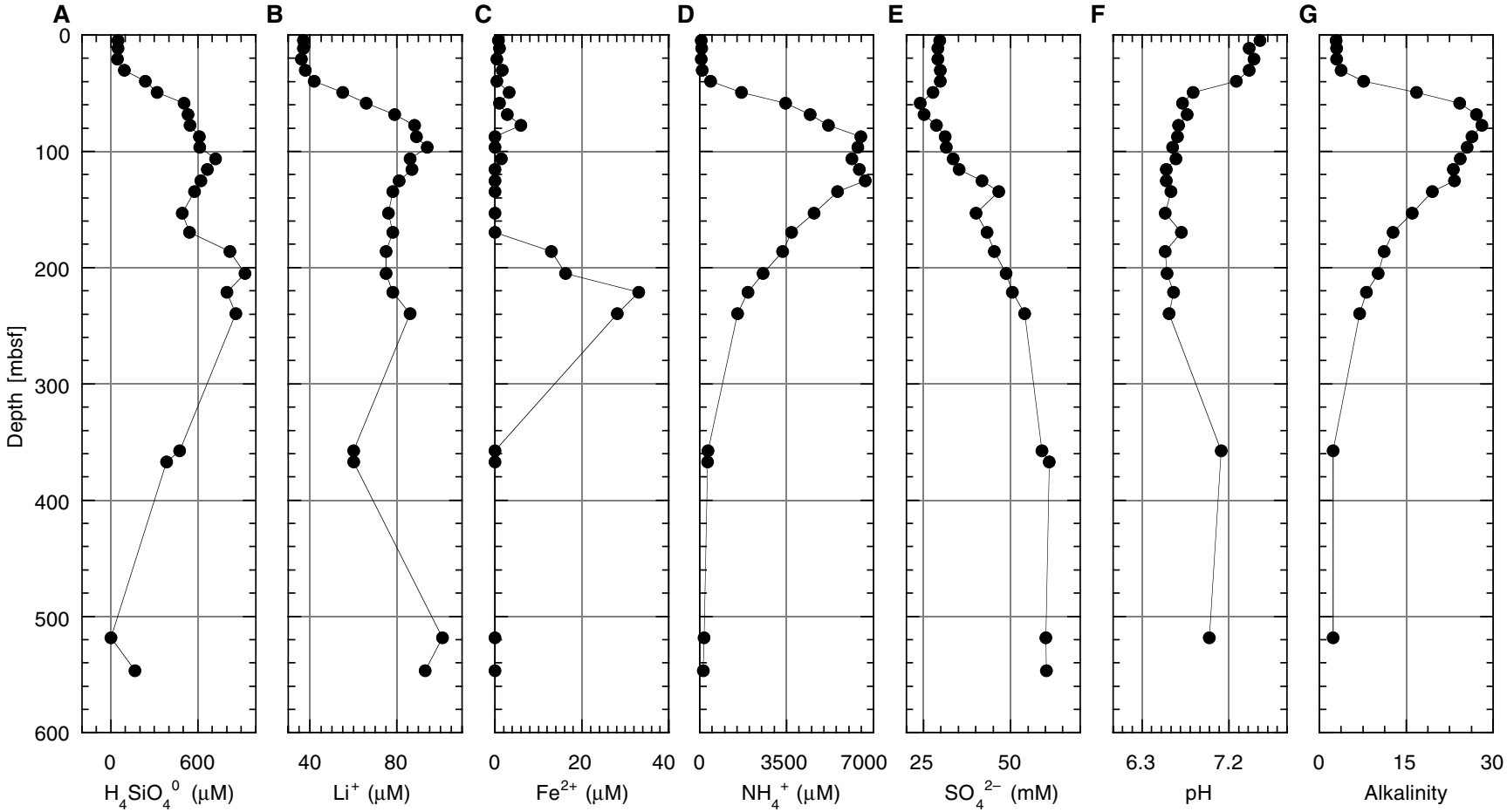

**Figure F17.** Concentration depth profiles. The concentrations of (**A**) $Na^+$, (**E**) $Sr^{2+}$, and (**F**) $SO_4^{2-}$ have been normalized by chlorinity to compensate for the concentration increase with increasing salinity. Unlike at previous sites, the excess concentrations of (**B**) $Ca^{2+}$, (**C**) $Mg^{2+}$, and (**D**) $K^+$ are not normalized by seawater but refer to the actual loss from the brine. Excess concentrations are calculated as $X_i - X_0 \times Cl_i^-/Cl_0^-$, where $X_i$ represents the concentration of the element at a certain depth, and $X_0$ refers to the normal seawater concentration of this element. Note that data from Site 1132 display a sodium/chlorinity ratio anomaly similar to that at Sites 1127 and 1131. For discussion, see **"Inorganic Geochemistry,"** p. 18, in the "Site 1131" chapter.

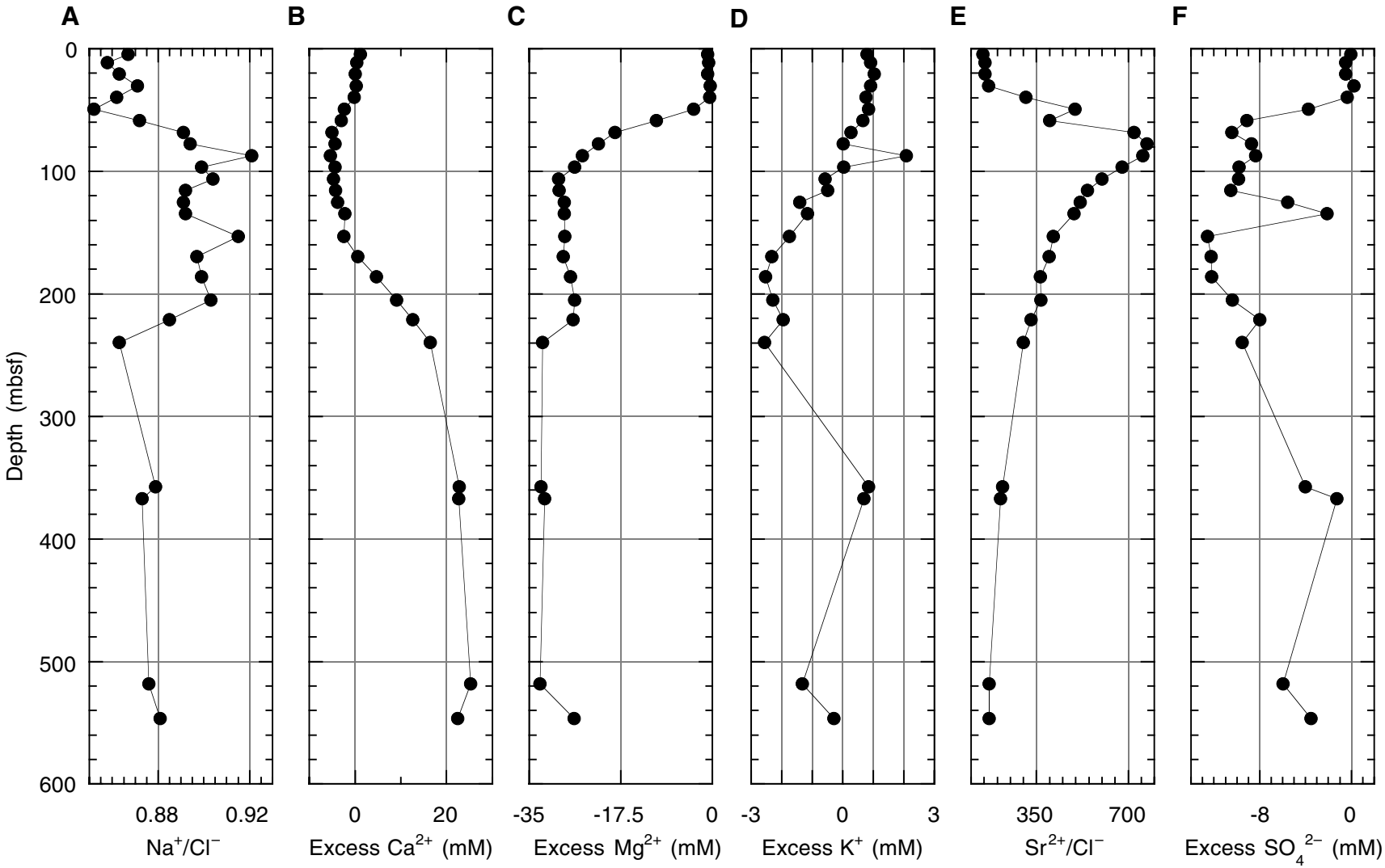

**Figure F18.** A plot of salinity vs. absolute depth (measured in meters below sea level [mbsl] rather than meters below seafloor [mbsf]) shows that the salinity values for Sites 1130 and 1132 stabilize at about the same depth, which suggests that the main body of the brine is situated ~520 mbsl. A schematic drawing of sequence boundary 2a shows that the brine crosscuts the sequence.

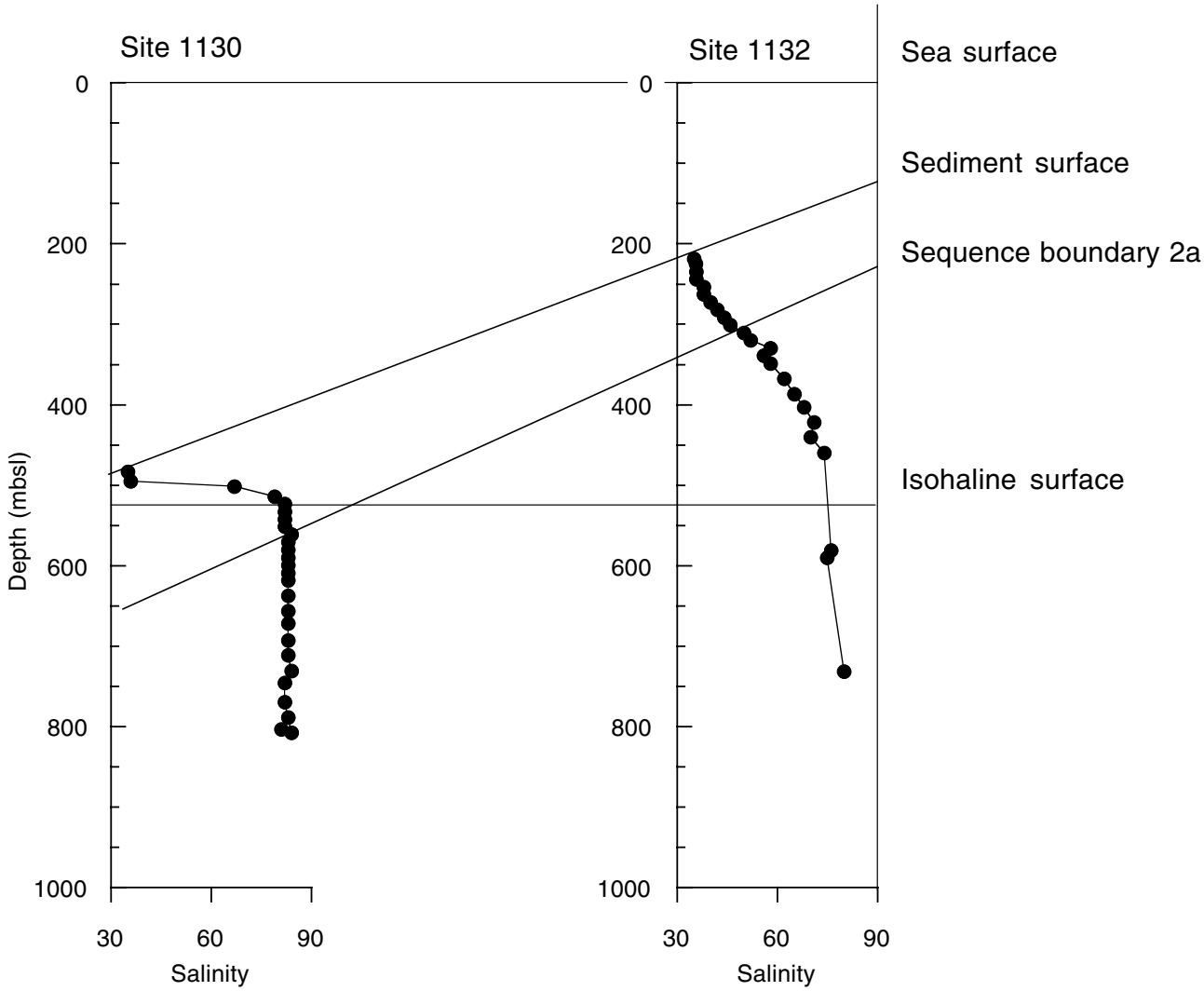

**Figure F19.** Variations in the concentration of aragonite (A), quartz (Q), LMC, HMC, and dolomite (D) at Site 1132 from XRD analysis. Calculations assume that the sediment is composed solely of these minerals and make no allowance for the presence of insoluble minerals (see **"Organic Geochemistry,"** p. 22) other than quartz.

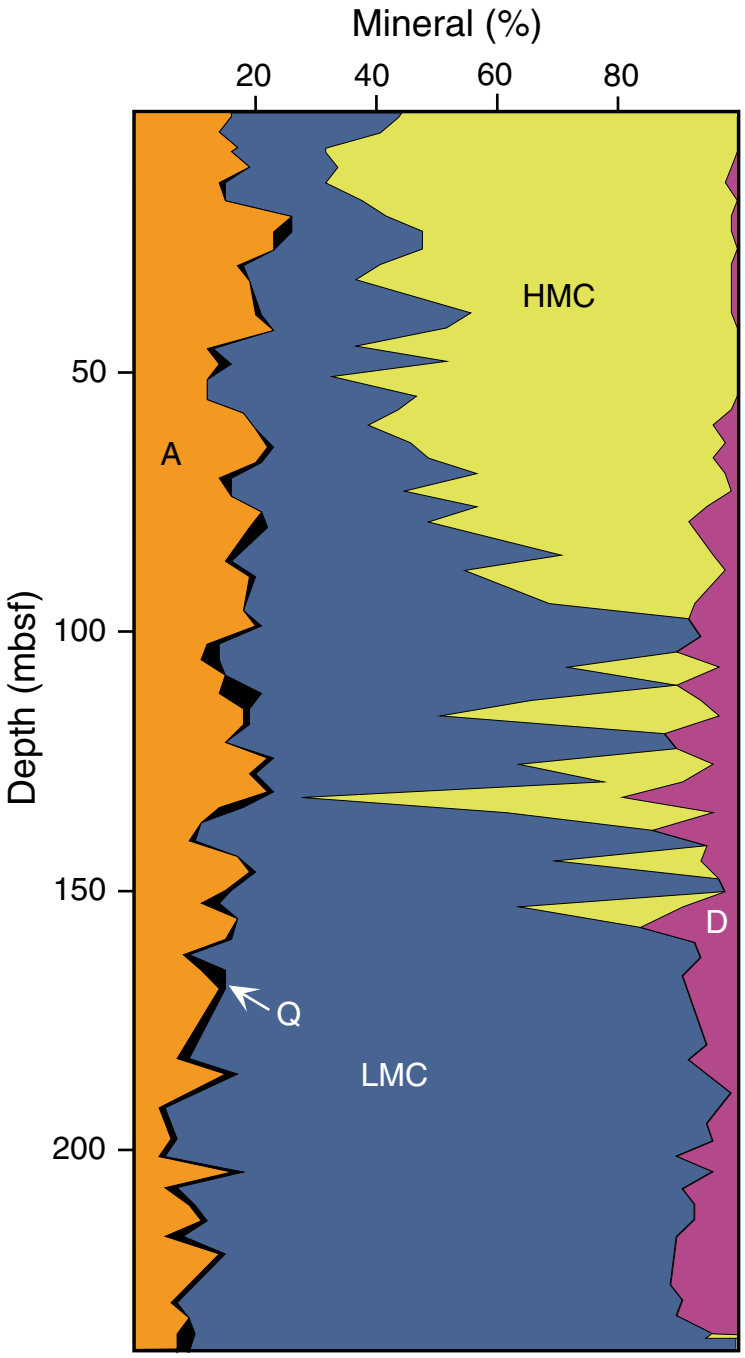

**Figure F20.** Composite figure of *P*-wave velocity, bulk density (solid circles = moisture and density [MAD]; lines = gamma-ray attenuation [GRA]), porosity, natural gamma radiation (NGR), and magnetic susceptibility for Site 1132. Recovery columns are shown on the left, and physical properties units on the right.

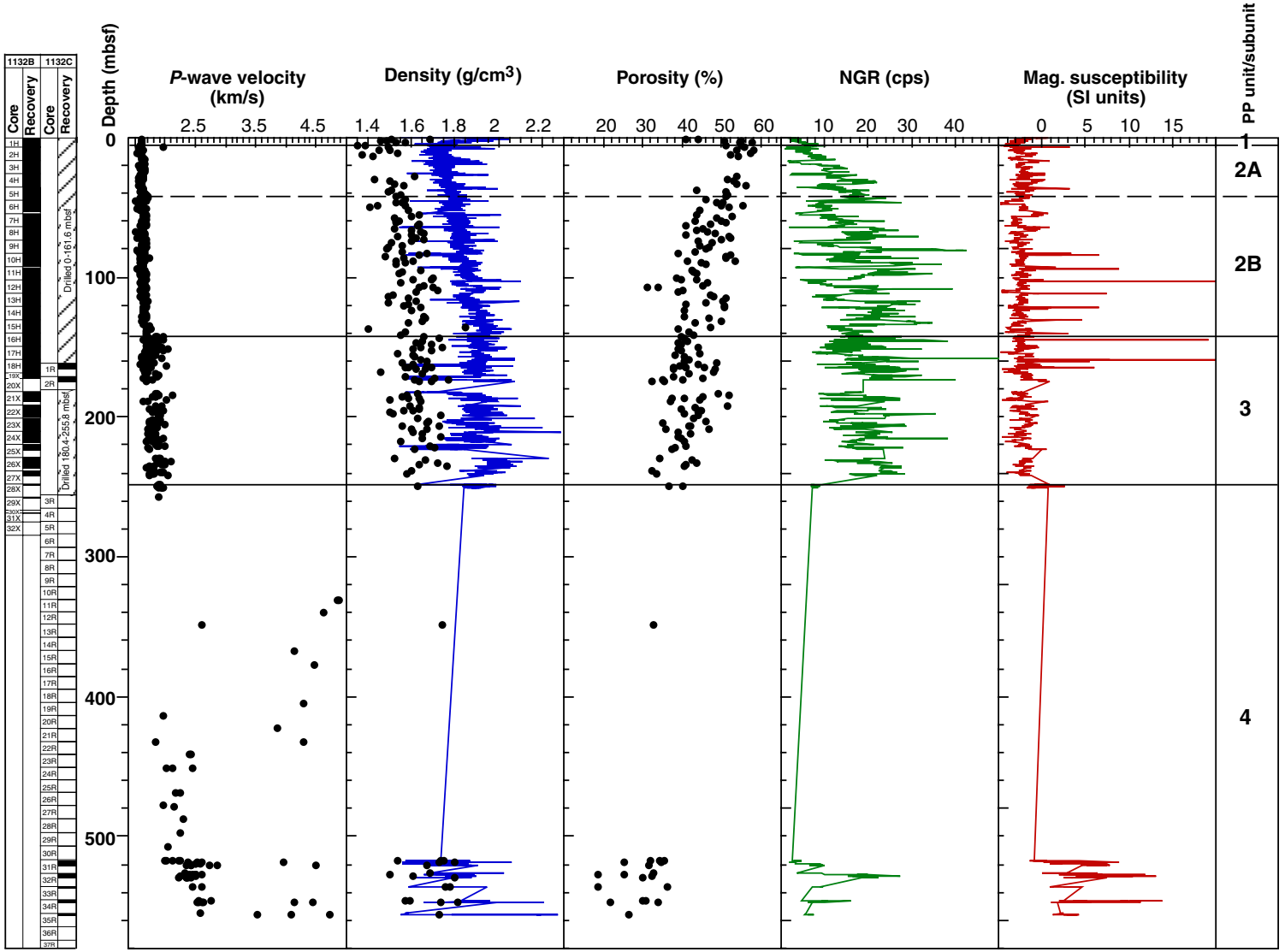

**Figure F21.** Shear strength data from Site 1132.

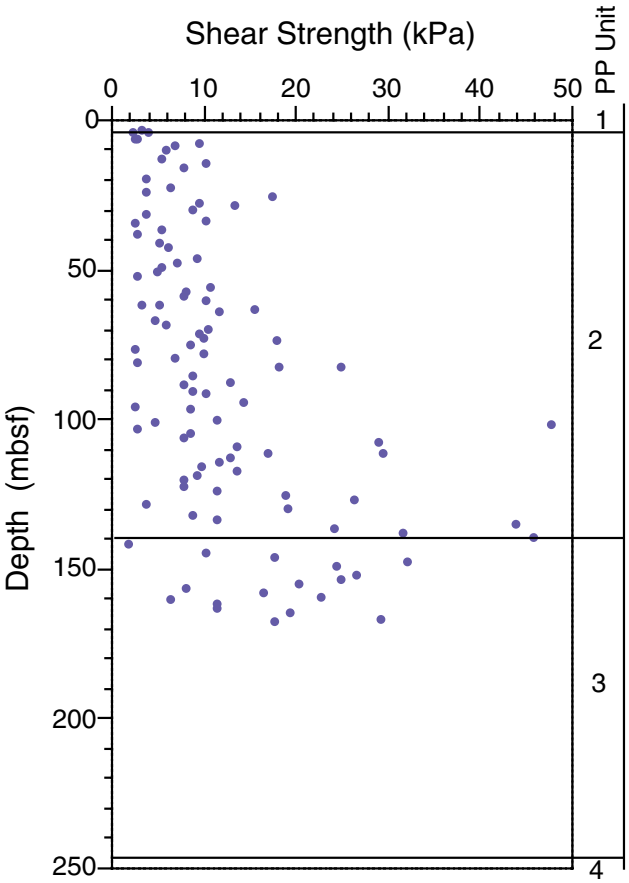

**Figure F22.** Thermal conductivity and gamma-ray attenuation (GRA) bulk density data from Site 1132.

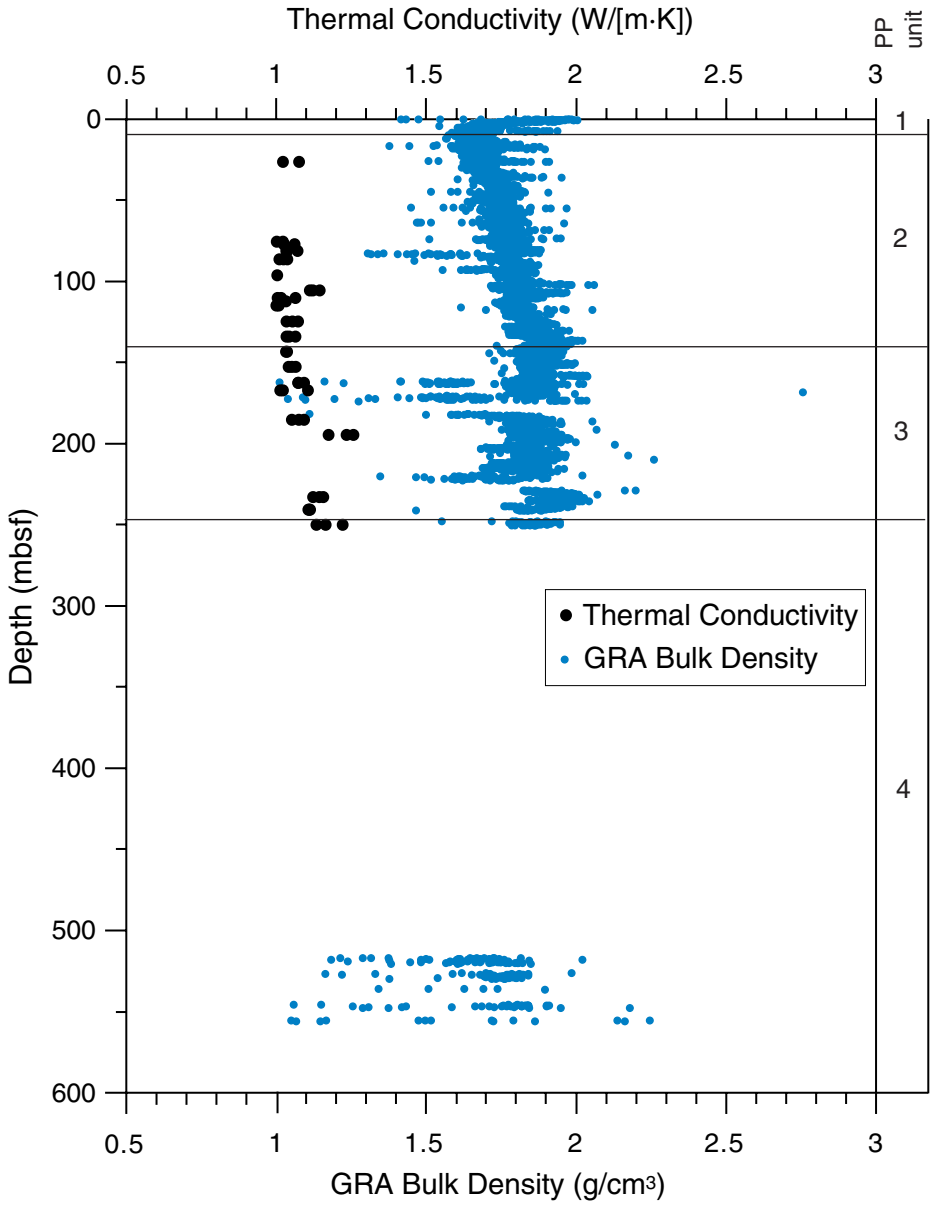

**Figure F23.** Variation of formation temperature with depth below seafloor for Site 1132. Expendable bathythermograph seafloor temperature = blue squares, mudline temperature from DVTP and Adara tools = green circles, Adara formation temperatures = red diamonds, and DVTP formation temperatures = purple triangles. Duplicate determinations are from different line fits to the temperature decay curve.

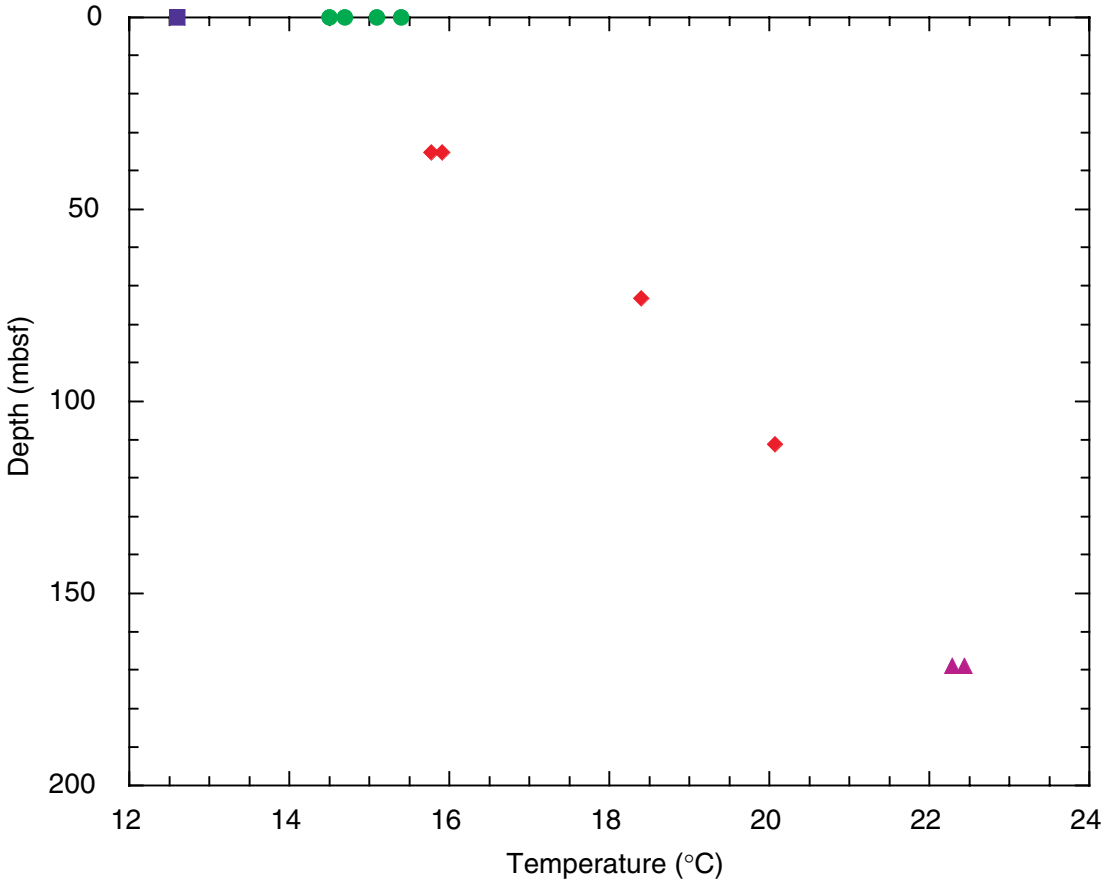

**Figure F24.** Summary of logging runs at Hole 1132C. Logging speed for both runs was 275 m/hr. Triple combo = triple combination logging tool; FMS = Formation MicroScanner; TD = total depth. See **"Downhole Measurements,"** p. 25, in the "Explanatory Notes" chapter for a description of the tool strings.

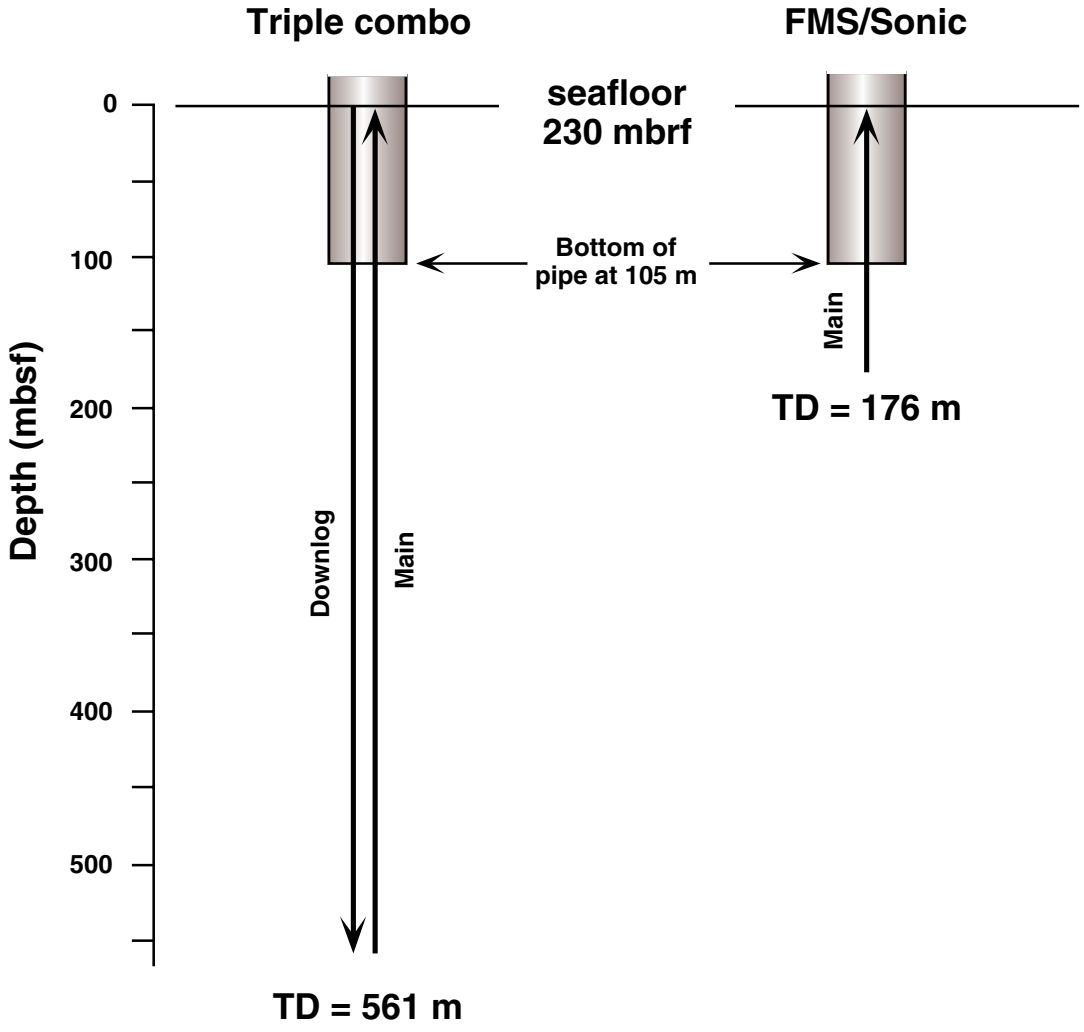

**Figure F25.** Summary of geophysical logs from the triple combination logging tool plotted vs. depth in the open-hole logged interval. The data plotted from left to right are core recovery; caliper and total gamma radiation (HSGR); porosity and density, scaled so that the two curves will coincide for a clean limestone; shallow, medium, and deep resistivity; sonic velocity; logging units; lithostratigraphic units; and biostratigraphic ages.

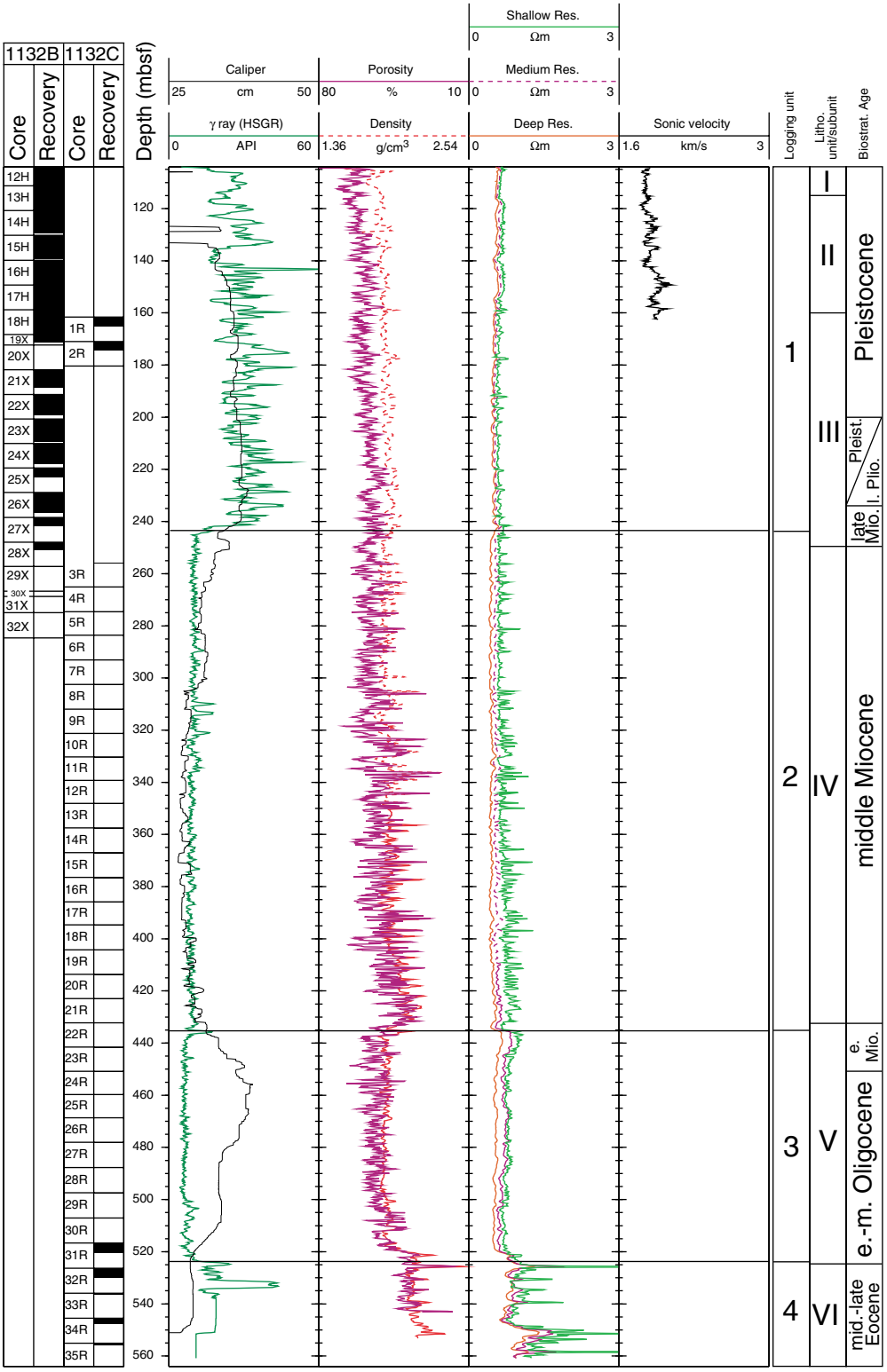

**Figure F26.** Summary of spectral gamma-ray logs plotted vs. depth for the open-hole logged interval. The data plotted from left to right are core recovery, total gamma radiation (HSGR) and computed (uranium-free) gamma radiation (HCGR), uranium, thorium, potassium and caliper, logging units, lithostratigraphic units, and biostratigraphic ages.

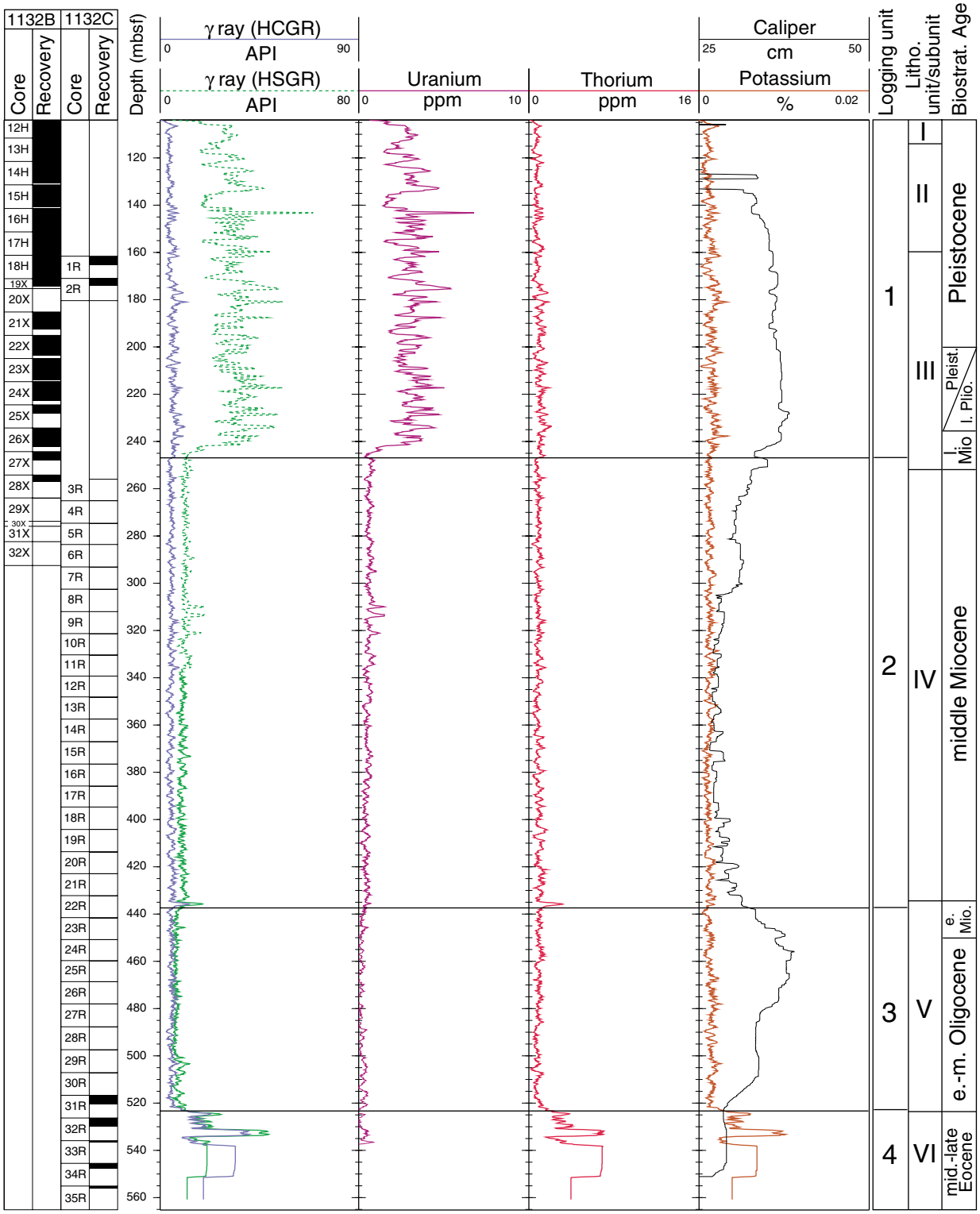

**Figure F27.** Summary of spectral gamma-ray logs plotted vs. depth (mbsf) for the interval logged through pipe. From left to right, columns are core recovery, total gamma radiation (HSGR) and computed (uranium-free) gamma radiation (HCGR), uranium, thorium, potassium, logging units, lithostratigraphic units, and biostratigraphic ages.

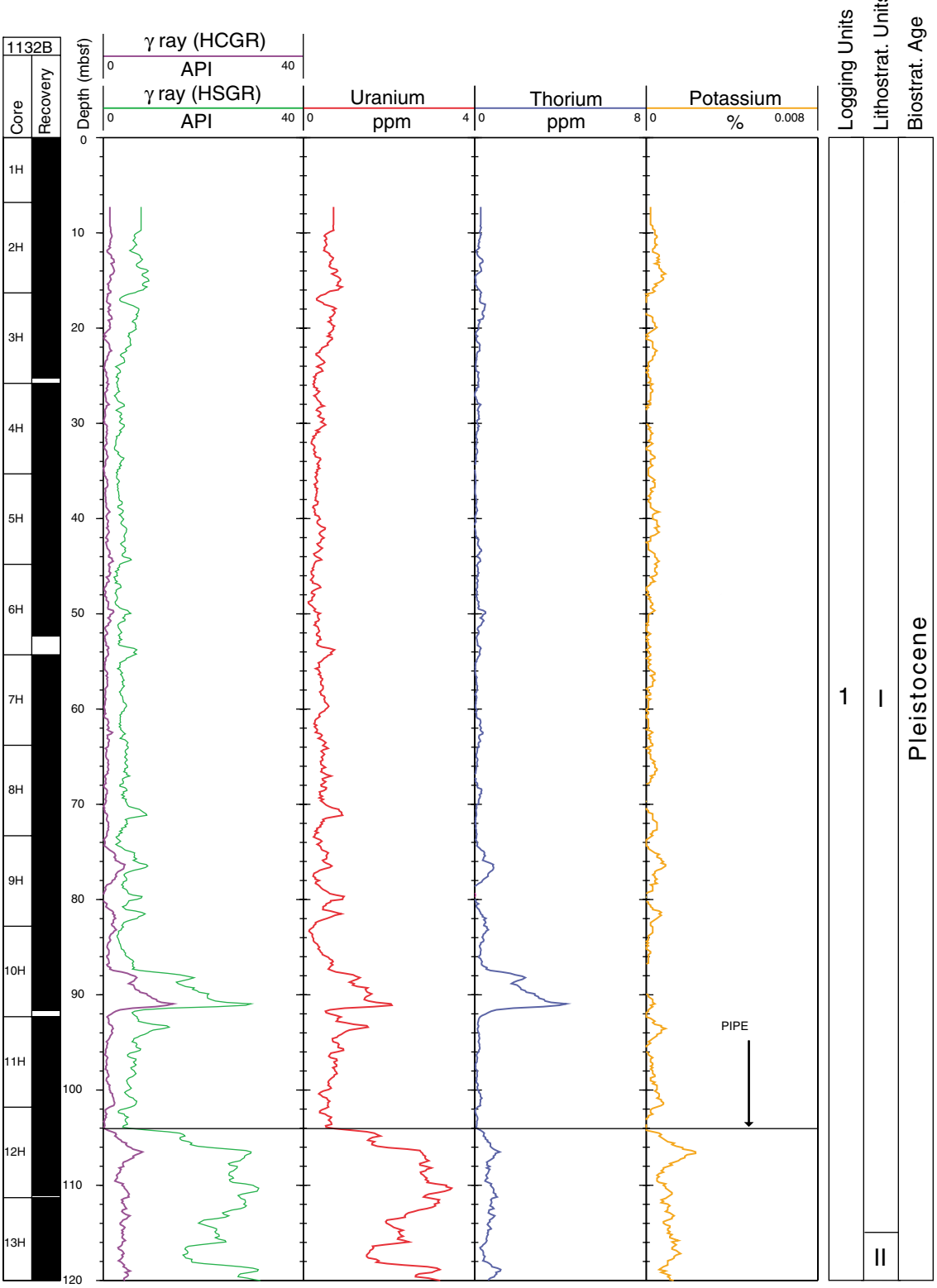

**Figure F28.** Seismic site-survey tracks for Site 1132 (Line AGSO169/13) in relation to other Leg 182 sites and the AGSO169 site-survey seismic lines. The bold trackline (part of AGSO169/13a) corresponds to the seismic line segment shown in Figure F29, p. 67.

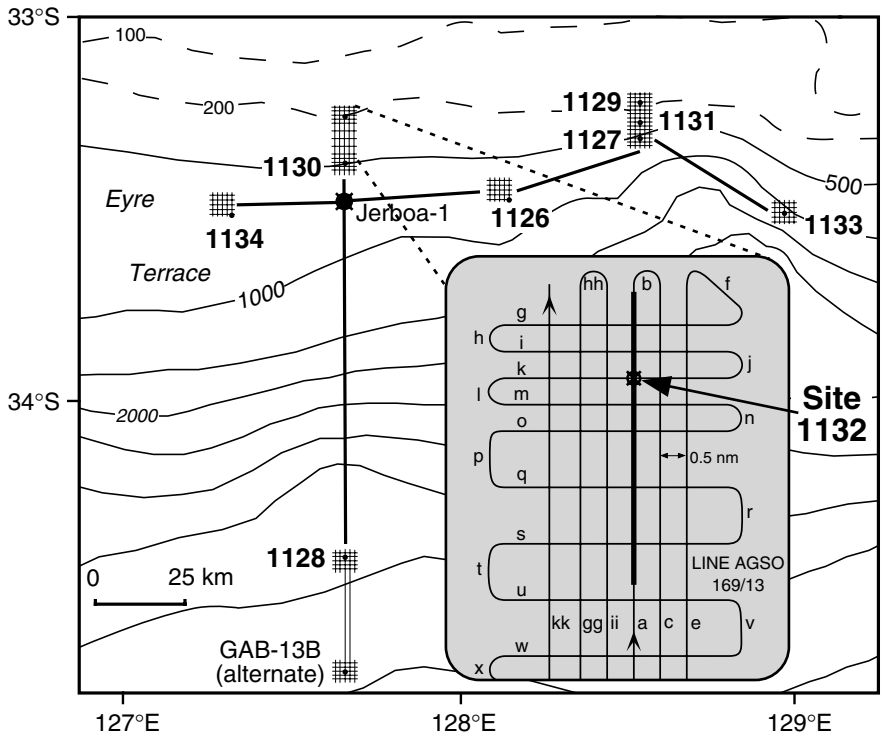

**Figure F29.** Portion of seismic Line AGSO169/13a showing interpreted seismic stratigraphic sequences predicted to be intersected at Site 1132, with planned (shown in white) and actual (shown in black) drill penetration. Note that the predicted seismic stratigraphy presented here is considerably different from the postdrill inferred stratigraphy presented in Figure **F31**, p. 69.

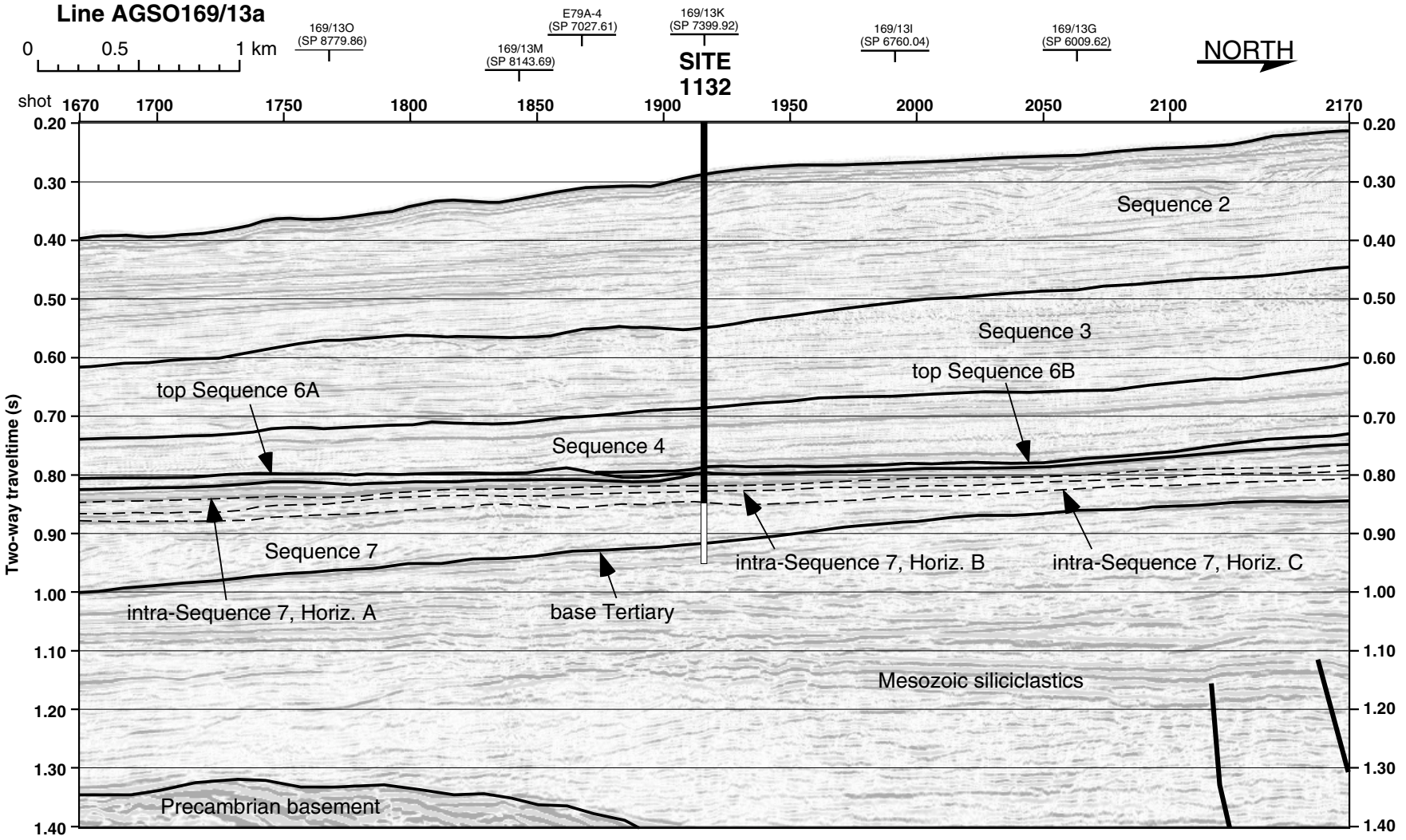

**Figure F30. A.** Plot showing relationship between predicted depths to seismic horizons and sequence boundaries (dashed) and corrected depths (arrowed) for Site 1132. In the absence of either a check-shot survey or a useful integrated sonic curve, this depth correction is based on an inference that the time–depth correlation line should fall immediately below the envelope of stacking velocity curves derived from six common depth points from site-survey seismic data immediately adjacent to this site, as was the case at Site 1130. **B.** Because of operational problems, the sonic tool could only be run over a small portion of the hole, and only a small segment of integrated sonic log, based on interval transit time data, can be plotted on A (heavy dashed line).

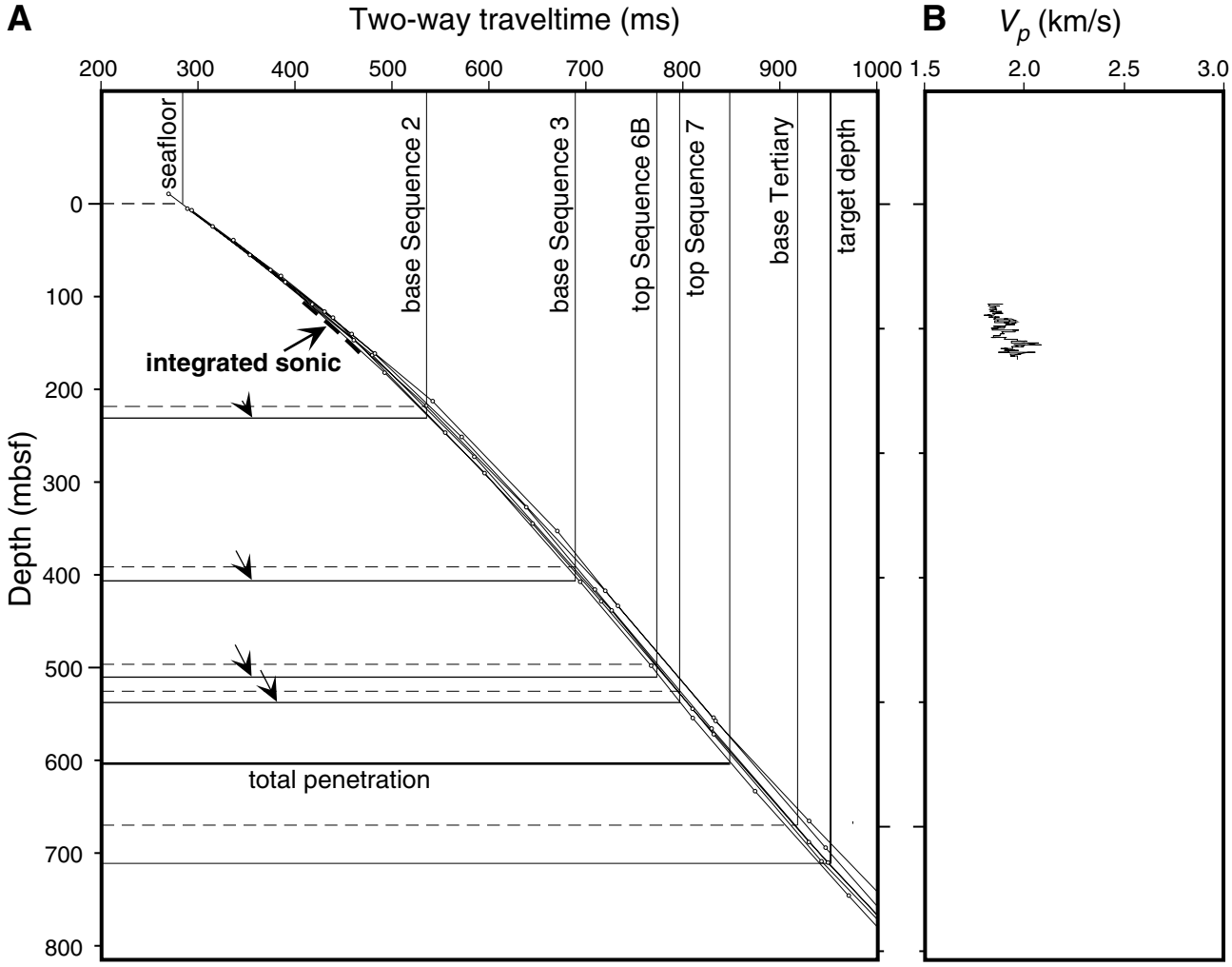

**Figure F31.** Tentative summary correlation between lithostratigraphic units, seismic sequences, biostratigraphic hiatuses, and ages at Site 1132. Note that the seismic stratigraphy inferred here is considerably different from the predicted stratigraphy presented in Figure F29, p. 67. NR = no recovery; ? in "Hiatuses" column = seismic data show missing section corresponding to these surfaces, although biostratigraphic data provide no constraint on the length of missing time.

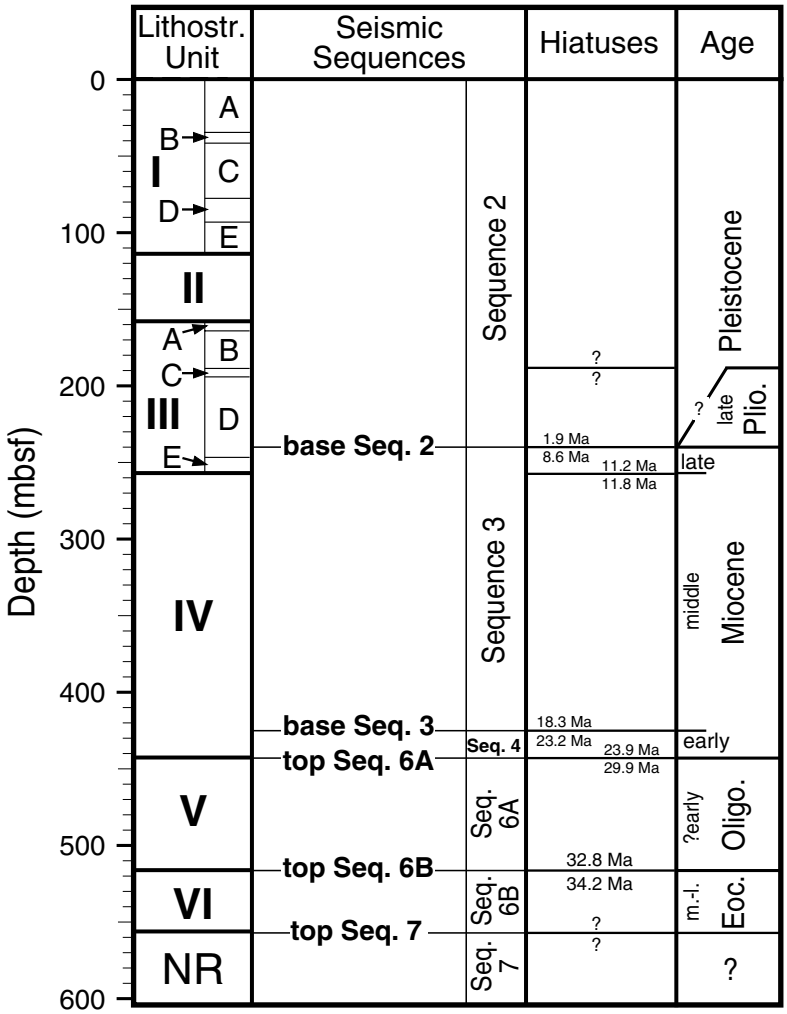

**Table T1.** Site 1132 coring summary. (See table note. Continued on next page.)

**Hole 1132A**

Latitude: –33.315950° (33°18.9570′S)
Longitude: 127.602170° (127°36.1302′E)
Seafloor (drill-pipe measurement from rig floor, mbrf): 229.7
Distance between rig floor and sea level (m): 11.7
Water depth (drill-pipe measurement from sea level, m): 218.0
Total depth (from rig floor, mbrf): 239.0
Penetration (mbsf): 9.3
Total number of cores: 1
Total core recovered (m): 9.23
Core recovery (%): 99.3

**Hole 1132B**

Latitude: –33.316190° (33°18.9714′S)
Longitude: 127.602200° (127°36.1320′E)
Seafloor (drill-pipe measurement from rig floor, mbrf): 230.2
Distance between rig floor and sea level (m): 11.7
Water depth (drill-pipe measurement from sea level, m): 218.5
Total depth (from rig floor): 514.8 mbrf
Penetration (mbsf): 284.6
Total number of cores: 32
Total length of cored section (m): 284.6
Total core recovered (m): 217.35
Core recovery (%): 76.37

**Hole 1132C**

Latitude: –33.316040° (33°18.9624′S)
Longitude: 127.602060° (127°36.1236′E)
Seafloor (drill-pipe measurement from rig floor, mbrf): 230.2
Distance between rig floor and sea level (m): 11.7
Water depth (drill-pipe measurement from sea level, m): 218.5
Total depth (from rig floor, mbrf): 833.4
Penetration (mbsf): 603.2
Total number of cores: 39
Total length of cored section (m): 366.2
Total number of drilled intervals: 2
Total length of drilled intervals (m): 237.0
Total core recovered (m): 22.42
Core recovery (%): 6.1

| Core | Date (Nov 1998) | Time (UTC + 8 hr) | Depth (mbsf) | Length cored (m) | Length recovered (m) | Recovery (%) | Comment |
|---|---|---|---|---|---|---|---|
| 182-1132A- | | | | | | | |
| 1H | 21 | 0105 | 0.00–9.30 | 9.3 | 9.23 | 99.3 | |
| Totals: | | | | 9.3 | 9.23 | 99.3 | |
| 182-1132B- | | | | | | | |
| 1H | 21 | 0145 | 0.00–6.80 | 6.8 | 6.78 | 99.7 | |
| 2H | 21 | 0210 | 6.80–16.30 | 9.5 | 9.42 | 99.2 | |
| 3H | 21 | 0315 | 16.30–25.80 | 9.5 | 8.97 | 94.4 | Oriented; nonmagnetic shoe |
| 4H | 21 | 0430 | 25.80–35.30 | 9.5 | 9.58 | 100.8 | Oriented; Adara |
| 5H | 21 | 0505 | 35.30–44.80 | 9.5 | 9.53 | 100.3 | $H_2S$; oriented; nonmagnetic shoe |
| 6H | 21 | 0545 | 44.80–54.30 | 9.5 | 7.58 | 79.8 | $H_2S$; oriented |
| 7H | 21 | 0625 | 54.30–63.80 | 9.5 | 9.84 | 103.6 | $H_2S$; oriented; nonmagnetic shoe |
| 8H | 21 | 0725 | 63.80–73.30 | 9.5 | 9.55 | 100.5 | $H_2S$; oriented; Adara |
| 9H | 21 | 0815 | 73.30–82.80 | 9.5 | 9.63 | 101.4 | $H_2S$; oriented; nonmagnetic shoe |
| 10H | 21 | 0855 | 82.80–92.30 | 9.5 | 8.88 | 93.5 | $H_2S$; oriented |
| 11H | 21 | 0940 | 92.30–101.80 | 9.5 | 9.48 | 99.8 | $H_2S$; oriented; nonmagnetic shoe |
| 12H | 21 | 1045 | 101.80–111.30 | 9.5 | 9.33 | 98.2 | $H_2S$; oriented; Adara |
| 13H | 21 | 1140 | 111.30–120.80 | 9.5 | 9.80 | 103.2 | $H_2S$; oriented; nonmagnetic shoe |
| 14H | 21 | 1215 | 120.80–130.30 | 9.5 | 8.83 | 93.0 | $H_2S$; oriented |
| 15H | 21 | 1310 | 130.30–139.80 | 9.5 | 8.90 | 93.7 | $H_2S$; oriented |
| 16H | 21 | 1350 | 139.80–149.30 | 9.5 | 10.16 | 107.0 | $H_2S$; oriented |
| 17H | 21 | 1440 | 149.30–158.80 | 9.5 | 9.81 | 103.3 | $H_2S$; oriented |
| 18H | 21 | 1540 | 158.80–168.30 | 9.5 | 9.61 | 101.2 | $H_2S$; oriented |
| 19X | 21 | 1730 | 168.30–172.30 | 4.0 | 2.99 | 74.8 | $H_2S$; DVTP |
| 20X | 21 | 1800 | 172.30–181.80 | 9.5 | 0.00 | 0.0 | No recovery |
| 21X | 21 | 1835 | 181.80–191.30 | 9.5 | 6.86 | 72.2 | $H_2S$ |
| 22X | 21 | 1910 | 191.30–200.70 | 9.4 | 8.15 | 86.7 | $H_2S$ |

Table T1 (continued).

| Core | Date (Nov 1998) | Time (UTC + 8 hr) | Depth (mbsf) | Length cored (m) | Length recovered (m) | Recovery (%) | Comment |
|---|---|---|---|---|---|---|---|
| 23X | 21 | 1945 | 200.70–210.10 | 9.4 | 8.22 | 87.5 | $H_2S$ |
| 24X | 21 | 2020 | 210.10–219.50 | 9.4 | 7.83 | 83.3 | $H_2S$ |
| 25X | 21 | 2050 | 219.50–228.90 | 9.4 | 3.44 | 36.6 | $H_2S$ |
| 26X | 21 | 2130 | 228.90–238.50 | 9.6 | 7.68 | 80.0 | $H_2S$ |
| 27X | 21 | 2205 | 238.50–247.90 | 9.4 | 3.33 | 35.4 | $H_2S$ |
| 28X | 21 | 2255 | 247.90–257.20 | 9.3 | 2.86 | 30.8 | $H_2S$ |
| 29X | 21 | 2330 | 257.20–266.70 | 9.5 | 0.26 | 2.7 | |
| 30X | 22 | 0015 | 266.70–268.70 | 2.0 | 0.01 | 0.5 | |
| 31X | 22 | 0110 | 268.70–275.00 | 6.3 | 0.03 | 0.5 | All to PALEO |
| 32X | 22 | 0150 | 275.00–284.60 | 9.6 | 0.01 | 0.1 | All to PALEO |
| Totals: | | | | 284.6 | 217.35 | 76.4 | |
| 182-1132C- | | | | | | | |
| | | ****Drilled from 0 to 161.60 mbsf**** | | | | | |
| 1R | 22 | 1205 | 161.60–171.00 | 9.4 | 3.60 | 38.3 | Minor $H_2S$ |
| 2R | 22 | 1240 | 171.00–180.40 | 9.4 | 3.20 | 34.0 | Minor $H_2S$ |
| | | ****Drilled from 180.40 to 255.80 mbsf**** | | | | | |
| 3R | 22 | 1530 | 255.80–265.10 | 9.3 | 0.16 | 1.7 | |
| 4R | 22 | 1600 | 265.10–274.60 | 9.5 | 0.06 | 0.6 | |
| 5R | 22 | 1620 | 274.60–283.60 | 9.0 | 0.07 | 0.8 | |
| 6R | 22 | 1645 | 283.60–293.10 | 9.5 | 0.03 | 0.3 | |
| 7R | 22 | 1710 | 293.10–302.50 | 9.4 | 0.12 | 1.3 | |
| 8R | 22 | 1750 | 302.50–312.00 | 9.5 | 0.13 | 1.4 | |
| 9R | 22 | 1810 | 312.00–321.30 | 9.3 | 0.04 | 0.4 | |
| 10R | 22 | 1845 | 321.30–330.30 | 9.0 | 0.13 | 1.4 | |
| 11R | 22 | 1915 | 330.30–339.30 | 9.0 | 0.30 | 3.3 | |
| 12R | 22 | 1945 | 339.30–348.10 | 8.8 | 0.16 | 1.8 | |
| 13R | 22 | 2005 | 348.10–357.50 | 9.4 | 0.21 | 2.2 | |
| 14R | 22 | 2115 | 357.50–367.00 | 9.5 | 0.12 | 1.3 | |
| 15R | 22 | 2155 | 367.00–376.50 | 9.5 | 0.20 | 2.1 | |
| 16R | 22 | 2230 | 376.50–385.80 | 9.3 | 0.30 | 3.2 | |
| 17R | 22 | 2310 | 385.80–394.70 | 8.9 | 0.12 | 1.4 | |
| 18R | 22 | 2340 | 394.70–404.20 | 9.5 | 0.24 | 2.5 | |
| 19R | 23 | 0025 | 404.20–413.60 | 9.4 | 0.15 | 1.6 | |
| 20R | 23 | 0100 | 413.60–422.90 | 9.3 | 0.25 | 2.7 | |
| 21R | 23 | 0140 | 422.90–432.20 | 9.3 | 0.26 | 2.8 | |
| 22R | 23 | 0215 | 432.20–441.50 | 9.3 | 0.13 | 1.4 | |
| 23R | 23 | 0250 | 441.50–450.80 | 9.3 | 0.21 | 2.3 | |
| 24R | 23 | 0330 | 450.80–459.70 | 8.9 | 0.17 | 1.9 | |
| 25R | 23 | 0415 | 459.70–468.60 | 8.9 | 0.12 | 1.4 | |
| 26R | 23 | 0445 | 468.60–478.00 | 9.4 | 0.22 | 2.3 | |
| 27R | 23 | 0525 | 478.00–487.70 | 9.7 | 0.20 | 2.1 | |
| 28R | 23 | 0600 | 487.70–497.40 | 9.7 | 0.21 | 2.2 | |
| 29R | 23 | 0640 | 497.40–507.10 | 9.7 | 0.26 | 2.7 | |
| 30R | 23 | 0720 | 507.10–516.70 | 9.6 | 0.19 | 2.0 | |
| 31R | 23 | 0810 | 516.70–526.30 | 9.6 | 3.92 | 40.8 | |
| 32R | 23 | 0855 | 526.30–535.90 | 9.6 | 3.45 | 35.9 | |
| 33R | 23 | 0945 | 535.90–545.50 | 9.6 | 0.57 | 5.9 | |
| 34R | 23 | 1025 | 545.50–555.10 | 9.6 | 2.07 | 21.6 | |
| 35R | 23 | 1125 | 555.10–564.80 | 9.7 | 0.85 | 8.8 | |
| 36R | 23 | 1220 | 564.80–574.40 | 9.6 | 0.00 | 0.0 | No recovery |
| 37R | 23 | 1255 | 574.40–584.00 | 9.6 | 0.00 | 0.0 | No recovery |
| 38R | 23 | 1325 | 584.00–593.60 | 9.6 | 0.00 | 0.0 | No recovery |
| 39R | 23 | 1355 | 593.60–603.20 | 9.6 | 0.00 | 0.0 | No recovery |
| Coring totals: | | | | 366.2 | 22.42 | 6.1 | |
| Drilled total: | | | | 237.0 | | | |
| Total: | | | | 603.2 | | | |

Note: UTC = Universal Time Coordinated, Adara = Adara temperature tool, DVTP = Davis-Villinger temperature probe, PALEO = Paleontology Laboratory.

**Table T2.** Datum levels used for the calculation of the Site 1132 sedimentation rate.

| Datum type | Datum level | Age (Ma) | Midpoint (mbsf) | Stratigraphic error (m) | Fossil group | Datum level code | Upper sample | | Lower sample | |
|---|---|---|---|---|---|---|---|---|---|---|
| | | | | | | | Core, section, interval (cm) | Depth (mbsf) | Core, section, interval (cm) | Depth (mbsf) |
| | | | | | | | 182-1132B- | | 182-1132B- | |
| T | *P. lacunosa* | 0.45 | 116.12 | 4.99 | 1 | 1 | 12H-CC, 4-7 | 111.10 | 13H-CC, 0-5 | 121.05 |
| T | *G. tosaensis* | 0.65 | 134.42 | 4.79 | 4 | 2 | 14H-CC, 6-9 | 129.60 | 15H-CC, 14-17 | 139.17 |
| | Brunhes/Matuyama | 0.78 | 184.05 | 0.75 | | 3 | 19X | 170 | 21X | 181 |
| B | *G. truncatulinoides* | 2 | 194.03 | 5.40 | 4 | 4 | 21X-CC, 28-31 | 188.63 | 22X-CC, 33-36 | 199.42 |
| T | *C. macintyrei* | 1.67 | 220.44 | 2.51 | 1 | 5 | 24X-CC, 33-36 | 217.90 | 25X-2, 134-136 | 222.34 |
| | Top of Jaramillo | 0.99 | 221.72 | 0.72 | | 6 | | | | |
| B | *G. plesiotumida* | 8.3 | 246.27 | 4.46 | 4 | 7 | 27X-CC, 34-37 | 241.80 | 28X-CC, 32-35 | 250.73 |
| T | *R. pseudoumbilicus* | 3.75 | 246.30 | 4.46 | 1 | 8 | 27X-CC, 34-37 | 241.80 | 28X-CC, 32-35 | 250.73 |
| T | *Z. nepenthes* | 4.2 | 246.30 | 4.46 | 4 | 9 | 27X-CC, 34-37 | 241.80 | 28X-CC, 32-35 | 250.73 |
| T | *G. cibaoensis* | 4.6 | 246.30 | 4.46 | 4 | 10 | 27X-CC, 34-37 | 241.80 | 28X-CC, 32-35 | 250.73 |
| T | *G. dehiscens* | 5.8 | 246.30 | 4.46 | 4 | 11 | 27X-CC, 34-37 | 241.80 | 28X-CC, 32-35 | 250.73 |
| B | *Z. nepenthes* | 11.8 | 254.08 | 3.35 | 4 | 12 | 27X-CC, 34-37 | 241.80 | 28X-CC, 32-35 | 250.73 |
| | | | | | | | 182-1132C- | | 182-1132C- | |
| T | *S. heteromorphus* | 13.6 | 352.87 | 4.75 | 1 | 13 | 13R-CC, 0-2 | 348.10 | 14R-CC, 10-12 | 357.60 |
| B | *S. heteromorphus* | 18.2 | 418.48 | 4.66 | 1 | 14 | 20R-CC, 22-25 | 413.82 | 21R-CC, 23-26 | 423.13 |
| B | *G. dehiscens* | 23.2 | 446.31 | 4.63 | 4 | 15 | 23R-CC, 18-21 | 441.68 | 24R-CC, 14-17 | 450.94 |
| T | *D. bisectus* | 23.9 | 446.30 | 4.60 | 1 | 16 | | | | |
| T | *C. altus* | 26.1 | 483.06 | 4.86 | 1 | 17 | 27R-CC, 17-20 | 478.17 | 28R-CC, 20-21 | 487.90 |
| T | *R. umbilicus* | 32.3 | 513.94 | 6.67 | 1 | 18 | 30R-CC, 17-19 | 507.27 | 31R-CC, 16-18 | 520.60 |

Notes: T = top of taxon stratigraphic range, B = bottom of taxon stratigraphic range. Midpoint = is the middle depth between the sample where the taxon occurs and the adjacent sample where it does not occur. Stratigraphic error = one-half the distance between these two samples. Datum level code = the number assigned to the datum level on Figure **F10,** p. 48. Fossil groups: 1 = calcareous nannofossils, 4 = planktonic foraminifers.

**Table T3.** Composition of headspace gases, Holes 1132B and 1132C.

| Core, section | Depth (mbsf) | $CO_2$ (ppmv) | $H_2S$ (ppmv) | $C_1$ (ppmv) | $C_2$ (ppmv) | $C_1/C_2$ |
|---|---|---|---|---|---|---|
| 182-1132B- | | | | | | |
| 1H-4 | 4.50 | NA | NA | 2 | | |
| 2H-4 | 11.30 | NA | NA | 2 | | |
| 3H-4 | 20.80 | NA | NA | 2 | | |
| 4H-4 | 30.30 | NA | NA | 2 | | |
| 5H-4 | 39.80 | NA | NA | 3 | | |
| 6H-4 | 49.30 | NA | NA | 9 | | |
| 7H-4 | 58.80 | NA | NA | 20 | 1 | 20 |
| 8H-4 | 68.30 | 13,195 | 1,430 | 17 | 1 | 17 |
| 9H-4 | 77.80 | 15,426 | 1,324 | 22 | 1 | 17 |
| 10H-4 | 87.30 | 21,693 | 1,588 | 40 | 3 | 15 |
| 11H-4 | 96.80 | 18,900 | 1,496 | 30 | 2 | 14 |
| 12H-4 | 106.30 | 15,286 | 698 | 36 | 3 | 13 |
| 13H-4 | 115.80 | 25,378 | 1,389 | 52 | 4 | 12 |
| 14H-4 | 125.30 | 16,025 | 136 | 38 | 4 | 11 |
| 15H-4 | 134.80 | 12,396 | | 32 | 3 | 11 |
| 16H-4 | 144.30 | 22,781 | | 48 | 5 | 10 |
| 17H-4 | 153.30 | 17,511 | | 43 | 4 | 10 |
| 18H-4 | 163.30 | 11,282 | | 32 | 4 | 9 |
| 19X-2 | 169.80 | 10,347 | | 20 | 2 | 9 |
| 21X-4 | 186.30 | 17,158 | | 33 | 4 | 9 |
| 22X-4 | 195.80 | 13,484 | | 25 | 3 | 8 |
| 23X-4 | 205.20 | 8,255 | | 17 | 2 | 9 |
| 24X-4 | 214.60 | NA | NA | 33 | 4 | 8 |
| 25X-2 | 221.00 | NA | NA | 20 | 2 | 9 |
| 26X-4 | 233.40 | NA | NA | 19 | 2 | 9 |
| 27X-2 | 240.00 | NA | NA | 18 | 2 | 11 |
| 28X-2 | 249.40 | NA | NA | 12 | 1 | 14 |
| 29X-CC | 257.20 | NA | NA | 6 | | |
| 182-1132C- | | | | | | |
| 1R-1 | 161.60 | 13,286 | | 41 | 5 | 9 |
| 2R-2 | 172.50 | 15,712 | | 54 | 7 | 8 |
| 28R-CC | 487.70 | NA | NA | 2 | | |
| 29R-CC | 497.40 | NA | NA | 3 | | |
| 31R-1 | 518.23 | NA | NA | 2 | | |
| 32R-2 | 527.67 | NA | NA | 2 | | |
| 34R-1 | 547.00 | NA | NA | 2 | | |
| 35R-1 | 555.92 | NA | NA | 2 | | |

Notes: NA = not analyzed; blank = not detected.

**Table T4.** Calcium carbonate ($CaCO_3$), organic carbon ($C_{org}$), nitrogen (N), and sulfur (S) data, Hole 1132B. (See table notes. Continued on next page.)

| Core, section, interval (cm) | Depth (mbsf) | $CaCO_3$ (wt%) | $C_{org}$ (wt%) | N (wt%) | S (wt%) |
|---|---|---|---|---|---|
| 182-1132B- | | | | | |
| 1H-1, 60-61 | 0.60 | 93.5 | 0.34 | | 0.02 |
| 1H-3, 60-61 | 3.60 | 93.1 | NA | NA | NA |
| 1H-5, 60-61 | 6.60 | 93.1 | 0.48 | 0.07 | 0.02 |
| 2H-1, 60-61 | 7.40 | 94.9 | 0.18 | | 0.13 |
| 2H-3, 60-61 | 10.40 | 93.0 | NA | NA | NA |
| 2H-5, 60-61 | 13.40 | 92.2 | 0.51 | 0.06 | |
| 3H-1, 60-61 | 16.90 | 95.6 | 0.19 | 0.03 | 0.19 |
| 3H-3, 60-61 | 19.90 | 91.8 | NA | NA | NA |
| 3H-5, 60-61 | 22.90 | 92.0 | 0.51 | 0.06 | |
| 4H-1, 60-61 | 26.40 | 94.0 | 0.26 | | 0.25 |
| 4H-3, 60-61 | 29.40 | 90.3 | NA | NA | NA |
| 4H-5, 60-61 | 32.40 | 91.6 | 0.54 | 0.07 | |
| 5H-3, 60-61 | 38.90 | 91.9 | 0.36 | 0.05 | |
| 5H-5, 60-61 | 41.90 | 93.6 | 0.31 | 0.05 | |
| 6H-1, 60-61 | 45.40 | 92.1 | 0.54 | 0.06 | 0.21 |
| 6H-3, 60-61 | 48.40 | 91.3 | NA | NA | NA |
| 6H-5, 60-61 | 51.40 | 92.0 | 0.52 | 0.06 | |
| 7H-1, 95-96 | 55.25 | 92.4 | 0.64 | 0.06 | |
| 7H-3, 60-61 | 57.90 | 91.0 | NA | NA | NA |
| 7H-5, 60-61 | 60.90 | 91.2 | 0.60 | 0.06 | |
| 8H-1, 60-61 | 64.40 | 90.7 | 0.67 | 0.08 | |
| 8H-3, 60-61 | 67.40 | 90.5 | NA | NA | NA |
| 8H-5, 60-61 | 70.40 | 92.6 | 0.52 | 0.05 | |
| 9H-1, 60-61 | 73.90 | 94.9 | 0.47 | 0.04 | 0.08 |
| 9H-3, 60-61 | 76.90 | 92.4 | NA | NA | NA |
| 9H-5, 60-61 | 79.90 | 91.2 | 0.46 | 0.05 | |
| 10H-3, 60-61 | 86.40 | 92.6 | 0.38 | 0.05 | |
| 10H-5, 60-61 | 89.40 | 90.4 | 0.71 | 0.06 | 0.22 |
| 11H-3, 60-61 | 95.90 | 91.4 | 0.41 | 0.03 | |
| 11H-5, 60-61 | 98.90 | 92.8 | 0.44 | | |
| 12H-1, 60-61 | 102.40 | 90.7 | 0.42 | | |
| 12H-3, 60-61 | 105.40 | 90.1 | NA | NA | NA |
| 12H-5, 60-61 | 108.40 | 92.8 | 0.23 | | |
| 13H-1, 60-61 | 111.90 | 92.6 | 0.39 | 0.04 | |
| 13H-3, 60-61 | 114.90 | 92.2 | NA | NA | NA |
| 13H-5, 60-61 | 117.90 | 89.9 | 0.71 | 0.05 | |
| 14H-1, 60-61 | 121.40 | 92.5 | 0.33 | | |
| 14H-3, 60-61 | 124.40 | 91.3 | NA | NA | NA |
| 14H-5, 60-61 | 127.40 | 91.6 | 0.46 | 0.05 | |
| 15H-1, 60-61 | 130.90 | 91.3 | 0.24 | 0.04 | |
| 15H-3, 60-61 | 133.90 | 87.3 | NA | NA | NA |
| 15H-5, 60-61 | 136.90 | 93.2 | 0.15 | | |
| 16H-1, 60-61 | 140.40 | 92.9 | 0.22 | | |
| 16H-3, 60-61 | 143.40 | 91.4 | NA | NA | NA |
| 16H-5, 60-61 | 146.40 | 90.0 | 0.51 | 0.05 | |
| 17H-1, 60-61 | 149.90 | 91.4 | 0.40 | | |
| 17H-3, 60-61 | 152.40 | 90.5 | NA | NA | NA |
| 17H-5, 60-61 | 155.40 | 89.7 | 0.50 | 0.06 | |
| 18H-1, 60-61 | 159.40 | 92.3 | 0.43 | | |
| 18H-3, 60-61 | 162.40 | 91.3 | NA | NA | NA |
| 18H-5, 60-61 | 165.40 | 91.1 | 0.32 | 0.03 | |
| 19X-1, 60-61 | 168.90 | 91.4 | 0.48 | 0.04 | |
| 21X-1, 60-61 | 182.40 | 89.9 | 0.35 | 0.05 | |
| 21X-3, 60-61 | 185.40 | 88.5 | NA | NA | NA |
| 22X-1, 60-61 | 191.90 | 86.9 | 0.80 | | |
| 22X-3, 60-61 | 194.90 | 90.3 | NA | NA | NA |
| 22X-5, 60-61 | 197.90 | 89.0 | 0.55 | | |
| 23X-1, 60-61 | 201.30 | 88.0 | 0.46 | | |
| 23X-3, 60-61 | 204.30 | 86.6 | NA | NA | NA |
| 23X-5, 60-61 | 207.30 | 87.4 | 0.37 | | |
| 24X-1, 60-61 | 210.70 | 88.6 | 0.76 | 0.05 | |
| 24X-3, 60-61 | 213.70 | 88.9 | NA | NA | NA |
| 24X-5, 60-61 | 216.70 | 87.0 | 0.47 | | |
| 25X-1, 60-61 | 220.10 | 90.7 | 0.56 | | |
| 26X-1, 60-61 | 229.50 | 85.9 | 0.52 | 0.04 | |

Table T4 (continued).

| Core, section, interval (cm) | Depth (mbsf) | $CaCO_3$ (wt%) | $C_{org}$ (wt%) | N (wt%) | S (wt%) |
|---|---|---|---|---|---|
| 26X-3, 60-61 | 232.50 | 89.7 | NA | NA | NA |
| 26X-5, 60-61 | 235.50 | 85.9 | 0.53 | 0.04 | |
| 27X-1, 60-61 | 239.10 | 86.9 | 0.65 | | |
| 28X-1, 60-61 | 248.50 | 90.5 | 0.17 | | |

Notes: NA = not analyzed, blank = not detected.

**Table T5.** Interstitial water geochemistry, Site 1132.

| Core, section, interval (cm) | Depth (mbsf) | pH | ppH | Alkalinity (mM) | Salinity | $Cl^-$ (mM) | $SO_4^{2-}$ (mM) | $Na^+$ (mM) | $K^+$ (mM) | $Mg^{2+}$ (mM) | $Ca^{2+}$ (mM) | $Sr^{2+}$ (μM) | $Li^+$ (μM) | $H_4SiO_4$ (μM) | $NH_4^+$ (μM) | $Fe^{2+}$ (μM) |
|---|---|---|---|---|---|---|---|---|---|---|---|---|---|---|---|---|
| 182-1132B- | | | | | | | | | | | | | | | | |
| 1H-3, 145-150 | 4.45 | 7.52 | 7.56 | 2.87 | 35.0 | 572 | 29.7 | 496 | 11.0 | 55.9 | 11.9 | 83 | 37 | 48 | 63 | 0.8 |
| 2H-3, 145-150 | 11.25 | 7.41 | 7.60 | 2.96 | 35.5 | 570 | 29.1 | 489 | 11.1 | 55.9 | 11.1 | 87 | 37 | 48 | 73 | 1.0 |
| 3H-3, 145-150 | 20.75 | 7.46 | 7.66 | 2.92 | 35.8 | 570 | 29.1 | 492 | 11.2 | 55.7 | 10.8 | 87 | 36 | 46 | 60 | 0.4 |
| 4H-3, 145-150 | 30.25 | 7.41 | 7.51 | 3.72 | 35.8 | 570 | 29.8 | 496 | 11.1 | 56.2 | 11.0 | 95 | 38 | 94 | 92 | 1.7 |
| 5H-3, 145-150 | 39.75 | 7.28 | 7.34 | 7.64 | 38.0 | 580 | 29.7 | 500 | 11.1 | 57.1 | 10.7 | 179 | 42 | 239 | 440 | 0.4 |
| 6H-3, 145-150 | 49.20 | 6.83 | 6.91 | 16.79 | 38.0 | 605 | 27.7 | 515 | 11.7 | 56.5 | 9.2 | 301 | 55 | 319 | 1675 | 3.3 |
| 7H-3, 145-150 | 58.75 | 6.72 | 6.67 | 24.26 | 40.0 | 639 | 24.0 | 557 | 12.1 | 52.8 | 9.1 | 256 | 66 | 505 | 3454 | 1.0 |
| 8H-3, 140-150 | 68.20 | 6.77 | 6.68 | 27.08 | 42.0 | 687 | 25.2 | 612 | 12.6 | 49.6 | 8.0 | 497 | 79 | 535 | 4445 | 2.8 |
| 9H-3, 145-150 | 77.70 | 6.68 | 6.62 | 28.05 | 44.0 | 721 | 28.7 | 644 | 12.9 | 49.8 | 9.2 | 557 | 88 | 547 | 5179 | 6.0 |
| 10H-3, 140-150 | 87.20 | 6.67 | | 26.36 | 46.0 | 764 | 31.3 | 704 | 15.8 | 51.0 | 9.0 | 578 | 89 | 612 | 6480 | 0.0 |
| 11H-3, 140-150 | 96.70 | 6.62 | 6.50 | 25.54 | 50.0 | 798 | 31.6 | 717 | 14.3 | 52.9 | 10.7 | 540 | 94 | 615 | 6355 | 0.0 |
| 12H-3, 140-150 | 106.20 | 6.65 | 6.66 | 24.33 | 52.0 | 836 | 33.6 | 756 | 14.4 | 53.6 | 11.1 | 501 | 86 | 721 | 6128 | 1.5 |
| 13H-3, 140-150 | 115.70 | 6.55 | 6.52 | 23.08 | 58.0 | 881 | 35.2 | 785 | 15.3 | 58.2 | 12.4 | 480 | 87 | 666 | 6422 | 0.0 |
| 14H-3, 140-150 | 125.20 | 6.55 | 6.57 | 23.34 | 56.0 | 914 | 41.8 | 814 | 14.9 | 62.5 | 13.5 | 472 | 81 | 620 | 6654 | 0.0 |
| 15H-3, 140-150 | 134.70 | 6.60 | 6.50 | 19.49 | 58.0 | 938 | 46.6 | 837 | 15.6 | 64.8 | 15.5 | 463 | 78 | 576 | 5550 | 0.0 |
| 17H-3, 140-150 | 153.20 | 6.54 | 6.48 | 16.02 | 62.0 | 1014 | 40.1 | 928 | 16.4 | 72.5 | 16.7 | 421 | 76 | 493 | 4601 | 0.0 |
| 19X-1, 140-150 | 169.70 | 6.71 | | 12.74 | 65.0 | 1069 | 43.2 | 958 | 16.8 | 77.6 | 20.8 | 426 | 78 | 544 | 3700 | 0.0 |
| 21X-3, 140-150 | 186.20 | 6.54 | | 11.21 | 68.0 | 1108 | 45.3 | 997 | 17.3 | 83.0 | 25.6 | 405 | 75 | 821 | 3345 | 13.0 |
| 23X-3, 140-150 | 205.10 | 6.56 | | 10.20 | 71.0 | 1139 | 48.7 | 1029 | 18.1 | 86.8 | 30.6 | 417 | 75 | 926 | 2542 | 16.2 |
| 25X-1, 140-150 | 220.90 | 6.63 | | 8.13 | 70.0 | 1128 | 50.6 | 998 | 18.2 | 85.4 | 33.9 | 371 | 78 | 801 | 1943 | 33.1 |
| 27X-1, 140-150 | 239.90 | 6.58 | | 6.96 | 74.0 | 1227 | 54.2 | 1059 | 19.4 | 89.4 | 39.6 | 367 | 86 | 863 | 1532 | 28.1 |
| 182-1132C- | | | | | | | | | | | | | | | | |
| 14R-CC, 9-10 | 357.59 | 7.12 | | 2.39 | 76.0 | 1216 | 59.1 | 1069 | 22.6 | 88.1 | 45.7 | 268 | 60 | 475 | 333 | 0.0 |
| 15R-CC, 17-18 | 367.17 | | | | 75.0 | 1203 | 61.1 | 1050 | 22.2 | 87.4 | 45.3 | 256 | 60 | 386 | 322 | 0.0 |
| 31R-1, 143-153 | 518.13 | 7.00 | | 2.37 | 80.0 | 1275 | 60.2 | 1117 | 21.5 | 93.6 | 49.4 | 216 | 101 | | 176 | 0.0 |
| 34R-1, 139-150 | 546.89 | | | | 75.0 | 1230 | 60.3 | 1084 | 21.7 | 95.7 | 45.6 | 207 | 93 | 166 | 139 | 0.0 |

**Table T6.** Summary of X-ray diffraction analysis, Site 1132.

| Leg | Site | Hole | Core | Type | Section | Top (cm) | Bottom (cm) | Depth (mbsf) | Aragonite (wt%) | Quartz (wt%) | LMC (wt%) | HMC (wt%) | Dolomite (wt%) |
|---|---|---|---|---|---|---|---|---|---|---|---|---|---|
| 182 | 1132 | B | 1 | H | 1 | 60.0 | 61.0 | 0.6 | 16 | 0 | 28 | 56 | 0 |
| 182 | 1132 | B | 1 | H | 3 | 60.0 | 61.0 | 3.6 | 14 | 0 | 27 | 59 | 0 |
| 182 | 1132 | B | 1 | H | 5 | 60.0 | 61.0 | 6.6 | 17 | 0 | 15 | 68 | 0 |
| 182 | 1132 | B | 2 | H | 1 | 60.0 | 61.0 | 7.4 | 16 | 0 | 16 | 68 | 0 |
| 182 | 1132 | B | 2 | H | 3 | 60.0 | 61.0 | 10.4 | 19 | 1 | 15 | 65 | 1 |
| 182 | 1132 | B | 2 | H | 5 | 60.0 | 61.0 | 13.4 | 14 | 0 | 18 | 66 | 2 |
| 182 | 1132 | B | 3 | H | 1 | 60.0 | 61.0 | 16.9 | 15 | 0 | 23 | 62 | 0 |
| 182 | 1132 | B | 3 | H | 3 | 60.0 | 61.0 | 19.9 | 26 | 0 | 16 | 58 | 1 |
| 182 | 1132 | B | 3 | H | 5 | 60.0 | 61.0 | 22.9 | 23 | 3 | 21 | 51 | 1 |
| 182 | 1132 | B | 4 | H | 1 | 60.0 | 61.0 | 26.4 | 23 | 0 | 25 | 52 | 0 |
| 182 | 1132 | B | 4 | H | 3 | 60.0 | 61.0 | 29.4 | 17 | 1 | 24 | 57 | 1 |
| 182 | 1132 | B | 4 | H | 5 | 60.0 | 61.0 | 32.4 | 19 | 1 | 18 | 61 | 1 |
| 182 | 1132 | B | 5 | H | 3 | 60.0 | 61.0 | 38.9 | 20 | 1 | 35 | 43 | 1 |
| 182 | 1132 | B | 5 | H | 5 | 60.0 | 61.0 | 41.9 | 23 | 0 | 29 | 48 | 0 |
| 182 | 1132 | B | 6 | H | 1 | 60.0 | 61.0 | 45.4 | 12 | 0 | 25 | 63 | 0 |
| 182 | 1132 | B | 6 | H | 3 | 60.0 | 61.0 | 48.4 | 14 | 2 | 36 | 48 | 0 |
| 182 | 1132 | B | 6 | H | 5 | 60.0 | 61.0 | 51.4 | 12 | 0 | 21 | 67 | 0 |
| 182 | 1132 | B | 7 | H | 1 | 95.0 | 96.0 | 55.25 | 12 | 0 | 34 | 53 | 0 |
| 182 | 1132 | B | 7 | H | 3 | 60.0 | 61.0 | 57.9 | 18 | 1 | 26 | 55 | 1 |
| 182 | 1132 | B | 7 | H | 5 | 60.0 | 61.0 | 60.9 | 20 | 0 | 19 | 57 | 4 |
| 182 | 1132 | B | 8 | H | 1 | 60.0 | 61.0 | 64.4 | 22 | 1 | 23 | 52 | 2 |
| 182 | 1132 | B | 8 | H | 3 | 60.0 | 61.0 | 67.4 | 20 | 1 | 28 | 47 | 4 |
| 182 | 1132 | B | 8 | H | 5 | 60.0 | 61.0 | 70.4 | 14 | 1 | 41 | 41 | 2 |
| 182 | 1132 | B | 9 | H | 1 | 60.0 | 61.0 | 73.9 | 16 | 0 | 29 | 54 | 1 |
| 182 | 1132 | B | 9 | H | 3 | 60.0 | 61.0 | 76.9 | 21 | 1 | 35 | 39 | 5 |
| 182 | 1132 | B | 9 | H | 5 | 60.0 | 61.0 | 79.9 | 19 | 2 | 27 | 43 | 8 |
| 182 | 1132 | B | 10 | H | 3 | 60.0 | 61.0 | 86.4 | 15 | 1 | 55 | 25 | 4 |
| 182 | 1132 | B | 10 | H | 5 | 60.0 | 61.0 | 89.4 | 19 | 2 | 35 | 43 | 2 |
| 182 | 1132 | B | 11 | H | 3 | 60.0 | 61.0 | 95.9 | 18 | 1 | 51 | 24 | 7 |
| 182 | 1132 | B | 11 | H | 5 | 60.0 | 61.0 | 98.9 | 20 | 1 | 71 | 0 | 8 |
| 182 | 1132 | B | 12 | H | 1 | 60.0 | 61.0 | 102.4 | 12 | 1 | 80 | 0 | 6 |
| 182 | 1132 | B | 12 | H | 3 | 60.0 | 61.0 | 105.4 | 11 | 3 | 76 | 0 | 10 |
| 182 | 1132 | B | 12 | H | 5 | 60.0 | 61.0 | 108.4 | 15 | 0 | 57 | 25 | 3 |
| 182 | 1132 | B | 13 | H | 1 | 60.0 | 61.0 | 111.9 | 14 | 6 | 69 | 0 | 10 |
| 182 | 1132 | B | 13 | H | 3 | 60.0 | 61.0 | 114.9 | 18 | 1 | 47 | 28 | 6 |
| 182 | 1132 | B | 13 | H | 5 | 60.0 | 61.0 | 117.9 | 18 | 1 | 31 | 46 | 3 |
| 182 | 1132 | B | 14 | H | 1 | 60.0 | 61.0 | 121.4 | 15 | 0 | 73 | 0 | 12 |
| 182 | 1132 | B | 14 | H | 3 | 60.0 | 61.0 | 124.4 | 22 | 1 | 67 | 0 | 10 |
| 182 | 1132 | B | 14 | H | 5 | 60.0 | 61.0 | 127.4 | 19 | 1 | 44 | 32 | 4 |
| 182 | 1132 | B | 15 | H | 1 | 60.0 | 61.0 | 130.9 | 22 | 1 | 55 | 13 | 9 |
| 182 | 1132 | B | 15 | H | 3 | 60.0 | 61.0 | 133.9 | 14 | 3 | 10 | 52 | 19 |
| 182 | 1132 | B | 15 | H | 5 | 60.0 | 61.0 | 136.9 | 11 | 0 | 51 | 34 | 4 |
| 182 | 1132 | B | 16 | H | 1 | 60.0 | 61.0 | 140.4 | 9 | 1 | 75 | 0 | 14 |
| 182 | 1132 | B | 16 | H | 3 | 60.0 | 61.0 | 143.4 | 17 | 1 | 77 | 0 | 5 |
| 182 | 1132 | B | 16 | H | 5 | 60.0 | 61.0 | 146.4 | 19 | 1 | 50 | 24 | 6 |
| 182 | 1132 | B | 17 | H | 1 | 60.0 | 61.0 | 149.9 | 15 | 1 | 81 | 0 | 3 |
| 182 | 1132 | B | 17 | H | 3 | 60.0 | 61.0 | 152.4 | 11 | 3 | 84 | 0 | 2 |
| 182 | 1132 | B | 17 | H | 5 | 60.0 | 61.0 | 155.4 | 17 | 1 | 46 | 28 | 9 |
| 182 | 1132 | B | 18 | H | 1 | 60.0 | 61.0 | 159.4 | 15 | 1 | 68 | 0 | 16 |
| 182 | 1132 | B | 18 | H | 3 | 60.0 | 61.0 | 162.4 | 8 | 1 | 84 | 0 | 7 |
| 182 | 1132 | B | 18 | H | 5 | 60.0 | 61.0 | 165.4 | 11 | 4 | 79 | 0 | 6 |
| 182 | 1132 | B | 19 | X | 1 | 60.0 | 61.0 | 168.9 | 14 | 1 | 76 | 0 | 9 |
| 182 | 1132 | B | 21 | X | 1 | 60.0 | 61.0 | 182.4 | 7 | 2 | 86 | 0 | 5 |
| 182 | 1132 | B | 21 | X | 3 | 60.0 | 61.0 | 185.4 | 15 | 1 | 75 | 0 | 8 |
| 182 | 1132 | B | 22 | X | 1 | 60.0 | 61.0 | 191.9 | 4 | 1 | 93 | 0 | 1 |
| 182 | 1132 | B | 22 | X | 3 | 60.0 | 61.0 | 194.9 | 5 | 1 | 91 | 0 | 3 |
| 182 | 1132 | B | 22 | X | 5 | 60.0 | 61.0 | 197.9 | 6 | 1 | 88 | 0 | 5 |
| 182 | 1132 | B | 23 | X | 1 | 60.0 | 61.0 | 201.3 | 4 | 1 | 91 | 0 | 4 |
| 182 | 1132 | B | 23 | X | 3 | 60.0 | 61.0 | 204.3 | 16 | 2 | 72 | 0 | 10 |
| 182 | 1132 | B | 23 | X | 5 | 60.0 | 61.0 | 207.3 | 5 | 2 | 89 | 0 | 4 |
| 182 | 1132 | B | 24 | X | 1 | 60.0 | 61.0 | 210.7 | 9 | 1 | 81 | 0 | 9 |
| 182 | 1132 | B | 24 | X | 3 | 60.0 | 61.0 | 213.7 | 11 | 1 | 81 | 0 | 7 |
| 182 | 1132 | B | 24 | X | 5 | 60.0 | 61.0 | 216.7 | 5 | 3 | 85 | 0 | 7 |
| 182 | 1132 | B | 25 | X | 1 | 60.0 | 61.0 | 220.1 | 14 | 1 | 75 | 0 | 10 |
| 182 | 1132 | B | 26 | X | 1 | 60.0 | 61.0 | 229.5 | 6 | 1 | 82 | 0 | 11 |
| 182 | 1132 | B | 26 | X | 3 | 60.0 | 61.0 | 232.5 | 9 | 1 | 82 | 0 | 9 |
| 182 | 1132 | B | 26 | X | 5 | 60.0 | 61.0 | 235.5 | 7 | 2 | 80 | 0 | 10 |
| 182 | 1132 | B | 27 | X | 1 | 60.0 | 61.0 | 239.1 | 7 | 2 | 87 | 0 | 4 |

Notes: LMC = low-Mg calcite, HMC = high-Mg calcite. This table is also available in **ASCII format.**

**Table T7.** Discrete *P*-wave velocity measurements using PWS1, PWS2, and PWS3, Site 1132.

| Leg | Site | Hole | Core | Type | Section | Interval (cm) | Depth (mbsf) | PWS 1, 2, or 3 | $V_p$ (km/s) |
|---|---|---|---|---|---|---|---|---|---|
| 182 | 1132 | B | 1 | H | 1 | 86.9 | 0.87 | 2 | 1.5958 |
| 182 | 1132 | B | 1 | H | 2 | 33.7 | 1.84 | 2 | 1.6071 |
| 182 | 1132 | B | 1 | H | 3 | 61.6 | 3.62 | 2 | 1.6027 |
| 182 | 1132 | B | 1 | H | 3 | 114.3 | 4.14 | 2 | 1.5965 |
| 182 | 1132 | B | 1 | H | 4 | 49.0 | 4.99 | 2 | 1.6033 |
| 182 | 1132 | B | 1 | H | 4 | 91.8 | 5.42 | 2 | 1.6109 |
| 182 | 1132 | B | 1 | H | 4 | 130.4 | 5.80 | 2 | 1.5703 |
| 182 | 1132 | B | 1 | H | 5 | 12.3 | 6.12 | 2 | 1.5799 |
| 182 | 1132 | B | 1 | H | 5 | 61.0 | 6.61 | 2 | 1.5714 |
| 182 | 1132 | B | 1 | H | 5 | 61.0 | 6.61 | 2 | 1.5714 |
| 182 | 1132 | B | 2 | H | 1 | 130.4 | 8.10 | 2 | 1.5595 |
| 182 | 1132 | B | 2 | H | 1 | 41.9 | 7.22 | 3 | 1.9692 |
| 182 | 1132 | B | 2 | H | 2 | 100.8 | 9.31 | 1 | 1.6223 |
| 182 | 1132 | B | 2 | H | 2 | 16.3 | 8.46 | 2 | 1.5903 |
| 182 | 1132 | B | 2 | H | 2 | 69.5 | 9.00 | 2 | 1.5928 |
| 182 | 1132 | B | 2 | H | 2 | 100.8 | 9.31 | 2 | 1.5757 |
| 182 | 1132 | B | 2 | H | 2 | 133.4 | 9.63 | 2 | 1.5637 |
| 182 | 1132 | B | 2 | H | 3 | 20.9 | 10.01 | 2 | 1.5787 |
| 182 | 1132 | B | 2 | H | 3 | 56.7 | 10.37 | 2 | 1.5714 |
| 182 | 1132 | B | 2 | H | 3 | 98.7 | 10.79 | 2 | 1.5282 |
| 182 | 1132 | B | 2 | H | 3 | 127.6 | 11.08 | 2 | 1.5824 |
| 182 | 1132 | B | 2 | H | 4 | 20.3 | 11.50 | 2 | 1.6071 |
| 182 | 1132 | B | 2 | H | 4 | 57.9 | 11.88 | 2 | 1.5776 |
| 182 | 1132 | B | 2 | H | 4 | 102.6 | 12.33 | 2 | 1.5679 |
| 182 | 1132 | B | 2 | H | 4 | 129.5 | 12.60 | 2 | 1.5799 |
| 182 | 1132 | B | 2 | H | 5 | 29.3 | 13.09 | 2 | 1.6002 |
| 182 | 1132 | B | 2 | H | 5 | 73.4 | 13.53 | 2 | 1.6027 |
| 182 | 1132 | B | 2 | H | 5 | 113.6 | 13.94 | 2 | 1.6190 |
| 182 | 1132 | B | 2 | H | 6 | 19.9 | 14.50 | 2 | 1.6109 |
| 182 | 1132 | B | 2 | H | 6 | 56.1 | 14.86 | 2 | 1.6008 |
| 182 | 1132 | B | 2 | H | 6 | 83.9 | 15.14 | 2 | 1.5946 |
| 182 | 1132 | B | 2 | H | 7 | 27.8 | 15.58 | 2 | 1.6096 |
| 182 | 1132 | B | 2 | H | 7 | 65.5 | 15.96 | 2 | 1.6483 |
| 182 | 1132 | B | 3 | H | 2 | 99.0 | 18.79 | 2 | 1.6536 |
| 182 | 1132 | B | 3 | H | 2 | 137.2 | 19.17 | 2 | 1.6096 |
| 182 | 1132 | B | 3 | H | 2 | 137.2 | 19.17 | 2 | 1.6033 |
| 182 | 1132 | B | 3 | H | 3 | 33.2 | 19.63 | 2 | 1.5619 |
| 182 | 1132 | B | 3 | H | 3 | 68.6 | 19.99 | 2 | 1.5934 |
| 182 | 1132 | B | 3 | H | 3 | 105.2 | 20.35 | 2 | 1.6300 |
| 182 | 1132 | B | 3 | H | 3 | 125.2 | 20.55 | 2 | 1.6236 |
| 182 | 1132 | B | 3 | H | 4 | 18.5 | 20.99 | 2 | 1.5953 |
| 182 | 1132 | B | 3 | H | 4 | 50.7 | 21.31 | 2 | 1.6053 |
| 182 | 1132 | B | 3 | H | 4 | 82.3 | 21.62 | 2 | 1.6268 |
| 182 | 1132 | B | 3 | H | 4 | 111.4 | 21.91 | 2 | 1.5878 |
| 182 | 1132 | B | 3 | H | 4 | 133.2 | 22.13 | 2 | 1.6609 |
| 182 | 1132 | B | 3 | H | 5 | 34.0 | 22.64 | 2 | 1.6609 |
| 182 | 1132 | B | 3 | H | 5 | 68.0 | 22.98 | 2 | 1.6569 |
| 182 | 1132 | B | 3 | H | 5 | 108.7 | 23.39 | 2 | 1.6306 |
| 182 | 1132 | B | 3 | H | 5 | 133.1 | 23.63 | 2 | 1.6090 |
| 182 | 1132 | B | 3 | H | 6 | 18.8 | 23.99 | 2 | 1.6450 |
| 182 | 1132 | B | 3 | H | 6 | 63.7 | 24.44 | 2 | 1.6358 |
| 182 | 1132 | B | 3 | H | 6 | 96.1 | 24.76 | 2 | 1.6281 |
| 182 | 1132 | B | 3 | H | 6 | 126.3 | 25.06 | 2 | 1.6424 |
| 182 | 1132 | B | 4 | H | 1 | 95.9 | 26.76 | 2 | 1.5903 |
| 182 | 1132 | B | 4 | H | 1 | 132.3 | 27.12 | 2 | 1.5769 |
| 182 | 1132 | B | 4 | H | 2 | 34.2 | 27.64 | 2 | 1.6203 |
| 182 | 1132 | B | 4 | H | 2 | 70.2 | 28.00 | 2 | 1.5977 |
| 182 | 1132 | B | 4 | H | 2 | 107.8 | 28.38 | 2 | 1.5637 |
| 182 | 1132 | B | 4 | H | 2 | 133.2 | 28.63 | 2 | 1.6217 |
| 182 | 1132 | B | 4 | H | 3 | 27.6 | 29.08 | 2 | 1.5983 |
| 182 | 1132 | B | 4 | H | 3 | 69.5 | 29.50 | 2 | 1.6287 |
| 182 | 1132 | B | 4 | H | 3 | 106.8 | 29.87 | 2 | 1.6197 |
| 182 | 1132 | B | 4 | H | 3 | 128.7 | 30.09 | 2 | 1.5848 |
| 182 | 1132 | B | 4 | H | 4 | 21.8 | 30.52 | 2 | 1.5766 |

Note: Only a portion of this table appears here. The complete table is available in **ASCII format.**

**Table T8.** Gamma-ray attenuation densiometry measurements from the multisensor track, Site 1132.

| Leg | Site | Hole | Core | Type | Section | Interval (cm) | Depth (mbsf) | Density (g/cm$^3$) | Corrected density (g/cm$^3$) |
|---|---|---|---|---|---|---|---|---|---|
| 182 | 1132 | A | 1 | H | 1 | 3.0 | 0.03 | 1.511 | 1.433 |
| 182 | 1132 | A | 1 | H | 1 | 7.0 | 0.07 | 1.548 | 1.473 |
| 182 | 1132 | A | 1 | H | 1 | 11.0 | 0.11 | 1.618 | 1.547 |
| 182 | 1132 | A | 1 | H | 1 | 15.0 | 0.15 | 1.691 | 1.625 |
| 182 | 1132 | A | 1 | H | 1 | 19.0 | 0.19 | 1.827 | 1.771 |
| 182 | 1132 | A | 1 | H | 1 | 23.0 | 0.23 | 1.881 | 1.828 |
| 182 | 1132 | A | 1 | H | 1 | 27.0 | 0.27 | 1.923 | 1.873 |
| 182 | 1132 | A | 1 | H | 1 | 31.0 | 0.31 | 2.017 | 1.974 |
| 182 | 1132 | A | 1 | H | 1 | 35.0 | 0.35 | 2.026 | 1.983 |
| 182 | 1132 | A | 1 | H | 1 | 39.0 | 0.39 | 2.008 | 1.964 |
| 182 | 1132 | A | 1 | H | 1 | 43.0 | 0.43 | 2.019 | 1.976 |
| 182 | 1132 | A | 1 | H | 1 | 47.0 | 0.47 | 1.917 | 1.867 |
| 182 | 1132 | A | 1 | H | 1 | 51.0 | 0.51 | 1.907 | 1.856 |
| 182 | 1132 | A | 1 | H | 1 | 55.0 | 0.55 | 1.914 | 1.864 |
| 182 | 1132 | A | 1 | H | 1 | 59.0 | 0.59 | 1.935 | 1.886 |
| 182 | 1132 | A | 1 | H | 1 | 63.0 | 0.63 | 1.888 | 1.836 |
| 182 | 1132 | A | 1 | H | 1 | 67.0 | 0.67 | 1.943 | 1.895 |
| 182 | 1132 | A | 1 | H | 1 | 71.0 | 0.71 | 1.924 | 1.874 |
| 182 | 1132 | A | 1 | H | 1 | 75.0 | 0.75 | 1.923 | 1.873 |
| 182 | 1132 | A | 1 | H | 1 | 79.0 | 0.79 | 1.999 | 1.955 |
| 182 | 1132 | A | 1 | H | 1 | 83.0 | 0.83 | 1.965 | 1.918 |
| 182 | 1132 | A | 1 | H | 1 | 87.0 | 0.87 | 2.007 | 1.963 |
| 182 | 1132 | A | 1 | H | 1 | 91.0 | 0.91 | 2.033 | 1.991 |
| 182 | 1132 | A | 1 | H | 1 | 95.0 | 0.95 | 1.964 | 1.917 |
| 182 | 1132 | A | 1 | H | 1 | 99.0 | 0.99 | 1.977 | 1.931 |
| 182 | 1132 | A | 1 | H | 1 | 103.0 | 1.03 | 1.988 | 1.943 |
| 182 | 1132 | A | 1 | H | 1 | 107.0 | 1.07 | 1.979 | 1.933 |
| 182 | 1132 | A | 1 | H | 1 | 111.0 | 1.11 | 1.982 | 1.936 |
| 182 | 1132 | A | 1 | H | 1 | 115.0 | 1.15 | 1.962 | 1.915 |
| 182 | 1132 | A | 1 | H | 1 | 119.0 | 1.19 | 1.958 | 1.911 |
| 182 | 1132 | A | 1 | H | 1 | 123.0 | 1.23 | 1.963 | 1.916 |
| 182 | 1132 | A | 1 | H | 1 | 127.0 | 1.27 | 1.909 | 1.858 |
| 182 | 1132 | A | 1 | H | 1 | 131.0 | 1.31 | 1.955 | 1.908 |
| 182 | 1132 | A | 1 | H | 1 | 135.0 | 1.35 | 1.933 | 1.884 |
| 182 | 1132 | A | 1 | H | 1 | 139.0 | 1.39 | 1.872 | 1.819 |
| 182 | 1132 | A | 1 | H | 1 | 143.0 | 1.43 | –0.331 | –0.535 |
| 182 | 1132 | A | 1 | H | 2 | 3.0 | 1.53 | 1.905 | 1.854 |
| 182 | 1132 | A | 1 | H | 2 | 7.0 | 1.57 | 1.937 | 1.888 |
| 182 | 1132 | A | 1 | H | 2 | 11.0 | 1.61 | 1.853 | 1.799 |
| 182 | 1132 | A | 1 | H | 2 | 15.0 | 1.65 | 1.988 | 1.943 |
| 182 | 1132 | A | 1 | H | 2 | 19.0 | 1.69 | 1.931 | 1.882 |
| 182 | 1132 | A | 1 | H | 2 | 23.0 | 1.73 | 1.884 | 1.832 |
| 182 | 1132 | A | 1 | H | 2 | 27.0 | 1.77 | 1.856 | 1.802 |
| 182 | 1132 | A | 1 | H | 2 | 31.0 | 1.81 | 1.857 | 1.803 |
| 182 | 1132 | A | 1 | H | 2 | 35.0 | 1.85 | 1.849 | 1.794 |
| 182 | 1132 | A | 1 | H | 2 | 39.0 | 1.89 | 1.828 | 1.772 |
| 182 | 1132 | A | 1 | H | 2 | 43.0 | 1.93 | 1.857 | 1.803 |
| 182 | 1132 | A | 1 | H | 2 | 47.0 | 1.97 | 1.829 | 1.773 |
| 182 | 1132 | A | 1 | H | 2 | 51.0 | 2.01 | 1.873 | 1.820 |
| 182 | 1132 | A | 1 | H | 2 | 55.0 | 2.05 | 1.863 | 1.809 |
| 182 | 1132 | A | 1 | H | 2 | 59.0 | 2.09 | 1.814 | 1.757 |
| 182 | 1132 | A | 1 | H | 2 | 63.0 | 2.13 | 1.799 | 1.741 |
| 182 | 1132 | A | 1 | H | 2 | 67.0 | 2.17 | 1.833 | 1.777 |
| 182 | 1132 | A | 1 | H | 2 | 71.0 | 2.21 | 1.800 | 1.742 |
| 182 | 1132 | A | 1 | H | 2 | 75.0 | 2.25 | 1.805 | 1.747 |
| 182 | 1132 | A | 1 | H | 2 | 79.0 | 2.29 | 1.803 | 1.745 |
| 182 | 1132 | A | 1 | H | 2 | 83.0 | 2.33 | 1.755 | 1.694 |
| 182 | 1132 | A | 1 | H | 2 | 87.0 | 2.37 | 1.799 | 1.741 |
| 182 | 1132 | A | 1 | H | 2 | 91.0 | 2.41 | 1.771 | 1.711 |
| 182 | 1132 | A | 1 | H | 2 | 95.0 | 2.45 | 1.730 | 1.667 |
| 182 | 1132 | A | 1 | H | 2 | 99.0 | 2.49 | 1.759 | 1.698 |
| 182 | 1132 | A | 1 | H | 2 | 103.0 | 2.53 | 1.775 | 1.715 |
| 182 | 1132 | A | 1 | H | 2 | 107.0 | 2.57 | 1.828 | 1.772 |

Note: Only a portion of this table appears here. The complete table is available in **ASCII format.**

**Table T9.** Magnetic susceptibility measurements from the multisensor track, Site 1132.

| Leg | Site | Hole | Core | Type | Section | Interval (cm) | Depth (mbsf) | Magnetic susceptibility ($10^{-6}$; SI units) | Corrected susceptibility ($10^{-6}$; SI units) |
|---|---|---|---|---|---|---|---|---|---|
| 182 | 1132 | A | 1 | H | 1 | 3.0 | 0.03 | –0.80 | –0.80 |
| 182 | 1132 | A | 1 | H | 1 | 11.0 | 0.11 | –1.40 | –1.40 |
| 182 | 1132 | A | 1 | H | 1 | 19.0 | 0.19 | –0.80 | –0.80 |
| 182 | 1132 | A | 1 | H | 1 | 27.0 | 0.27 | –1.70 | –1.70 |
| 182 | 1132 | A | 1 | H | 1 | 35.0 | 0.35 | –2.30 | –2.30 |
| 182 | 1132 | A | 1 | H | 1 | 43.0 | 0.43 | –2.00 | –2.00 |
| 182 | 1132 | A | 1 | H | 1 | 51.0 | 0.51 | –1.80 | –1.80 |
| 182 | 1132 | A | 1 | H | 1 | 59.0 | 0.59 | –2.20 | –2.20 |
| 182 | 1132 | A | 1 | H | 1 | 67.0 | 0.67 | –2.80 | –2.80 |
| 182 | 1132 | A | 1 | H | 1 | 75.0 | 0.75 | –2.70 | –2.70 |
| 182 | 1132 | A | 1 | H | 1 | 83.0 | 0.83 | –2.70 | –2.70 |
| 182 | 1132 | A | 1 | H | 1 | 91.0 | 0.91 | –3.00 | –3.00 |
| 182 | 1132 | A | 1 | H | 1 | 99.0 | 0.99 | –2.30 | –2.30 |
| 182 | 1132 | A | 1 | H | 1 | 107.0 | 1.07 | –2.80 | –2.80 |
| 182 | 1132 | A | 1 | H | 1 | 115.0 | 1.15 | –2.30 | –2.30 |
| 182 | 1132 | A | 1 | H | 1 | 123.0 | 1.23 | –2.70 | –2.70 |
| 182 | 1132 | A | 1 | H | 1 | 131.0 | 1.31 | –2.70 | –2.70 |
| 182 | 1132 | A | 1 | H | 1 | 139.0 | 1.39 | –3.20 | –3.20 |
| 182 | 1132 | A | 1 | H | 2 | 3.0 | 1.53 | –2.70 | –2.70 |
| 182 | 1132 | A | 1 | H | 2 | 11.0 | 1.61 | –2.60 | –2.60 |
| 182 | 1132 | A | 1 | H | 2 | 19.0 | 1.69 | –3.00 | –3.00 |
| 182 | 1132 | A | 1 | H | 2 | 27.0 | 1.77 | –3.00 | –3.00 |
| 182 | 1132 | A | 1 | H | 2 | 35.0 | 1.85 | –3.20 | –3.20 |
| 182 | 1132 | A | 1 | H | 2 | 43.0 | 1.93 | –3.00 | –3.00 |
| 182 | 1132 | A | 1 | H | 2 | 51.0 | 2.01 | –3.20 | –3.20 |
| 182 | 1132 | A | 1 | H | 2 | 59.0 | 2.09 | –3.10 | –3.10 |
| 182 | 1132 | A | 1 | H | 2 | 67.0 | 2.17 | –3.70 | –3.70 |
| 182 | 1132 | A | 1 | H | 2 | 75.0 | 2.25 | –3.10 | –3.10 |
| 182 | 1132 | A | 1 | H | 2 | 83.0 | 2.33 | –3.50 | –3.50 |
| 182 | 1132 | A | 1 | H | 2 | 91.0 | 2.41 | –3.80 | –3.80 |
| 182 | 1132 | A | 1 | H | 2 | 99.0 | 2.49 | –3.40 | –3.40 |
| 182 | 1132 | A | 1 | H | 2 | 107.0 | 2.57 | –3.70 | –3.70 |
| 182 | 1132 | A | 1 | H | 2 | 115.0 | 2.65 | –3.70 | –3.70 |
| 182 | 1132 | A | 1 | H | 2 | 123.0 | 2.73 | –3.20 | –3.20 |
| 182 | 1132 | A | 1 | H | 2 | 131.0 | 2.81 | –3.20 | –3.20 |
| 182 | 1132 | A | 1 | H | 2 | 139.0 | 2.89 | –3.80 | –3.80 |
| 182 | 1132 | A | 1 | H | 2 | 147.0 | 2.97 | –3.50 | –3.50 |
| 182 | 1132 | A | 1 | H | 3 | 3.0 | 3.03 | –2.10 | –2.10 |
| 182 | 1132 | A | 1 | H | 3 | 11.0 | 3.11 | –2.00 | –2.00 |
| 182 | 1132 | A | 1 | H | 3 | 19.0 | 3.19 | –2.50 | –2.50 |
| 182 | 1132 | A | 1 | H | 3 | 27.0 | 3.27 | –2.40 | –2.40 |
| 182 | 1132 | A | 1 | H | 3 | 35.0 | 3.35 | –2.30 | –2.30 |
| 182 | 1132 | A | 1 | H | 3 | 43.0 | 3.43 | –2.90 | –2.90 |
| 182 | 1132 | A | 1 | H | 3 | 51.0 | 3.51 | –3.10 | –3.10 |
| 182 | 1132 | A | 1 | H | 3 | 59.0 | 3.59 | –3.40 | –3.40 |
| 182 | 1132 | A | 1 | H | 3 | 67.0 | 3.67 | –2.30 | –2.30 |
| 182 | 1132 | A | 1 | H | 3 | 75.0 | 3.75 | –2.60 | –2.60 |
| 182 | 1132 | A | 1 | H | 3 | 83.0 | 3.83 | –3.00 | –3.00 |
| 182 | 1132 | A | 1 | H | 3 | 91.0 | 3.91 | –2.70 | –2.70 |
| 182 | 1132 | A | 1 | H | 3 | 99.0 | 3.99 | –3.10 | –3.10 |
| 182 | 1132 | A | 1 | H | 3 | 107.0 | 4.07 | –2.70 | –2.70 |
| 182 | 1132 | A | 1 | H | 3 | 115.0 | 4.15 | –3.00 | –3.00 |
| 182 | 1132 | A | 1 | H | 3 | 123.0 | 4.23 | –3.30 | –3.30 |
| 182 | 1132 | A | 1 | H | 3 | 131.0 | 4.31 | –3.00 | –3.00 |
| 182 | 1132 | A | 1 | H | 3 | 139.0 | 4.39 | –2.80 | –2.80 |
| 182 | 1132 | A | 1 | H | 4 | 3.0 | 4.53 | –3.50 | –3.50 |
| 182 | 1132 | A | 1 | H | 4 | 11.0 | 4.61 | –3.70 | –3.70 |
| 182 | 1132 | A | 1 | H | 4 | 19.0 | 4.69 | –3.40 | –3.40 |
| 182 | 1132 | A | 1 | H | 4 | 27.0 | 4.77 | –3.90 | –3.90 |
| 182 | 1132 | A | 1 | H | 4 | 35.0 | 4.85 | –4.30 | –4.30 |
| 182 | 1132 | A | 1 | H | 4 | 43.0 | 4.93 | –3.90 | –3.90 |
| 182 | 1132 | A | 1 | H | 4 | 51.0 | 5.01 | –4.10 | –4.10 |
| 182 | 1132 | A | 1 | H | 4 | 59.0 | 5.09 | –4.20 | –4.20 |
| 182 | 1132 | A | 1 | H | 4 | 67.0 | 5.17 | –4.00 | –4.00 |

Note: Only a portion of this table appears here. The complete table is available in **ASCII format.**

**Table T10.** Natural gamma-ray measurements from the multisensor track, Site 1132.

| Leg | Site | Hole | Core | Type | Section | Interval (cm) | Depth (mbsf) | NGR (cps) |
|---|---|---|---|---|---|---|---|---|
| 182 | 1132 | A | 1 | H | 1 | 11.0 | 0.11 | 2.50 |
| 182 | 1132 | A | 1 | H | 1 | 27.0 | 0.27 | 1.27 |
| 182 | 1132 | A | 1 | H | 1 | 43.0 | 0.43 | 3.58 |
| 182 | 1132 | A | 1 | H | 1 | 59.0 | 0.59 | 3.62 |
| 182 | 1132 | A | 1 | H | 1 | 75.0 | 0.75 | 2.81 |
| 182 | 1132 | A | 1 | H | 1 | 91.0 | 0.91 | 3.19 |
| 182 | 1132 | A | 1 | H | 1 | 107.0 | 1.07 | 3.77 |
| 182 | 1132 | A | 1 | H | 1 | 123.0 | 1.23 | 4.69 |
| 182 | 1132 | A | 1 | H | 2 | 11.0 | 1.61 | 3.31 |
| 182 | 1132 | A | 1 | H | 2 | 27.0 | 1.77 | 2.73 |
| 182 | 1132 | A | 1 | H | 2 | 43.0 | 1.93 | 2.50 |
| 182 | 1132 | A | 1 | H | 2 | 59.0 | 2.09 | 2.69 |
| 182 | 1132 | A | 1 | H | 2 | 75.0 | 2.25 | 4.54 |
| 182 | 1132 | A | 1 | H | 2 | 91.0 | 2.41 | 3.81 |
| 182 | 1132 | A | 1 | H | 2 | 107.0 | 2.57 | 3.31 |
| 182 | 1132 | A | 1 | H | 2 | 123.0 | 2.73 | 2.50 |
| 182 | 1132 | A | 1 | H | 2 | 139.0 | 2.89 | 4.31 |
| 182 | 1132 | A | 1 | H | 3 | 11.0 | 3.11 | 4.69 |
| 182 | 1132 | A | 1 | H | 3 | 27.0 | 3.27 | 4.77 |
| 182 | 1132 | A | 1 | H | 3 | 43.0 | 3.43 | 5.81 |
| 182 | 1132 | A | 1 | H | 3 | 59.0 | 3.59 | 5.54 |
| 182 | 1132 | A | 1 | H | 3 | 75.0 | 3.75 | 5.39 |
| 182 | 1132 | A | 1 | H | 3 | 91.0 | 3.91 | 4.73 |
| 182 | 1132 | A | 1 | H | 3 | 107.0 | 4.07 | 5.42 |
| 182 | 1132 | A | 1 | H | 3 | 123.0 | 4.23 | 4.92 |
| 182 | 1132 | A | 1 | H | 4 | 11.0 | 4.61 | 6.12 |
| 182 | 1132 | A | 1 | H | 4 | 27.0 | 4.77 | 8.31 |
| 182 | 1132 | A | 1 | H | 4 | 43.0 | 4.93 | 7.04 |
| 182 | 1132 | A | 1 | H | 4 | 59.0 | 5.09 | 7.19 |
| 182 | 1132 | A | 1 | H | 4 | 75.0 | 5.25 | 7.19 |
| 182 | 1132 | A | 1 | H | 4 | 91.0 | 5.41 | 8.23 |
| 182 | 1132 | A | 1 | H | 4 | 107.0 | 5.57 | 8.15 |
| 182 | 1132 | A | 1 | H | 4 | 123.0 | 5.73 | 10.19 |
| 182 | 1132 | A | 1 | H | 4 | 139.0 | 5.89 | 9.54 |
| 182 | 1132 | A | 1 | H | 5 | 11.0 | 6.11 | 5.46 |
| 182 | 1132 | A | 1 | H | 5 | 27.0 | 6.27 | 5.39 |
| 182 | 1132 | A | 1 | H | 5 | 43.0 | 6.43 | 6.54 |
| 182 | 1132 | A | 1 | H | 5 | 59.0 | 6.59 | 5.65 |
| 182 | 1132 | A | 1 | H | 5 | 75.0 | 6.75 | 5.65 |
| 182 | 1132 | A | 1 | H | 5 | 91.0 | 6.91 | 6.81 |
| 182 | 1132 | A | 1 | H | 5 | 107.0 | 7.07 | 6.62 |
| 182 | 1132 | A | 1 | H | 5 | 123.0 | 7.23 | 6.27 |
| 182 | 1132 | A | 1 | H | 5 | 139.0 | 7.39 | 8.50 |
| 182 | 1132 | A | 1 | H | 6 | 11.0 | 7.61 | 7.42 |
| 182 | 1132 | A | 1 | H | 6 | 27.0 | 7.77 | 8.15 |
| 182 | 1132 | A | 1 | H | 6 | 43.0 | 7.93 | 5.77 |
| 182 | 1132 | A | 1 | H | 6 | 59.0 | 8.09 | 6.00 |
| 182 | 1132 | A | 1 | H | 6 | 75.0 | 8.25 | 4.50 |
| 182 | 1132 | A | 1 | H | 7 | 11.0 | 8.61 | 5.46 |
| 182 | 1132 | A | 1 | H | 7 | 27.0 | 8.77 | 5.85 |
| 182 | 1132 | A | 1 | H | 7 | 43.0 | 8.93 | 4.27 |
| 182 | 1132 | B | 1 | H | 1 | 11.0 | 0.11 | 1.58 |
| 182 | 1132 | B | 1 | H | 1 | 27.0 | 0.27 | 2.39 |
| 182 | 1132 | B | 1 | H | 1 | 43.0 | 0.43 | 1.92 |
| 182 | 1132 | B | 1 | H | 1 | 59.0 | 0.59 | 2.04 |
| 182 | 1132 | B | 1 | H | 1 | 75.0 | 0.75 | 2.12 |
| 182 | 1132 | B | 1 | H | 1 | 91.0 | 0.91 | 3.31 |
| 182 | 1132 | B | 1 | H | 1 | 107.0 | 1.07 | 2.69 |
| 182 | 1132 | B | 1 | H | 1 | 123.0 | 1.23 | 3.54 |
| 182 | 1132 | B | 1 | H | 1 | 139.0 | 1.39 | 3.08 |
| 182 | 1132 | B | 1 | H | 2 | 11.0 | 1.61 | 3.23 |
| 182 | 1132 | B | 1 | H | 2 | 27.0 | 1.77 | 2.89 |
| 182 | 1132 | B | 1 | H | 2 | 43.0 | 1.93 | 3.23 |
| 182 | 1132 | B | 1 | H | 2 | 59.0 | 2.09 | 4.46 |

Notes: NGR = natural gamma radiation. Only a portion of this table appears here. The complete table is available in **ASCII format.**

**Table T11.** Thermal conductivity measurements, Site 1132.

| Leg | Site | Hole | Core | Type | Section | Interval (cm) | Depth (mbsf) | Thermal conductivity (W/[m·K]) |
|---|---|---|---|---|---|---|---|---|
| 182 | 1132 | B | 2 | H | 3 | 75.0 | 10.55 | 0.828 |
| 182 | 1132 | B | 2 | H | 3 | 75.0 | 10.55 | 0.817 |
| 182 | 1132 | B | 2 | H | 3 | 75.0 | 10.55 | 0.828 |
| 182 | 1132 | B | 3 | H | 3 | 75.0 | 20.05 | 0.865 |
| 182 | 1132 | B | 3 | H | 3 | 75.0 | 20.05 | 0.898 |
| 182 | 1132 | B | 3 | H | 3 | 75.0 | 20.05 | 0.906 |
| 182 | 1132 | B | 4 | H | 3 | 75.0 | 29.55 | 0.916 |
| 182 | 1132 | B | 4 | H | 3 | 75.0 | 29.55 | 0.908 |
| 182 | 1132 | B | 4 | H | 3 | 75.0 | 29.55 | 0.912 |
| 182 | 1132 | B | 5 | H | 3 | 75.0 | 39.05 | 0.965 |
| 182 | 1132 | B | 5 | H | 3 | 75.0 | 39.05 | 0.952 |
| 182 | 1132 | B | 5 | H | 3 | 75.0 | 39.05 | 0.949 |
| 182 | 1132 | B | 4 | H | 1 | 75.0 | 26.55 | 1.076 |
| 182 | 1132 | B | 4 | H | 1 | 75.0 | 26.55 | 1.022 |
| 182 | 1132 | B | 4 | H | 1 | 75.0 | 26.55 | 0.989 |
| 182 | 1132 | B | 4 | H | 5 | 75.0 | 32.55 | 0.934 |
| 182 | 1132 | B | 4 | H | 5 | 75.0 | 32.55 | 0.902 |
| 182 | 1132 | B | 4 | H | 5 | 75.0 | 32.55 | 0.896 |
| 182 | 1132 | B | 6 | H | 3 | 75.0 | 48.55 | 0.880 |
| 182 | 1132 | B | 6 | H | 3 | 75.0 | 48.55 | 0.881 |
| 182 | 1132 | B | 6 | H | 3 | 75.0 | 48.55 | 0.895 |
| 182 | 1132 | B | 7 | H | 3 | 75.0 | 58.05 | 0.903 |
| 182 | 1132 | B | 7 | H | 3 | 75.0 | 58.05 | 0.926 |
| 182 | 1132 | B | 7 | H | 3 | 75.0 | 58.05 | 0.935 |
| 182 | 1132 | B | 8 | H | 3 | 75.0 | 67.55 | 0.959 |
| 182 | 1132 | B | 8 | H | 3 | 75.0 | 67.55 | 0.977 |
| 182 | 1132 | B | 8 | H | 3 | 75.0 | 67.55 | 0.956 |
| 182 | 1132 | B | 8 | H | 6 | 90.0 | 72.20 | 0.933 |
| 182 | 1132 | B | 8 | H | 6 | 90.0 | 72.20 | 0.874 |
| 182 | 1132 | B | 8 | H | 6 | 90.0 | 72.20 | 0.900 |
| 182 | 1132 | B | 9 | H | 2 | 60.0 | 75.40 | 1.001 |
| 182 | 1132 | B | 9 | H | 2 | 60.0 | 75.40 | 0.992 |
| 182 | 1132 | B | 9 | H | 2 | 60.0 | 75.40 | 1.022 |
| 182 | 1132 | B | 9 | H | 3 | 71.0 | 77.01 | 1.025 |
| 182 | 1132 | B | 9 | H | 3 | 71.0 | 77.01 | 1.061 |
| 182 | 1132 | B | 9 | H | 3 | 71.0 | 77.01 | 1.025 |
| 182 | 1132 | B | 9 | H | 6 | 68.0 | 81.48 | 1.071 |
| 182 | 1132 | B | 9 | H | 6 | 68.0 | 81.48 | 1.037 |
| 182 | 1132 | B | 9 | H | 6 | 68.0 | 81.48 | 1.033 |
| 182 | 1132 | B | 10 | H | 3 | 64.0 | 86.44 | 1.037 |
| 182 | 1132 | B | 10 | H | 3 | 64.0 | 86.44 | 1.010 |
| 182 | 1132 | B | 10 | H | 3 | 64.0 | 86.44 | 1.024 |
| 182 | 1132 | B | 11 | H | 3 | 71.0 | 96.01 | 0.964 |
| 182 | 1132 | B | 11 | H | 3 | 71.0 | 96.01 | 1.003 |
| 182 | 1132 | B | 11 | H | 3 | 71.0 | 96.01 | 0.997 |
| 182 | 1132 | B | 12 | H | 3 | 63.0 | 105.43 | 1.112 |
| 182 | 1132 | B | 12 | H | 3 | 63.0 | 105.43 | 1.122 |
| 182 | 1132 | B | 12 | H | 3 | 63.0 | 105.43 | 1.145 |
| 182 | 1132 | B | 12 | H | 6 | 95.0 | 110.25 | 1.064 |
| 182 | 1132 | B | 12 | H | 6 | 95.0 | 110.25 | 1.016 |
| 182 | 1132 | B | 12 | H | 6 | 95.0 | 110.25 | 1.004 |
| 182 | 1132 | B | 13 | H | 1 | 79.0 | 112.09 | 1.018 |
| 182 | 1132 | B | 13 | H | 1 | 79.0 | 112.09 | 1.020 |
| 182 | 1132 | B | 13 | H | 1 | 79.0 | 112.09 | 1.032 |
| 182 | 1132 | B | 13 | H | 3 | 75.0 | 115.05 | 1.000 |
| 182 | 1132 | B | 13 | H | 3 | 75.0 | 115.05 | 0.999 |
| 182 | 1132 | B | 13 | H | 3 | 75.0 | 115.05 | 1.008 |
| 182 | 1132 | B | 14 | H | 3 | 75.0 | 124.55 | 1.073 |
| 182 | 1132 | B | 14 | H | 3 | 75.0 | 124.55 | 1.034 |
| 182 | 1132 | B | 14 | H | 3 | 75.0 | 124.55 | 1.054 |
| 182 | 1132 | B | 15 | H | 3 | 85.0 | 134.15 | 1.064 |
| 182 | 1132 | B | 15 | H | 3 | 85.0 | 134.15 | 1.043 |
| 182 | 1132 | B | 15 | H | 3 | 85.0 | 134.15 | 1.034 |
| 182 | 1132 | B | 16 | H | 3 | 75.0 | 143.55 | 0.993 |

Note: Only a portion of this table appears here. The complete table is available in **ASCII format.**

**Table T12.** In situ formation temperature estimates, Site 1132.

| Leg, core, section | Depth (mbsf) | Mudline temperature (°C) | Formation temperature (°C) | Fitting error (°C) |
|---|---|---|---|---|
| 182-1132B-4H | 0 | 14.5 | | |
| | 0 | >14.1 | | |
| | 35.30 | | 15.91 | 0.005 |
| | 35.30 | | 15.78 | 0.005 |
| 182-1132B-8H | 0 | <14.9 | | |
| | 73.30 | | 18.40 | 0.007 |
| 182-1132B-12H | 0 | <14.7 | | |
| | 111.30 | 14.7 | 20.07 | 0.005 |
| | 111.30 | 15.1 | | |
| 182-1132B-17H | 0 | 15.4 | | |
| | 169.00 | | 22.44 | 0.380 |
| | 169.00 | | 22.29 | 0.120 |

Notes: Average mudline temperature = 1.92°C. Additional estimate of seafloor temperature using an expendable bathythermograph = 12.55–12.61. This table is also available in **ASCII format.**

**Table T13.** Index properties measurements, Site 1132.

| Leg | Site | Hole | Core | Type | Section | Top (cm) | Bottom (cm) | Depth (mbsf) | Bulk water content (%) | Dry water content (%) | Bulk density (g/cm³) | Dry density (g/cm³) | Grain density (g/cm³) | Porosity (%) | Void ratio |
|---|---|---|---|---|---|---|---|---|---|---|---|---|---|---|---|
| 182 | 1132 | A | 1 | H | 1 | 86.0 | 88.0 | 0.86 | 27.9 | 38.6 | 1.51 | 1.09 | 1.84 | 41.0 | 0.70 |
| 182 | 1132 | A | 1 | H | 2 | 86.0 | 88.0 | 2.36 | 38.5 | 62.6 | 1.46 | 0.90 | 1.98 | 54.7 | 1.21 |
| 182 | 1132 | A | 1 | H | 3 | 86.0 | 88.0 | 3.86 | 35.7 | 55.4 | 1.57 | 1.01 | 2.22 | 54.6 | 1.20 |
| 182 | 1132 | A | 1 | H | 4 | 86.0 | 88.0 | 5.36 | 38.6 | 63.0 | 1.35 | 0.83 | 1.69 | 51.0 | 1.04 |
| 182 | 1132 | A | 1 | H | 5 | 86.0 | 88.0 | 6.86 | 38.3 | 62.1 | 1.49 | 0.92 | 2.08 | 55.8 | 1.26 |
| 182 | 1132 | A | 1 | H | 6 | 86.0 | 88.0 | 8.36 | 37.9 | 61.1 | 1.45 | 0.90 | 1.93 | 53.6 | 1.15 |
| 182 | 1132 | B | 1 | H | 1 | 86.0 | 88.0 | 0.86 | 26.7 | 36.4 | 1.68 | 1.23 | 2.20 | 43.8 | 0.78 |
| 182 | 1132 | B | 1 | H | 2 | 86.0 | 88.0 | 2.36 | 35.0 | 53.8 | 1.48 | 0.96 | 1.95 | 50.7 | 1.03 |
| 182 | 1132 | B | 1 | H | 3 | 86.0 | 88.0 | 3.86 | 38.7 | 63.1 | 1.53 | 0.94 | 2.22 | 57.8 | 1.37 |
| 182 | 1132 | B | 1 | H | 4 | 86.0 | 88.0 | 5.36 | 40.4 | 67.9 | 1.39 | 0.83 | 1.83 | 54.8 | 1.21 |
| 182 | 1132 | B | 2 | H | 2 | 86.0 | 88.0 | 9.16 | 39.6 | 65.6 | 1.50 | 0.90 | 2.15 | 58.0 | 1.38 |
| 182 | 1132 | B | 2 | H | 3 | 86.0 | 88.0 | 10.66 | 38.3 | 62.1 | 1.54 | 0.95 | 2.22 | 57.4 | 1.35 |
| 182 | 1132 | B | 2 | H | 4 | 86.0 | 88.0 | 12.16 | 38.9 | 63.8 | 1.37 | 0.84 | 1.76 | 52.2 | 1.09 |
| 182 | 1132 | B | 2 | H | 5 | 86.0 | 88.0 | 13.66 | 38.8 | 63.5 | 1.42 | 0.87 | 1.89 | 54.0 | 1.17 |
| 182 | 1132 | B | 4 | H | 2 | 86.0 | 88.0 | 28.16 | 34.3 | 52.2 | 1.61 | 1.06 | 2.30 | 53.9 | 1.17 |
| 182 | 1132 | B | 4 | H | 3 | 86.0 | 88.0 | 29.66 | 36.8 | 58.2 | 1.43 | 0.90 | 1.86 | 51.4 | 1.06 |
| 182 | 1132 | B | 4 | H | 4 | 86.0 | 88.0 | 31.16 | 36.3 | 56.9 | 1.50 | 0.96 | 2.03 | 53.1 | 1.13 |
| 182 | 1132 | B | 4 | H | 5 | 86.0 | 88.0 | 32.66 | 36.3 | 56.9 | 1.52 | 0.97 | 2.10 | 53.8 | 1.16 |
| 182 | 1132 | B | 4 | H | 6 | 86.0 | 88.0 | 34.16 | 36.8 | 58.2 | 1.56 | 0.99 | 2.25 | 56.1 | 1.28 |
| 182 | 1132 | B | 5 | H | 2 | 86.0 | 88.0 | 37.66 | 29.6 | 42.0 | 1.51 | 1.06 | 1.88 | 43.5 | 0.77 |
| 182 | 1132 | B | 5 | H | 3 | 86.0 | 88.0 | 39.16 | 35.0 | 54.0 | 1.49 | 0.97 | 1.97 | 51.0 | 1.04 |
| 182 | 1132 | B | 5 | H | 4 | 86.0 | 88.0 | 40.66 | 34.0 | 51.5 | 1.55 | 1.02 | 2.11 | 51.5 | 1.06 |
| 182 | 1132 | B | 5 | H | 5 | 86.0 | 88.0 | 42.16 | 34.1 | 51.7 | 1.53 | 1.01 | 2.06 | 51.0 | 1.04 |
| 182 | 1132 | B | 5 | H | 6 | 86.0 | 88.0 | 43.66 | 29.9 | 42.7 | 1.57 | 1.10 | 2.03 | 45.8 | 0.85 |
| 182 | 1132 | B | 6 | H | 1 | 124.0 | 126.0 | 46.04 | 33.7 | 50.9 | 1.52 | 1.01 | 2.03 | 50.2 | 1.01 |
| 182 | 1132 | B | 6 | H | 1 | 132.0 | 134.0 | 46.12 | 32.0 | 47.0 | 1.56 | 1.06 | 2.06 | 48.5 | 0.94 |
| 182 | 1132 | B | 6 | H | 3 | 71.0 | 73.0 | 48.51 | 35.4 | 54.7 | 1.44 | 0.93 | 1.86 | 49.8 | 0.99 |
| 182 | 1132 | B | 6 | H | 3 | 73.0 | 75.0 | 48.53 | 36.2 | 56.7 | 1.57 | 1.00 | 2.24 | 55.4 | 1.24 |
| 182 | 1132 | B | 6 | H | 4 | 72.0 | 74.0 | 50.02 | 37.8 | 60.8 | 1.41 | 0.87 | 1.82 | 51.9 | 1.08 |
| 182 | 1132 | B | 6 | H | 5 | 72.0 | 74.0 | 51.52 | 28.6 | 40.0 | 1.58 | 1.13 | 2.02 | 44.2 | 0.79 |
| 182 | 1132 | B | 7 | H | 1 | 87.0 | 89.0 | 55.17 | 27.3 | 37.6 | 1.64 | 1.19 | 2.11 | 43.7 | 0.78 |
| 182 | 1132 | B | 7 | H | 2 | 55.0 | 57.0 | 56.35 | 33.6 | 50.7 | 1.60 | 1.06 | 2.24 | 52.6 | 1.11 |
| 182 | 1132 | B | 7 | H | 3 | 66.0 | 68.0 | 57.96 | 32.9 | 49.1 | 1.52 | 1.02 | 1.99 | 48.8 | 0.95 |
| 182 | 1132 | B | 7 | H | 4 | 46.0 | 48.0 | 59.26 | 33.1 | 49.5 | 1.54 | 1.03 | 2.06 | 49.9 | 0.99 |
| 182 | 1132 | B | 7 | H | 4 | 62.0 | 64.0 | 59.42 | 28.8 | 40.5 | 1.53 | 1.09 | 1.92 | 43.1 | 0.76 |
| 182 | 1132 | B | 7 | H | 5 | 49.0 | 51.0 | 60.79 | 34.2 | 52.1 | 1.53 | 1.00 | 2.05 | 51.0 | 1.04 |
| 182 | 1132 | B | 7 | H | 6 | 49.0 | 51.0 | 62.29 | 29.4 | 41.6 | 1.64 | 1.16 | 2.18 | 47.0 | 0.89 |
| 182 | 1132 | B | 7 | H | 7 | 9.0 | 11.0 | 63.39 | 25.7 | 34.6 | 1.63 | 1.21 | 2.04 | 40.9 | 0.69 |
| 182 | 1132 | B | 8 | H | 1 | 81.0 | 83.0 | 64.61 | 30.3 | 43.4 | 1.52 | 1.06 | 1.93 | 45.0 | 0.82 |
| 182 | 1132 | B | 8 | H | 2 | 68.0 | 70.0 | 65.98 | 28.0 | 38.9 | 1.60 | 1.15 | 2.04 | 43.6 | 0.77 |
| 182 | 1132 | B | 8 | H | 3 | 68.0 | 70.0 | 67.48 | 28.9 | 40.7 | 1.64 | 1.17 | 2.18 | 46.4 | 0.87 |
| 182 | 1132 | B | 8 | H | 4 | 26.0 | 28.0 | 68.56 | 29.9 | 42.6 | 1.65 | 1.16 | 2.24 | 48.2 | 0.93 |
| 182 | 1132 | B | 8 | H | 4 | 94.0 | 96.0 | 69.24 | 26.1 | 35.3 | 1.60 | 1.18 | 2.00 | 40.8 | 0.69 |
| 182 | 1132 | B | 8 | H | 5 | 82.0 | 84.0 | 70.62 | 34.4 | 52.5 | 1.54 | 1.01 | 2.08 | 51.6 | 1.07 |
| 182 | 1132 | B | 8 | H | 6 | 79.0 | 81.0 | 72.09 | 33.0 | 49.3 | 1.62 | 1.09 | 2.28 | 52.3 | 1.10 |
| 182 | 1132 | B | 8 | H | 7 | 27.0 | 29.0 | 73.07 | 30.8 | 44.4 | 1.66 | 1.15 | 2.28 | 49.8 | 0.99 |
| 182 | 1132 | B | 9 | H | 1 | 40.0 | 42.0 | 73.70 | 28.0 | 39.0 | 1.60 | 1.15 | 2.05 | 43.8 | 0.78 |
| 182 | 1132 | B | 9 | H | 2 | 69.0 | 71.0 | 75.49 | 32.4 | 48.0 | 1.50 | 1.02 | 1.94 | 47.6 | 0.91 |
| 182 | 1132 | B | 9 | H | 3 | 69.0 | 71.0 | 76.99 | 29.1 | 41.1 | 1.56 | 1.10 | 1.98 | 44.2 | 0.79 |
| 182 | 1132 | B | 9 | H | 4 | 67.0 | 69.0 | 78.47 | 32.0 | 47.0 | 1.49 | 1.01 | 1.90 | 46.6 | 0.87 |
| 182 | 1132 | B | 9 | H | 5 | 67.0 | 69.0 | 79.97 | 31.8 | 46.6 | 1.49 | 1.01 | 1.88 | 46.1 | 0.86 |
| 182 | 1132 | B | 9 | H | 6 | 67.0 | 69.0 | 81.47 | 28.2 | 39.3 | 1.56 | 1.12 | 1.96 | 43.0 | 0.75 |
| 182 | 1132 | B | 9 | H | 7 | 25.0 | 27.0 | 82.55 | 24.0 | 31.5 | 1.67 | 1.27 | 2.08 | 39.0 | 0.64 |
| 182 | 1132 | B | 10 | H | 1 | 116.0 | 118.0 | 83.96 | 32.7 | 48.6 | 1.64 | 1.10 | 2.30 | 52.2 | 1.09 |
| 182 | 1132 | B | 10 | H | 2 | 70.0 | 72.0 | 85.00 | 35.1 | 54.2 | 1.48 | 0.96 | 1.95 | 50.8 | 1.03 |
| 182 | 1132 | B | 10 | H | 3 | 69.0 | 71.0 | 86.49 | 33.5 | 50.3 | 1.56 | 1.04 | 2.13 | 51.1 | 1.05 |
| 182 | 1132 | B | 10 | H | 4 | 66.0 | 68.0 | 87.96 | 34.1 | 51.8 | 1.60 | 1.06 | 2.27 | 53.4 | 1.15 |
| 182 | 1132 | B | 10 | H | 4 | 117.0 | 119.0 | 88.47 | 27.5 | 38.0 | 1.53 | 1.11 | 1.89 | 41.2 | 0.70 |
| 182 | 1132 | B | 10 | H | 5 | 70.0 | 72.0 | 89.50 | 29.1 | 41.0 | 1.57 | 1.12 | 2.01 | 44.7 | 0.81 |
| 182 | 1132 | B | 10 | H | 6 | 69.0 | 71.0 | 90.99 | 30.6 | 44.1 | 1.53 | 1.06 | 1.96 | 45.8 | 0.84 |
| 182 | 1132 | B | 11 | H | 2 | 74.0 | 76.0 | 94.54 | 26.5 | 36.0 | 1.64 | 1.21 | 2.10 | 42.4 | 0.74 |
| 182 | 1132 | B | 11 | H | 3 | 72.0 | 74.0 | 96.02 | 28.3 | 39.4 | 1.56 | 1.12 | 1.96 | 42.9 | 0.75 |
| 182 | 1132 | B | 11 | H | 4 | 74.0 | 76.0 | 97.54 | 28.8 | 40.5 | 1.54 | 1.10 | 1.94 | 43.4 | 0.77 |
| 182 | 1132 | B | 11 | H | 6 | 48.0 | 50.0 | 100.28 | 23.2 | 30.2 | 1.70 | 1.31 | 2.12 | 38.4 | 0.62 |
| 182 | 1132 | B | 11 | H | 6 | 142.0 | 144.0 | 101.22 | 25.2 | 33.7 | 1.60 | 1.20 | 1.98 | 39.5 | 0.65 |

Note: Only a portion of this table appears here. The complete table is available in **ASCII format.**

**Table T14.** Undrained shear strength measurements, Site 1132.

| Leg | Site | Hole | Core | Type | Section | Interval (cm) | Depth (mbsf) | Maximum shear strength (kPa) |
|---|---|---|---|---|---|---|---|---|
| 182 | 1132 | A | 1 | H | 2 | 120.3 | 2.70 | 3.18 |
| 182 | 1132 | A | 1 | H | 3 | 70.6 | 3.71 | 3.95 |
| 182 | 1132 | A | 1 | H | 4 | 117.7 | 5.68 | 2.74 |
| 182 | 1132 | A | 1 | H | 5 | 114.2 | 7.14 | 9.33 |
| 182 | 1132 | B | 1 | H | 3 | 65.9 | 3.66 | 2.20 |
| 182 | 1132 | B | 1 | H | 4 | 115.5 | 5.66 | 2.53 |
| 182 | 1132 | B | 2 | H | 1 | 133.2 | 8.13 | 6.70 |
| 182 | 1132 | B | 2 | H | 2 | 123.1 | 9.53 | 5.82 |
| 182 | 1132 | B | 2 | H | 4 | 136.3 | 12.66 | 5.27 |
| 182 | 1132 | B | 2 | H | 5 | 122.9 | 14.03 | 9.99 |
| 182 | 1132 | B | 2 | H | 6 | 93.5 | 15.23 | 7.79 |
| 182 | 1132 | B | 3 | H | 2 | 131.2 | 19.11 | 3.62 |
| 182 | 1132 | B | 3 | H | 4 | 122.8 | 22.03 | 6.15 |
| 182 | 1132 | B | 3 | H | 5 | 118.5 | 23.49 | 3.51 |
| 182 | 1132 | B | 3 | H | 6 | 120.1 | 25.00 | 17.23 |
| 182 | 1132 | B | 4 | H | 1 | 127.7 | 27.08 | 9.44 |
| 182 | 1132 | B | 4 | H | 2 | 118.8 | 28.49 | 13.28 |
| 182 | 1132 | B | 4 | H | 3 | 112.1 | 29.92 | 8.78 |
| 182 | 1132 | B | 4 | H | 4 | 106.3 | 31.36 | 3.62 |
| 182 | 1132 | B | 4 | H | 5 | 125.9 | 33.06 | 10.10 |
| 182 | 1132 | B | 4 | H | 6 | 83.7 | 34.14 | 2.31 |
| 182 | 1132 | B | 5 | H | 1 | 133.0 | 36.63 | 5.38 |
| 182 | 1132 | B | 5 | H | 2 | 115.9 | 37.96 | 2.74 |
| 182 | 1132 | B | 5 | H | 4 | 121.0 | 41.01 | 5.16 |
| 182 | 1132 | B | 5 | H | 5 | 112.0 | 42.42 | 5.93 |
| 182 | 1132 | B | 6 | H | 1 | 118.5 | 45.99 | 9.11 |
| 182 | 1132 | B | 6 | H | 2 | 126.8 | 47.57 | 7.03 |
| 182 | 1132 | B | 6 | H | 3 | 108.6 | 48.89 | 5.27 |
| 182 | 1132 | B | 6 | H | 4 | 123.1 | 50.53 | 4.72 |
| 182 | 1132 | B | 6 | H | 5 | 123.3 | 52.03 | 2.74 |
| 182 | 1132 | B | 7 | H | 1 | 130.2 | 55.60 | 10.54 |
| 182 | 1132 | B | 7 | H | 2 | 107.4 | 56.87 | 8.01 |
| 182 | 1132 | B | 7 | H | 3 | 133.7 | 58.64 | 7.79 |
| 182 | 1132 | B | 7 | H | 4 | 118.3 | 59.98 | 10.10 |
| 182 | 1132 | B | 7 | H | 5 | 133.8 | 61.64 | 3.18 |
| 182 | 1132 | B | 7 | H | 5 | 106.9 | 61.37 | 5.05 |
| 182 | 1132 | B | 7 | H | 6 | 128.4 | 63.08 | 15.37 |
| 182 | 1132 | B | 7 | H | 7 | 22.1 | 63.52 | 11.64 |
| 182 | 1132 | B | 8 | H | 2 | 101.0 | 66.31 | 4.61 |
| 182 | 1132 | B | 8 | H | 3 | 114.8 | 67.95 | 5.82 |
| 182 | 1132 | B | 8 | H | 4 | 116.5 | 69.46 | 10.43 |
| 182 | 1132 | B | 8 | H | 5 | 134.7 | 71.15 | 9.44 |
| 182 | 1132 | B | 8 | H | 6 | 106.4 | 72.36 | 9.88 |
| 182 | 1132 | B | 8 | H | 7 | 20.1 | 73.00 | 17.89 |
| 182 | 1132 | B | 9 | H | 1 | 124.4 | 74.54 | 8.45 |
| 182 | 1132 | B | 9 | H | 2 | 125.5 | 76.06 | 2.31 |
| 182 | 1132 | B | 9 | H | 3 | 103.6 | 77.34 | 9.77 |
| 182 | 1132 | B | 9 | H | 4 | 130.7 | 79.11 | 6.81 |
| 182 | 1132 | B | 9 | H | 5 | 122.0 | 80.52 | 2.63 |
| 182 | 1132 | B | 9 | H | 6 | 129.1 | 82.09 | 18.00 |
| 182 | 1132 | B | 9 | H | 7 | 15.9 | 82.46 | 24.81 |
| 182 | 1132 | B | 10 | H | 2 | 107.2 | 85.37 | 8.67 |
| 182 | 1132 | B | 10 | H | 3 | 120.0 | 87.00 | 12.73 |
| 182 | 1132 | B | 10 | H | 4 | 101.1 | 88.31 | 7.68 |
| 182 | 1132 | B | 10 | H | 5 | 132.0 | 90.12 | 8.78 |
| 182 | 1132 | B | 10 | H | 6 | 87.7 | 91.18 | 10.10 |
| 182 | 1132 | B | 11 | H | 1 | 135.1 | 93.65 | 14.27 |
| 182 | 1132 | B | 11 | H | 2 | 130.9 | 95.11 | 2.53 |
| 182 | 1132 | B | 11 | H | 3 | 103.2 | 96.33 | 8.34 |
| 182 | 1132 | B | 11 | H | 5 | 142.2 | 99.72 | 11.20 |
| 182 | 1132 | B | 11 | H | 6 | 110.6 | 100.91 | 4.50 |
| 182 | 1132 | B | 11 | H | 7 | 34.8 | 101.65 | 47.53 |

Note: Only a portion of this table appears here. The complete table is available in **ASCII format.**

**Table T15.** *P*-wave velocity measurements from the multisensor track, Site 1132.

| Leg | Site | Hole | Core | Type | Section | Interval (cm) | Depth (mbsf) | $V_p$ (km/s) |
|---|---|---|---|---|---|---|---|---|
| 182 | 1132 | A | 1 | H | 1 | 3.0 | 0.03 | 1.8234 |
| 182 | 1132 | A | 1 | H | 1 | 7.0 | 0.07 | 4.1116 |
| 182 | 1132 | A | 1 | H | 1 | 11.0 | 0.11 | 4.0450 |
| 182 | 1132 | A | 1 | H | 1 | 15.0 | 0.15 | 4.0051 |
| 182 | 1132 | A | 1 | H | 1 | 19.0 | 0.19 | 4.0321 |
| 182 | 1132 | A | 1 | H | 1 | 23.0 | 0.23 | 3.8780 |
| 182 | 1132 | A | 1 | H | 1 | 27.0 | 0.27 | 4.0469 |
| 182 | 1132 | A | 1 | H | 1 | 31.0 | 0.31 | 3.7695 |
| 182 | 1132 | A | 1 | H | 1 | 35.0 | 0.35 | 4.0469 |
| 182 | 1132 | A | 1 | H | 1 | 43.0 | 0.43 | 4.0271 |
| 182 | 1132 | A | 1 | H | 1 | 47.0 | 0.47 | 4.0444 |
| 182 | 1132 | A | 1 | H | 1 | 51.0 | 0.51 | 4.0100 |
| 182 | 1132 | A | 1 | H | 1 | 59.0 | 0.59 | 4.0370 |
| 182 | 1132 | A | 1 | H | 1 | 63.0 | 0.63 | 3.9943 |
| 182 | 1132 | A | 1 | H | 1 | 67.0 | 0.67 | 3.7004 |
| 182 | 1132 | A | 1 | H | 1 | 71.0 | 0.71 | 3.9846 |
| 182 | 1132 | A | 1 | H | 1 | 75.0 | 0.75 | 3.9726 |
| 182 | 1132 | A | 1 | H | 1 | 79.0 | 0.79 | 3.9967 |
| 182 | 1132 | A | 1 | H | 1 | 83.0 | 0.83 | 3.9919 |
| 182 | 1132 | A | 1 | H | 1 | 87.0 | 0.87 | 3.9919 |
| 182 | 1132 | A | 1 | H | 1 | 95.0 | 0.95 | 3.9894 |
| 182 | 1132 | A | 1 | H | 1 | 99.0 | 0.99 | 3.9967 |
| 182 | 1132 | A | 1 | H | 1 | 103.0 | 1.03 | 3.6654 |
| 182 | 1132 | A | 1 | H | 1 | 107.0 | 1.07 | 4.0137 |
| 182 | 1132 | A | 1 | H | 1 | 111.0 | 1.11 | 3.9870 |
| 182 | 1132 | A | 1 | H | 1 | 115.0 | 1.15 | 4.0162 |
| 182 | 1132 | A | 1 | H | 1 | 123.0 | 1.23 | 3.8339 |
| 182 | 1132 | A | 1 | H | 1 | 127.0 | 1.27 | 4.0064 |
| 182 | 1132 | A | 1 | H | 1 | 131.0 | 1.31 | 4.0089 |
| 182 | 1132 | A | 1 | H | 1 | 135.0 | 1.35 | 3.9943 |
| 182 | 1132 | A | 1 | H | 1 | 139.0 | 1.39 | 3.9810 |
| 182 | 1132 | A | 1 | H | 1 | 143.0 | 1.43 | 1.8440 |
| 182 | 1132 | A | 1 | H | 2 | 3.0 | 1.53 | 3.1336 |
| 182 | 1132 | A | 1 | H | 2 | 7.0 | 1.57 | 4.0775 |
| 182 | 1132 | A | 1 | H | 2 | 11.0 | 1.61 | 4.0541 |
| 182 | 1132 | A | 1 | H | 2 | 15.0 | 1.65 | 4.0260 |
| 182 | 1132 | A | 1 | H | 2 | 19.0 | 1.69 | 4.0298 |
| 182 | 1132 | A | 1 | H | 2 | 23.0 | 1.73 | 4.0348 |
| 182 | 1132 | A | 1 | H | 2 | 27.0 | 1.77 | 4.0224 |
| 182 | 1132 | A | 1 | H | 2 | 31.0 | 1.81 | 4.0298 |
| 182 | 1132 | A | 1 | H | 2 | 35.0 | 1.85 | 4.0249 |
| 182 | 1132 | A | 1 | H | 2 | 43.0 | 1.93 | 4.0213 |
| 182 | 1132 | A | 1 | H | 2 | 47.0 | 1.97 | 3.6810 |
| 182 | 1132 | A | 1 | H | 2 | 51.0 | 2.01 | 4.0041 |
| 182 | 1132 | A | 1 | H | 2 | 55.0 | 2.05 | 3.9895 |
| 182 | 1132 | A | 1 | H | 2 | 59.0 | 2.09 | 3.9968 |
| 182 | 1132 | A | 1 | H | 2 | 63.0 | 2.13 | 3.6483 |
| 182 | 1132 | A | 1 | H | 2 | 67.0 | 2.17 | 3.9703 |
| 182 | 1132 | A | 1 | H | 2 | 71.0 | 2.21 | 3.9895 |
| 182 | 1132 | A | 1 | H | 2 | 75.0 | 2.25 | 3.9440 |
| 182 | 1132 | A | 1 | H | 2 | 79.0 | 2.29 | 3.9511 |
| 182 | 1132 | A | 1 | H | 2 | 83.0 | 2.33 | 3.7101 |
| 182 | 1132 | A | 1 | H | 2 | 87.0 | 2.37 | 1.8648 |
| 182 | 1132 | A | 1 | H | 2 | 91.0 | 2.41 | 2.1823 |
| 182 | 1132 | A | 1 | H | 2 | 95.0 | 2.45 | 3.4010 |
| 182 | 1132 | A | 1 | H | 2 | 99.0 | 2.49 | 3.9835 |
| 182 | 1132 | A | 1 | H | 2 | 103.0 | 2.53 | 3.9619 |
| 182 | 1132 | A | 1 | H | 2 | 107.0 | 2.57 | 3.9835 |
| 182 | 1132 | A | 1 | H | 2 | 111.0 | 2.61 | 3.9823 |
| 182 | 1132 | A | 1 | H | 2 | 115.0 | 2.65 | 3.9799 |
| 182 | 1132 | A | 1 | H | 2 | 119.0 | 2.69 | 3.9895 |
| 182 | 1132 | A | 1 | H | 2 | 123.0 | 2.73 | 3.9703 |
| 182 | 1132 | A | 1 | H | 2 | 131.0 | 2.81 | 3.9847 |
| 182 | 1132 | A | 1 | H | 2 | 135.0 | 2.85 | 3.9775 |
| 182 | 1132 | A | 1 | H | 2 | 139.0 | 2.89 | 3.9727 |

Note: Only a portion of this table appears here. The complete table is available in **ASCII format.**

**Table T16.** Differences between depths to seismic horizons and corrected depths.

| Seismic horizons | Predicted intersection (mbsf) | ITT corrected depth (mbsf) | Difference (m) |
|---|---|---|---|
| Base of Sequence 2 | 218 | 230 | +12 |
| Base of Sequence 3 | 391 | 406 | +15 |
| Top of Sequence 6B | 496 | 510 | +14 |
| Top of Sequence 7 | 525 | 537 | +12 |
| Base of Cenozoic | 670 | | |

Notes: Predicted intersection depths were derived using high-resolution site-survey seismic data stacking velocities. Corrected depths were based on interval transit-time (ITT) data.